

The fundamental parameters of astrophysical plasma turbulence and its dissipation: non-relativistic limit

Gregory G. Howes  †

Department of Physics and Astronomy, University of Iowa, Iowa City, IA 52242, USA

(Received 17 April 2024; revised 9 July 2024; accepted 18 July 2024)

A specific set of dimensionless plasma and turbulence parameters is introduced to characterize the nature of turbulence and its dissipation in weakly collisional space and astrophysical plasmas. Key considerations are discussed for the development of predictive models of the turbulent plasma heating that characterize the partitioning of dissipated turbulent energy between the ion and electron species and between the perpendicular and parallel degrees of freedom for each species. Identifying the kinetic physical mechanisms that govern the damping of the turbulent fluctuations is a critical first step in constructing such turbulent heating models. A set of ten general plasma and turbulence parameters are defined, and reasonable approximations along with the exploitation of existing scaling theories for magnetohydrodynamic turbulence are used to reduce this general set of ten parameters to just three parameters in the isotropic temperature case: the ion plasma beta, the ion-to-electron temperature ratio and the isotropic driving wavenumber. A critical step forward in this study is to identify the dependence of all of the proposed kinetic mechanisms for turbulent damping in terms of the same set of fundamental plasma and turbulence parameters. Analytical estimations of the scaling of each damping mechanism on these fundamental parameters are presented. The power of this approach is illustrated in the development of the first phase diagram for the turbulent damping mechanisms as a function of the ion plasma beta and isotropic driving wavenumber for unity ion-to-electron temperature ratio, showing the regions of this two-dimensional parameter space in which ion Landau and transit-time damping, electron Landau and transit-time damping, ion cyclotron damping, ion stochastic heating, collisionless magnetic reconnection and kinetic ‘viscous’ heating play a role in the damping of the turbulent fluctuations.

Key words: astrophysical plasmas, space plasma physics, plasma nonlinear phenomena

1. Introduction

Turbulence is a fundamental, yet incompletely understood, process in space and astrophysical plasmas that mediates the transfer of the energy of chaotic plasma flows and electromagnetic fields into the energy of the plasma particles, either as heat of the

† Email address for correspondence: gregory-howes@uiowa.edu

plasma species or as acceleration of a small population of particles (Howes 2017). The 2013 NRC Heliophysics Decadal Survey (National Research Council 2013) identifies plasma turbulence as a ubiquitous phenomenon occurring both within the heliosphere and throughout the Universe. Predicting the heating or acceleration of the different plasma species by turbulence, based on the observable turbulence and plasma parameters at large scales, constitutes one of the grand challenge problems in heliophysics and astrophysics.

Turbulent plasma heating plays a key role in governing the flow of energy in the heliosphere, impacting the mesoscale and macroscale evolution of key heliospheric environments comprising the coupled solar–terrestrial system and connecting the solar corona, solar wind and Earth’s magnetosphere. The accuracy of ongoing efforts (Mikić *et al.* 1999; Lionello, Linker & Mikić 2009; van der Holst *et al.* 2014; Adhikari *et al.* 2020) to model globally the flow of energy from the Sun through the interplanetary medium to the Earth, to the other planets and on to the boundary of the heliosphere with the surrounding interstellar medium (Opher *et al.* 2020) relies on the availability of prescriptive models of the turbulent plasma heating (Howes 2010; Chandran *et al.* 2011; Rowan, Sironi & Narayan 2017).

Such turbulent heating prescriptions are also critical for the interpretation of remote astronomical observations of emissions from black hole accretion disks, such as the ground-breaking observations by the Event Horizon Telescope of the supermassive black holes at the centre of M87 (Event Horizon Telescope Collaboration *et al.* 2019) and at Sagittarius A* in the Milky Way (Event Horizon Telescope Collaboration *et al.* 2022). In these cases, alternative turbulent heating prescriptions (Howes 2010; Rowan *et al.* 2017) have been shown to yield drastically different predictions for the emitted radiation (Chael, Narayan & Johnson 2019).

1.1. How does turbulence mediate energy transport and plasma heating?

The transport of energy mediated by plasma turbulence is depicted in figure 1 for the solar wind with ion plasma beta $\beta_i = 1$, where (a) a plot of the turbulent magnetic-energy wavenumber spectrum shows that Alfvénic energy injected into the turbulent cascade at the outer scale ($k_0 \rho_i = 10^{-4}$) is transferred nonlinearly without loss through the inertial range to the transition into the dissipation range at ion scales ($k \rho_i \sim 1$), where ρ_i is the ion Larmor radius. At the ion scales and smaller ($k \rho_i \gtrsim 1$), poorly understood mechanisms can remove energy from the turbulence, transferring energy to the ions (blue arrows) or electrons (magenta arrows). In figure 1(b), modern plasma turbulence theory (Goldreich & Sridhar (1995), hereafter GS95 or Boldyrev (2006), hereafter B06) predicts that the turbulent cascade generates a scale-dependent anisotropy in wavevector space (blue shaded region): isotropy at the driving scale ($k_{\perp 0} \rho_i = k_{\parallel 0} \rho_i = 10^{-4}$) develops into a significant anisotropy $k_{\perp} \gg k_{\parallel}$ as the cascade transfers energy to smaller scales¹. In addition, kinetic instabilities can generate unstable turbulent fluctuations with wavevectors $k \rho_i \sim 1$ (red ovals in both panels), which can mediate the non-local transfer of energy from the large-scale motions directly to the ion kinetic scales. I explicitly define ‘turbulence’ here as the collection of physical mechanisms involved in the conversion of the energy of large-scale plasma flows and magnetic fields into plasma heat or the energy of accelerated particles, including the nonlinear scale-to-scale energy transfer of the turbulent cascade, the mechanisms damping the turbulence at small scales and any possible instabilities that may generate turbulent fluctuations or govern non-local energy transfer.

¹Parallel and perpendicular here are defined relative to the local mean magnetic field direction.

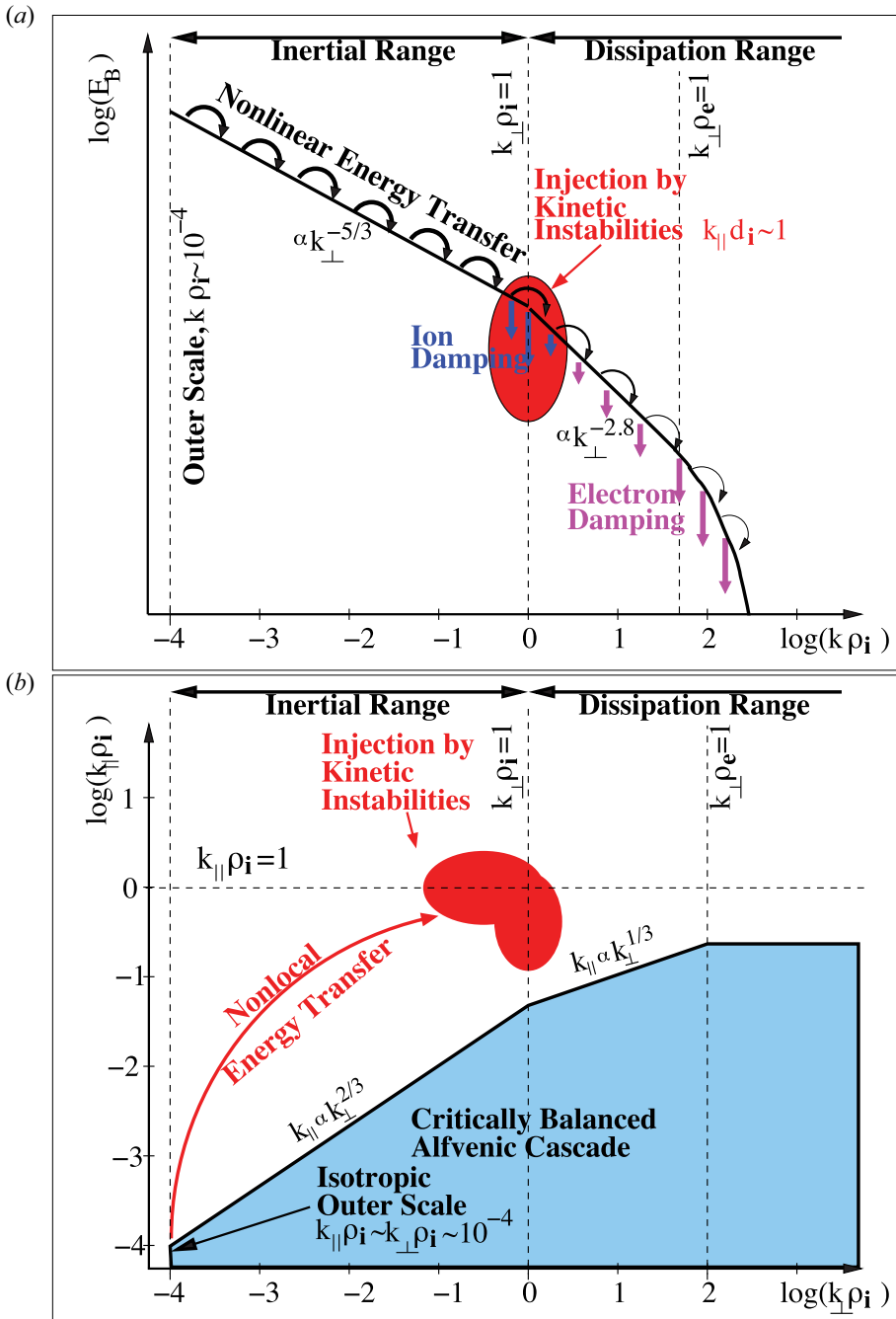


FIGURE 1. (a) Schematic diagram of the turbulent magnetic-energy spectrum in the solar wind with ion plasma beta $\beta_i = 1$, depicting the local transfer of Alfvénic energy from large scales (small wavenumbers k) to small scales (large k) through a turbulent cascade (black arrows). Instabilities may alter this energy flow by non-locally transporting energy directly to small, kinetic scales (red arrow). (b) In wavevector space, the local transfer of the Alfvénic turbulent cascade follows the anisotropic, critically balanced path, here plotted quantitatively for the case of the GS95 scaling theory.

1.2. What do we want to predict?

A long-term goal of the heliophysics community is to characterize the partitioning of turbulent energy in terms of observable plasma and turbulence parameters, producing a predictive heating model that can be used in numerical modelling of the global evolution of the heliosphere, thereby advancing our capability for predictive modelling of the coupled solar–terrestrial system. Understanding how the multiscale physics of plasma turbulence couples the large-scale plasma conditions and evolution to the microphysical heating and particle energization is essential to creating predictive heating models. Unfortunately, current numerical codes cannot simulate the vast dynamic range of scales inherent to the multiscale nature of heliospheric plasma turbulence while simultaneously capturing the kinetic physics governing the conversion of turbulent energy to some form of particle energy. Developing turbulent heating models that capture this coupling is one promising avenue for formulating predictive models at a computationally feasible cost. To develop such models, it is essential to establish a thorough understanding of the microphysical kinetic processes that govern the energization of particles.

In a statistically steady-state turbulent cascade in a weakly collisional astrophysical plasma, the energy injected into the turbulence at the outer scale is transferred locally in scale down to increasingly smaller scales until reaching the kinetic length scales at which damping mechanisms can collisionlessly remove energy from the turbulence and energize the different particle species, as depicted in [figure 1\(a\)](#). This local cascade of energy is mediated by nonlinear interactions among the turbulent fluctuations, such as between counterpropagating Alfvén wave packets, often denoted ‘Alfvén wave collisions’ (Kraichnan 1965; Sridhar & Goldreich 1994; Goldreich & Sridhar 1995; Ng & Bhattacharjee 1996; Galtier *et al.* 2000; Howes *et al.* 2012*b*; Drake *et al.* 2013; Howes & Nielson 2013; Howes *et al.* 2013; Nielson, Howes & Dorland 2013; Howes 2016; Verniero & Howes 2018; Verniero, Howes & Klein 2018; Ripperda *et al.* 2021; TenBarge *et al.* 2021). Non-local energy transfer mechanisms – such as kinetic instabilities driven by the large-scale dynamics that may cause the plasma conditions to deviate from local thermodynamic equilibrium – can also directly generate turbulent fluctuations at the small kinetic length scales, as illustrated in [figure 1\(b\)](#). Together, these mechanisms lead to a turbulent energy density cascade rate ε from the large scales down to the small scales of the turbulence. This nonlinear transfer of the turbulent energy density is ultimately damped at small scales by kinetic plasma physics mechanisms, converting the energy density of the small-scale turbulent plasma flows and magnetic fields into particle energy with a statistically steady-state total plasma energy density heating rate $Q \sim \varepsilon$.

For a single-ion-species plasma, such as a fully ionized hydrogenic plasma of protons and electrons, the primary deliverable of a turbulent heating model is the determination of the partitioning of the energy by the kinetic turbulent damping mechanisms between the ions and electrons, Q_i/Q_e . Unlike in the case of strongly collisional plasmas, in which the dissipated turbulent energy would be rapidly equilibrated between ion and electron species by collisions, under the weakly collisional plasma conditions typical of space and astrophysical plasmas, the differential heating of the plasma species can impact the thermodynamic evolution of the plasma on mesoscales and macroscales.

Furthermore, energy transferred to a given plasma species may lead to energization of the parallel degree of freedom or the perpendicular degrees of freedom relative to the direction of the local magnetic field. Thus, secondary deliverables of a turbulent heating model are measures of the anisotropic ion energy density heating rate $Q_{\perp,i}/Q_{\parallel,i}$ and the anisotropic electron energy density heating rate $Q_{\perp,e}/Q_{\parallel,e}$. In a strongly collisional plasma, the anisotropic heating for each species would be rapidly isotropized by collisions, but

Quantity	Symbol	Bounded
Turbulent energy density cascade rate	ε	
Plasma energy density heating rate	Q	
Ion-to-Electron heating ratio	Q_i/Q_e	Q_i/Q
Anisotropic ion energy density heating ratio	$Q_{\perp,i}/Q_{\parallel,i}$	$Q_{\perp,i}/Q_i$
Anisotropic electron energy density heating ratio	$Q_{\perp,e}/Q_{\parallel,e}$	$Q_{\perp,e}/Q_e$

TABLE 1. The key input quantities (top section) and deliverables (bottom section) for predictive turbulent heating models. Bounded quantities are normalized such that their values vary only over the interval $[0, 1]$.

weakly collisional plasmas allow the parallel and perpendicular² degrees of freedom to be energized independently (Kawazura, Barnes & Schekochihin 2019).

Different kinetic particle energization mechanisms may energize different degrees of freedom – e.g. Landau damping energizes particles parallel to the magnetic field, but cyclotron damping generally energizes particles perpendicular to the magnetic field – so determining $Q_{\perp,i}/Q_{\parallel,i}$ and $Q_{\perp,e}/Q_{\parallel,e}$ first requires one to identify which kinetic physical mechanisms govern the damping of the turbulent fluctuations as a function of the plasma and turbulence parameters. Therefore, identifying the contributing turbulent damping mechanisms as a function of the plasma and turbulence parameters is an additional deliverable of a predictive turbulent heating model. Such information about the dominant turbulent damping mechanisms, as a function of the key dimensionless parameters describing the turbulent plasma, can be concisely presented in a phase diagram for the dissipation of kinetic plasma turbulence, analogous to that developed for the behaviour of magnetic reconnection in astrophysical plasmas (Ji & Daughton 2011). A first attempt at a phase diagram for the turbulent damping mechanisms in weakly collisional space and astrophysical plasmas is presented here in figure 12. The reader may wish to skip ahead briefly to view figure 12 to appreciate a key goal of the analysis presented here.

The key input quantities for a turbulent heating model (ε , Q) and the deliverables (Q_i/Q_e , $Q_{\perp,i}/Q_{\parallel,i}$, $Q_{\perp,e}/Q_{\parallel,e}$) for a turbulent heating model are summarized in table 1. Note that, for ion cyclotron damping, which generally energizes only the perpendicular degrees of freedom in the ion velocity distribution function³, the anisotropic ion heating ratio $Q_{\perp,i}/Q_{\parallel,i}$ would be formally infinite. To avoid these inelegant infinities, we may choose to use alternative bounded versions of the heating ratios in the right column of Table 1 that vary only over the range $[0, 1]$. These bounded quantities are related to the original quantities by $Q_i/Q = (Q_i/Q_e)/[1 + (Q_i/Q_e)]$ for the species partition and $Q_{\perp,s}/Q_s = (Q_{\perp,s}/Q_{\parallel,s})/[1 + (Q_{\perp,s}/Q_{\parallel,s})]$ for the anisotropic heating ratio for each species.

It is worthwhile noting that the determination of the partitioning of the turbulent energy between ions and electrons Q_i/Q_e can be simplified by the properties of the turbulent cascade that are evident in figure 1(a). The inertial range is defined as the range of scales over which the turbulent energy density is transferred to smaller scales without loss, leading to a constant energy density cascade rate ε throughout this range. However, this standard definition of the inertial range from fluid turbulence theory neglects the

²Note that, under typical astrophysical plasma conditions in which the turbulent fluctuation frequencies are not much faster than the species cyclotron frequencies, $\omega \lesssim \Omega_s$, the two perpendicular degrees of freedom are rapidly equilibrated by the gyromotion of the particles about the magnetic field, leading to gyrotopical plasma conditions with $T_{\perp,1} \sim T_{\perp,2}$.

³Note that, in quasilinear theory, ions are scattered along contours of constant energy in the cyclotron wave frame, which in some cases can lead to parallel cooling (Hollweg & Isenberg 2002).

possibility of a non-local transfer of energy that may arise in weakly collisional plasmas and potential collisionless damping of compressible fluctuations at scales $k_{\perp}\rho_i \ll 1$. In the absence of these effects, the turbulent cascade rate ε at the onset of damping at ion kinetic scales at $k\rho_i \sim 1$ is the same as that determined at the outer scale of the turbulence at $k_0\rho_i \ll 1$. Therefore, the collisionless wave–particle interactions that serve to remove energy from the turbulent fluctuations and transfer that energy to the ions generally play a significant role only within the range of length scales similar to the ion kinetic length scales, $k\rho_i \sim 1$: (i) at larger scales $k\rho_i \ll 1$, the collisionless damping rate with the ions γ_i is typically negligible in comparison with the effective nonlinear frequency of the turbulent energy transfer $\gamma_i \ll \omega_{nl}$; and (ii) at smaller scales $k\rho_i \gg 1$, the gyromotion of the ions averages out the effect of the small-scale electromagnetic fluctuations, so the ions decouple from the turbulent fields and do not exchange significant energy. Whatever turbulent energy manages to cascade beyond the ion scales to smaller scales at $k\rho_i \gg 1$ will ultimately be deposited with the electrons. Thus, the task of determining Q_i/Q_e largely boils down to determining what fraction of the turbulent energy is damped on the ions as the cascade progresses through the ion kinetic scales at $k\rho_i \sim 1$.

Ultimately, the kinetic mechanisms that serve to damp the turbulent fluctuations at kinetic length scales depend on the nature of the turbulent fluctuations at those scales. Therefore, a viable strategy for developing a useful phase diagram for plasma turbulence is to use turbulence scaling theories (e.g. GS95 or B06) to predict the properties of the turbulent fluctuations upon reaching the ion and electron kinetic scales from the plasma and turbulence parameters at large scales. The primary aim of this investigation is to establish a theoretical framework upon which to base such predictions of the dominant turbulent damping mechanisms as a function of the plasma and turbulence parameters.

1.3. *What is the approach for developing a predictive turbulent heating model?*

The Buckingham Pi theorem (Buckingham 1914) uses dimensional analysis (Barenblatt 1996) to determine the minimum number of dimensionless parameters upon which the physical behaviour of a system depends. This approach is the key principle underlying the development of predictive models of turbulent plasma heating in terms of the fundamental dimensionless parameters of kinetic plasma turbulence. For sufficiently simple systems, in which there are not multiple physical quantities of importance that have the same dimensions, one can define a unique set of fundamental dimensionless parameters. But for more complicated systems, in which there may be more than one relevant physical quantity with the same dimensions, such as multiple characteristic length scales, the determination of the fundamental dimensionless parameters is generally non-unique. The case of kinetic turbulence in a weakly collisional plasma certainly falls into this more complicated category. In that situation, it is essential to use physical insight into the system's properties and behaviour to define a particular set of dimensionless parameters that is most useful in characterizing the behaviour of the system.

The goal of this paper is to define a particular set of fundamental dimensionless parameters that can be used to characterize the properties of kinetic plasma turbulence and its damping mechanisms. Modern scaling theories for anisotropic plasma turbulence can then be expressed in terms of these fundamental parameters to determine the properties of the turbulent fluctuations at the kinetic length scales at which kinetic physical mechanisms can act to remove energy from the turbulent fluctuations and energize the plasma particles. How those kinetic damping mechanisms depend on the plasma parameters and properties of the turbulent fluctuations can then be used to predict the dominant mechanisms for the damping of turbulence as a function of the dimensionless parameters, as summarized by the phase diagram presented in figure 12. All of this information can then be synthesized

to generate improved turbulent heating prescriptions for comparison with direct numerical simulations of turbulent dissipation and for use in global modelling efforts for space and astrophysical plasma systems, such as the heliosphere or supermassive black hole accretion disks.

2. The fundamental dimensionless parameters of kinetic plasma turbulence

The first step in developing a predictive model for plasma turbulence in weakly collisional space and astrophysical plasmas is to identify the key dimensionless parameters upon which the turbulent energy cascade and its dissipation depend. In this paper, the focus is to characterize kinetic plasma turbulence in the non-relativistic limit for sub-Alfvénic turbulent motions, a case widely applicable to the turbulent plasmas found ubiquitously in the heliosphere and throughout the universe. There are two categories of governing parameters: plasma parameters and turbulence parameters. Modern scaling theories for anisotropic plasma turbulence can be employed to reduce the number of parameters needed to characterize the turbulence, as described in § 3.1. The reduced set of dimensionless parameters can then be used to develop useful phase diagrams that identify the dominant physical mechanisms of turbulent dissipation and highlight which of these key parameters has the strongest impact on how particles are energized by the turbulence.

2.1. Plasma parameters

The plasma parameters play a critical role in determining the nature of the turbulent fluctuations and their interaction with the underlying particle velocity distributions. For simplicity of notation, we assume here a fully ionized, hydrogenic plasma of protons and electrons with bi-Maxwellian equilibrium velocity distributions characterized by separate parallel and perpendicular temperatures⁴ for each species, $T_{\parallel,s}$ and $T_{\perp,s}$. In this idealized case, the equilibrium ion and electron number densities are equal, $n_i = n_e$.

The first and most important plasma parameter is the parallel ion plasma beta, $\beta_{\parallel,i} = 8\pi n_i T_{\parallel,i} / B^2$, which characterizes the ratio of parallel thermal pressure to the magnetic pressure in the plasma and dominantly controls the phase speeds of different linear wave modes in a magnetized plasma. Note that with definitions for the parallel ion thermal velocity $v_{\parallel,i}^2 = 2T_{\parallel,i} / m_i$ and the Alfvén velocity $v_A^2 = B^2 / (4\pi n_i m_i)$, the parallel ion plasma beta can be alternatively expressed as $\beta_{\parallel,i} = v_{\parallel,i}^2 / v_A^2$. The definitions of all characteristic plasma quantities and useful conversion formulas are collected in table 2. The second parameter is the ion-to-electron parallel temperature ratio $\tau_{\parallel} = T_{\parallel,i} / T_{\parallel,e}$. The third and fourth parameters describe the ion and electron temperature anisotropies, $A_i = T_{\perp,i} / T_{\parallel,i}$ and $A_e = T_{\perp,e} / T_{\parallel,e}$. The fifth parameter characterizes the collisionality of the plasma by comparing the mean free path scale for electron–electron collisions relative with the parallel driving scale $k_{\parallel 0} \lambda_{\text{mfp},e}$.

Although for a hydrogenic plasma of protons and electrons the ion-to-electron mass ratio $\mu = m_i / m_e$ has a fixed physical value of 1836, this ratio is included as an additional independent parameter in the calculations below since a reduced mass ratio is often used in numerical simulations of plasma turbulence for reasons of computational efficiency. Note also that, once μ and τ_{\parallel} are specified⁵, the single dimensionless parameter $k_{\parallel 0} \lambda_{\text{mfp},e}$ is sufficient to specify all possible charged particle collision rates, since $v_{ee} / (k_{\parallel 0} v_{\parallel,e}) = 1 / (k_{\parallel 0} \lambda_{\text{mfp},e})$ and $v_{ei} \sim v_{ee}$, $v_{ii} \sim \mu^{-1/2} \tau_{\parallel}^{-3/2} v_{ee}$ and $v_{ie} \sim \mu^{-1} \tau_{\parallel}^{-3/2} v_{ee}$.

⁴Note that we absorb the Boltzmann constant into the temperature throughout this paper, giving temperature in units of energy.

⁵For weakly collisional plasmas, the mean free path depends on the thermal velocity of particles parallel to the magnetic field, and is therefore independent of the perpendicular temperature.

Characteristic Plasma Quantities	
Parameter	Symbol and Definition
Parallel Species Thermal Velocity	$v_{t\parallel,s} = \sqrt{2T_{\parallel,s}/m_s}$
Perpendicular Species Thermal Velocity	$v_{t\perp,s} = \sqrt{2T_{\perp,s}/m_s}$
Alfvén Velocity	$v_A = B_0/\sqrt{4\pi n_i m_i}$
Ion Acoustic Velocity	$c_s = \sqrt{T_{\parallel,i}/m_i}$
Species Cyclotron Frequency (Angular)	$\Omega_s = q_s B_0/m_s c$
Species Plasma Frequency (Angular)	$\omega_{ps} = \sqrt{4\pi n_s q_s^2/m_s}$
Electron–electron Collision Frequency	$\nu_{ee} = 2^{3/2} \pi n_e e^4 \ln \Lambda / (m_e^{1/2} T_{\parallel,e}^{3/2})$
Ion Larmor Radius	$\rho_i = v_{t\perp,i}/\Omega_i$
Ion Sound Larmor Radius	$\rho_s = c_s/\Omega_i$
Electron Larmor Radius	$\rho_e = v_{t\perp,e}/\Omega_e$
Species Inertial Length	$d_s = c/\omega_{ps}$
Species Debye Length	$\lambda_{D,s} = \sqrt{T_s/(4\pi n_s q_s^2)}$
Electron Mean Free Path	$\lambda_{\text{mfp},e} = v_{t\parallel,e}/\nu_{ee}$
Ion Mean Free Path	$\lambda_{\text{mfp},i} = v_{t\parallel,i}/\nu_{ii}$
Plasma Parameter	$\Lambda = n_e \lambda_{D,e}^3$
Parallel Driving Scale	$L_{\parallel 0}$
Perpendicular Driving Scale	$L_{\perp 0}$
Parallel Driving Wavenumber	$k_{\parallel 0} = 2\pi/L_{\parallel 0}$
Perpendicular Driving Wavenumber	$k_{\perp 0} = 2\pi/L_{\perp 0}$
Linear Wave Frequency and Damping* Rate	$\omega - i\gamma$

Useful Conversion Formulas

$d_i = c/\omega_{pi} = v_A/\Omega_i = \rho_i/\sqrt{\beta_{\parallel,i} A_i}$	$\nu_{ei} \sim \nu_{ee}$
$d_e = v_A \mu^{1/2}/\Omega_e = \rho_i/\sqrt{\beta_{\parallel,i} A_i \mu} = \rho_e \sqrt{\tau_{\parallel} \mu/(\beta_{\parallel,i} A_e)}$	$\nu_{ii} \sim \mu^{-1/2} \tau_{\parallel}^{-3/2} \nu_{ee}$
$\rho_s = \rho_i/\sqrt{2\tau_{\parallel} A_i}$	$\nu_{ie} \sim \mu^{-1} \tau_{\parallel}^{-3/2} \nu_{ee}$
$\rho_e = \rho_i/\sqrt{\tau_{\parallel} A_e \mu/A_i}$	$\lambda_{\text{mfp},i} = \lambda_{\text{mfp},e} \tau_{\parallel}^2$
$\beta_{\parallel,i} = v_{t\parallel,i}^2/v_A^2$	$\beta_{\perp,e} = \beta_{\parallel,i}/\tau_{\parallel}$

TABLE 2. Definitions of characteristic plasma quantities in cgs units and useful conversion relations, where $\beta_{\parallel,i}$, τ_{\parallel} , A_i and μ are defined in table 3. *Note that the linear wave damping rate is defined unconventionally here such that $\gamma > 0$ corresponds to wave damping, while $\gamma < 0$ corresponds to wave growth; this choice eliminates negative signs in the numerous formulas for damping rates presented in this paper.

Therefore, $(\beta_{\parallel,i}, \tau_{\parallel}, A_i, A_e, k_{\parallel 0} \lambda_{\text{mfp},e})$ are five key dimensionless plasma parameters that govern the properties of plasma turbulence, along with the fixed mass ratio μ . These plasma parameters are summarized in table 3.

Note that, if the plasma contains multiple ion species, possibly each with multiple charge states, the number of parameters increases dramatically, requiring a minimum of five new dimensionless parameters for each new species s : (i) mass ratio m_s/m_i , (ii) number density ratio n_s/n_e , (iii) charge ratio q_s/q_e , (iv) parallel temperature ratio $T_{\parallel,s}/T_{\parallel,i}$ and (v) temperature anisotropy $T_{\perp,s}/T_{\parallel,s}$. Partially ionized plasmas will similarly require additional dimensionless parameters to be characterized. Since the intention here is not to treat kinetic plasma turbulence in full generality, but rather to describe how one can use the Pi theorem and turbulence scaling theories to minimize the number of relevant dimensionless parameters, the remainder of this paper will focus on the case of a fully

Plasma Parameters	
Parameter	Symbol and Definition
Parallel Ion Plasma Beta	$\beta_{\parallel,i} = 8\pi n_i T_{\parallel,i} / B^2$
Ion-to-Electron Parallel Temperature Ratio	$\tau_{\parallel} = T_{\parallel,i} / T_{\parallel,e}$
Ion Temperature Anisotropy	$A_i = T_{\perp,i} / T_{\parallel,i}$
Electron Temperature Anisotropy	$A_e = T_{\perp,e} / T_{\parallel,e}$
Plasma Collisionality	$k_{\parallel 0} \lambda_{\text{mf},e}$
Ion-to-Electron Mass Ratio	$\mu = m_i / m_e$
Turbulence Parameters	
Parameter	Symbol and Definition
Perpendicular Driving Scale	$k_{\perp 0} \rho_i$
Driving-Scale Anisotropy	$k_{\parallel 0} / k_{\perp 0}$
Nonlinear Parameter	$\chi_0 = k_{\perp 0} \delta B_{\perp 0} \theta_0 / (k_{\parallel 0} B_0)$
Imbalance Parameter	Z_0^+ / Z_0^-
Driving Compressibility	$E_{\text{comp}} / E_{\text{inc}}$

TABLE 3. For the general case of homogeneous turbulence in a fully ionized, hydrogenic plasma with bi-Maxwellian equilibrium velocity distributions, these are the fundamental dimensionless parameters of kinetic plasma turbulence, including plasma parameters and turbulence parameters. Note that the Boltzmann constant is absorbed to give temperature in units of energy.

ionized, hydrogenic plasma of protons and electrons with bi-Maxwellian equilibrium velocity distributions. Refinements of turbulent heating models to include minor ions, such as the α particles that comprise a small fraction of ions in space and astrophysical plasmas, can be constructed following the same principles presented here.

2.2. Turbulence parameters

The turbulence parameters characterize the scale, amplitude and properties of the turbulent driving through five additional parameters. For simplicity, the focus here is restricted to only the case of turbulence in a spatially homogeneous system in which the scale length of gradients in the equilibrium quantities are much larger than the turbulent outer scale of the system. Dimensionless ratios of length scales are notationally simplified by characterizing the length scales of the turbulent fluctuations in terms of their perpendicular and parallel wavenumbers. Below quantities at the outer scale of the turbulence, commonly denoted the driving scale or energy injection scale, are denoted by the subscript ‘0’.

The driving of the turbulence can be characterized by three dimensionless parameters. The first parameter is the perpendicular wavenumber of the driving-scale fluctuations normalized by the ion Larmor radius, $k_{\perp 0} \rho_i$. The second parameter is the wavevector anisotropy of the fluctuations at the driving scale, $k_{\parallel 0} / k_{\perp 0}$. The third parameter is the nonlinearity parameter that characterizes the amplitude of the driving, $\chi_0 = (k_{\perp 0} \delta B_{\perp 0} \theta_0) / (k_{\parallel 0} B_0)$, where $\delta B_{\perp 0}$ is the amplitude of the perpendicular magnetic field fluctuations, B_0 is the equilibrium magnetic field magnitude and θ_0 is the angle of dynamic alignment at the driving scale in radians (Boldyrev 2006). In the next section, we demonstrate how modern scaling theories for anisotropic magnetohydrodynamic (MHD) turbulence can be used to combine these three dimensionless parameters into a single parameter, the isotropic driving wavenumber, $k_0 \rho_i$. Note also that, in principle, the dynamic alignment angle θ_0 at driving scale is an additional dimensionless parameter

(measured in radians), but dynamic alignment is typically understood to be a phenomenon that develops self-consistently due to the turbulence as it cascades to smaller scales, so we neglect this parameter at the outer scale⁶, generally taking $\theta_0 \sim 1$ rad.

The nature of the turbulent fluctuations at the driving scale also plays an important role in determining the ultimate fate of the turbulent energy. The fourth turbulence parameter is the imbalance parameter, measuring the ratio of the amplitudes in upward-to-downward Elsasser fields, Z_0^+/Z_0^- , where the Elsasser fields at the outer scale are defined by $Z_0^\pm = \delta U_{\perp,0} \pm \delta B_{\perp,0}/\sqrt{4\pi n_i m_i}$ (Elsasser 1950), and where $\delta U_{\perp,0}$ and $\delta B_{\perp,0}$ are the perpendicular perturbed plasma flow velocity and perpendicular perturbed magnetic field of the turbulent fluctuations at the driving scale. Formally, $\delta U_{\perp,0}$ and $\delta B_{\perp,0}$ are vectors in the plane perpendicular to the equilibrium magnetic field B_0 , but to calculate the ratio Z_0^+/Z_0^- , we simply take the amplitudes of the Elsasser fields, $Z_0^\pm = |Z_0^\pm|$. Physically, Alfvén wave packets propagating up the mean magnetic field have $Z^+ = 0$ and $Z^- \neq 0$, and those propagating down the field have $Z^+ \neq 0$ and $Z^- = 0$. The Elsasser fields effectively characterize the wave energy flux in each direction along the magnetic field⁷ of the typically dominant Alfvénic fluctuations in heliospheric plasma turbulence (Tu & Marsch 1995; Schekochihin *et al.* 2009; Bruno & Carbone 2013). Since the nonlinear interactions that mediate the turbulent cascade in Alfvénic turbulence at MHD scales arise only between counterpropagating and perpendicularly polarized Alfvén waves (Kraichnan 1965; Sridhar & Goldreich 1994; Goldreich & Sridhar 1995; Ng & Bhattacharjee 1996; Galtier *et al.* 2000; Howes & Nielson 2013; Howes 2015a), the imbalance plays an important role in characterizing the turbulence. The importance of Z_0^+/Z_0^- under sufficiently imbalanced conditions, such as occurs in the inner heliosphere where wave energy fluxes are dominantly anti-sunward, has been demonstrated clearly with the recent discovery of a new phenomenon known as the helicity barrier in plasma turbulence (Meyrand *et al.* 2021; Squire *et al.* 2022; Squire, Meyrand & Kunz 2023).

A fifth turbulence parameter is the ratio of the energy in compressible fluctuations to that in incompressible fluctuations, $E_{\text{comp}}/E_{\text{inc}}$. Since a magnetized plasma supports two distinct compressible wave modes, the fast and slow magnetosonic waves (differing by whether the thermal and magnetic pressure perturbations associated with the wave act in conjunction or in opposition), one could further characterize the compressible component of the turbulent fluctuations by the additional ratio of the energy in the fast magnetosonic fluctuations to the total energy of compressible fluctuations E_F/E_{comp} , where the total compressible energy is the sum of the contributions from fast-mode and slow-mode fluctuations, $E_{\text{comp}} = E_F + E_S$. The ratio E_F/E_{comp} is not included here as one of the fundamental parameters based on a study of the inertial range in solar wind turbulence at 1 AU that showed negligible energy in fast-mode mode fluctuations, or $E_F/E_{\text{comp}} \ll 1$ (Howes *et al.* 2012a). If significant energy exists in fast-mode fluctuations in other turbulent astrophysical plasmas, E_F/E_{comp} may need to be included.

Therefore, $(k_{\perp 0} \rho_i, k_{\parallel 0}/k_{\perp 0}, \chi_0, Z_0^+/Z_0^-, E_{\text{comp}}/E_{\text{inc}})$ are five key dimensionless turbulence parameters that govern the properties of plasma turbulence. These turbulence parameters are summarized in table 3.

⁶Reflection-driven turbulence, as expected to occur in the inner heliosphere, is a likely exception to turbulent driving with $\theta_0 \sim 1$ rad, since sunward Alfvén waves born through reflection will be aligned with the anti-sunward Alfvén waves from which they were generated (Perez & Chandran 2013; Chandran & Perez 2019).

⁷Note that the imbalance of counterpropagating wave energy fluxes in plasma turbulence has alternatively been characterized in the literature using the cross-helicity (Dobrowolny, Mangeney & Veltri 1980; Matthaeus, Goldstein & Smith 1982; Marsch & Tu 1990; Perez & Boldyrev 2009, 2010) or the normalized Poynting flux (Hnat, Chapman & Rowlands 2003; Di Mare & Howes 2024).

If the restriction to spatially homogeneous turbulent plasmas is relaxed, the large-scale context of the turbulent plasma can also impact the nonlinear dynamics of the turbulence and the evolution of the turbulent fluctuations. In the solar wind, the spherical expansion of the solar wind governs the evolution of the plasma equilibrium temperatures with heliocentric radius, possibly triggering kinetic temperature anisotropy instabilities that can mediate non-local transfer of energy to small scales, as depicted in [figure 1\(b\)](#). In rotating plasmas, such as found in the solar convection zone, the turbulence may be driven with helical motions that can initiate the growth of magnetic field energy through a dynamo effect (Parker 1955; Glatzmaier 1984, 1985; Parker 1993; Ossendrijver 2003). Differential rotation in astrophysical accretion disks, which can trigger plasma turbulence through the magnetorotational instability (Balbus & Hawley 1991; Hawley & Balbus 1991; Balbus & Hawley 1998), has been recently shown to generate turbulence with a dominant fraction of its energy in compressible fluctuations (Kawazura *et al.* 2022). The inclusion of self-gravitational effects in the plasma, which play an important role in governing the dynamics of the multi-phase interstellar medium in molecular clouds and star-forming regions, adds significant additional complexity to the nature of the turbulent cascade. Finally, kinetic instabilities arising in the foot and ramp regions of collisionless shocks (Brown *et al.* 2023) can generate turbulent fluctuations that are swept into the downstream region. In all of these astrophysically relevant cases, additional dimensionless turbulence parameters will be required to characterize properly the turbulent fluctuations and their evolution.

2.3. What happened to the Reynolds number?

Readers familiar with studies of MHD turbulence may find what appear to be two glaring omissions in the proposed list of plasma and turbulence parameters in [table 3](#) since it does not include the Reynolds number, $Re = LU_0/\nu$, or the magnetic Reynolds number, $Re_M = LU_0/\eta$. The Reynolds number is a dimensionless quantity that characterizes the ratio of the amplitude of the convective term $\mathbf{U} \cdot \nabla \mathbf{U}$ to that of the viscous diffusion term $\nu \nabla^2 \mathbf{U}$ in the MHD momentum equation; the magnetic Reynolds number characterizes the ratio of the amplitude of the inductive term $\nabla \times (\mathbf{U} \times \mathbf{B})$ to that of the resistive diffusion term $\eta \nabla^2 \mathbf{B}$ in the MHD induction equation.

The kinematic viscosity ν and resistivity η are transport coefficients that are rigorously defined by an extension of the Chapman–Enskog procedure for magnetohydrodynamic systems (Spitzer 1962; Grad 1963; Braginskii 1965) in the limit of small but finite mean free path relative to the gradient scale, $\lambda_{\text{mfp}}/L \ll 1$. As illustrated by [figure 11](#), however, for many space and astrophysical plasma systems of interest, the scales at which energy is removed from the turbulence (beginning at the small-scale end of the inertial range) are weakly collisional, with $\lambda_{\text{mfp}}/L \gtrsim 1$ or $\lambda_{\text{mfp}}/L \gg 1$. In these complementary limits of moderate to large mean free path, relevant to space and astrophysical plasmas, the procedure to calculate the viscosity and resistivity ceases to be valid. In fact, the standard Laplacian viscosity and resistivity terms are likely to be poor approximations to the physical mechanisms that are believed to remove energy from weakly collisional plasma turbulence (see [§ 5.1](#) for a list of proposed damping mechanisms). Since it is not possible to define clearly the viscosity or resistivity in a weakly collisional system, it is also not possible to define the Reynolds number or magnetic Reynolds number in weakly collisional, kinetic plasma turbulence. Thus, we are forced to choose alternative dimensionless numbers that characterize the plasma and turbulence in weakly collisional systems, so one of the primary aims of this paper is to propose the specific set of fundamental dimensionless plasma and turbulence parameters that are suitable for characterizing kinetic plasma turbulence, presented here in [table 3](#).

3. Scaling theories for anisotropic plasma turbulence

The key to predicting the evolution of the turbulent fluctuations as energy is cascaded to ever smaller scales, and therefore also to developing a useful phase diagram for plasma turbulence, is to use turbulence scaling theories to predict the properties of the turbulence upon reaching the ion kinetic scales from the characteristics of the turbulence at large scales. In particular, we will include the two prominent theories for the anisotropic cascade of Alfvénic turbulence in MHD plasmas, the Goldreich–Sridhar 1995 (GS95) formulation for weak and strong MHD turbulence (Sridhar & Goldreich 1994; Goldreich & Sridhar 1995), and the modification of this theory by Boldyrev 2006 (B06) that accounts for a weakening of the nonlinearity by dynamic alignment (Boldyrev 2006). Note that, since these are MHD theories of plasma turbulence – where strong collisionality is assumed in the standard MHD approximation (Kulsrud 1983; Gurnett & Bhattacharjee 2017) – the equilibrium species temperatures are assumed to be isotropic and equal, corresponding to $\tau_{\parallel} = A_i = A_e = 1$. For the case of weakly collisional plasma turbulence that is relevant to most space and astrophysical plasma environments, these theories may need to be modified appropriately, but such development of refined turbulence theories is beyond the scope of the treatment here.

The particular scalings of the parallel wavenumber, intermediate wavenumber, alignment angle, and magnetic field perturbation as a function of the perpendicular wavenumber are given by

$$k_{\parallel} \propto k_{\perp}^{2/(3+\alpha)}, \quad (3.1)$$

$$k_i \propto k_{\perp}^{3/(3+\alpha)}, \quad (3.2)$$

$$\theta \propto k_{\perp}^{-\alpha/(3+\alpha)}, \quad (3.3)$$

$$\delta B_{\perp} \propto k_{\perp}^{-1/(3+\alpha)}, \quad (3.4)$$

where $\alpha = 0$ corresponds to the GS95 theory and $\alpha = 1$ corresponds to the B06 theory. Here the turbulent fluctuations as a function of scale are characterized by the three spatial components of the wavevector relative to the local magnetic field direction: (i) the parallel wavenumber k_{\parallel} ; and (ii) the intermediate wavenumber k_i and (iii) the perpendicular wavenumber k_{\perp} , which together describe the anisotropy of the fluctuations in the plane perpendicular to the local magnetic field, $k_i \ll k_{\perp}$, arising from the dynamic alignment of the fluctuations (Boldyrev 2006; Mason, Cattaneo & Boldyrev 2006; Boldyrev, Mason & Cattaneo 2009; Perez *et al.* 2012) and predicting the development of current sheets at small scales. These scaling theories predict the scaling of k_{\parallel} , k_i , the angle of dynamic alignment θ (in radians), and the amplitude of the perpendicular magnetic field fluctuations δB_{\perp} as a function of the perpendicular wavenumber k_{\perp} .

These theories yield specific predictions for the perpendicular magnetic-energy spectrum of turbulence in the MHD regime, $k_{\perp} \rho_i \gg 1$, and for the scale-dependent anisotropy of the turbulence, a qualitative feature that is well established in MHD turbulence (Cho & Vishniac 2000; Maron & Goldreich 2001; Cho, Lazarian & Vishniac 2002; Cho & Lazarian 2003; Mason *et al.* 2006; Boldyrev *et al.* 2009; Narita *et al.* 2010; Sahraoui *et al.* 2010; Chen *et al.* 2011, 2012; Perez *et al.* 2012; Roberts, Li & Jeska 2015). The perpendicular magnetic-energy spectrum for the two theories is given by

$$E_{B_{\perp}}(k_{\perp}) \propto \frac{(\delta B_{\perp})^2}{k_{\perp}} \propto k_{\perp}^{-(5+\alpha)/(3+\alpha)} = \begin{cases} k_{\perp}^{-5/3} & \alpha = 0 \\ k_{\perp}^{-3/2} & \alpha = 1 \end{cases}. \quad (3.5)$$

The parallel-to-perpendicular wavevector anisotropy is given by

$$\frac{k_{\parallel}}{k_{\perp}} \propto k_{\perp}^{-(1+\alpha)/(3+\alpha)} = \begin{cases} k_{\perp}^{-1/3} & \alpha = 0 \\ k_{\perp}^{-1/2} & \alpha = 1 \end{cases}, \quad (3.6)$$

demonstrating that both theories predict that the turbulent fluctuations develop a scale-dependent anisotropy, whereby the fluctuations become progressively more elongated along the magnetic field as they cascade to smaller scale, eventually yielding $k_{\parallel}/k_{\perp} \ll 1$ at sufficiently small scales. This k_{\parallel}/k_{\perp} anisotropy follows from the imposition of the condition of critical balance between the linear and nonlinear time scales of the turbulence (Goldreich & Sridhar 1995; Mallet, Schekochihin & Chandran 2015). The intermediate-to-perpendicular wavevector anisotropy is given by

$$\frac{k_i}{k_{\perp}} \propto k_{\perp}^{-\alpha/(3+\alpha)} = \begin{cases} k_{\perp}^0 & \alpha = 0 \\ k_{\perp}^{-1/4} & \alpha = 1 \end{cases}. \quad (3.7)$$

Here, the GS95 theory predicts no development of anisotropy in the perpendicular plane, at odds with the findings of current sheets at small perpendicular scales in numerical simulations (Matthaeus & Montgomery 1980; Meneguzzi, Frisch & Pouquet 1981; Uritsky *et al.* 2010; Zhdankin *et al.* 2012, 2013) and spacecraft observations (Borovsky 2008; Osman *et al.* 2011). The B06 theory predicts the development of anisotropy in the perpendicular plane, corresponding to the development of current sheets with $k_i/k_{\perp} \ll 1$ at sufficiently small scales, potentially triggering tearing instabilities (Furth, Killeen & Rosenbluth 1963; Zocco & Schekochihin 2011) that enable magnetic reconnection to disrupt the turbulent cascade (Boldyrev & Loureiro 2017; Loureiro & Boldyrev 2017a, b; Mallet, Schekochihin & Chandran 2017a, b; Walker, Boldyrev & Loureiro 2018).

It is worthwhile emphasizing that the idea of critical balance in the turbulent cascade does not imply that all of the turbulent energy is concentrated at the parallel wavenumber $k_{\parallel}^{\text{cb}}$ determined by critical balance. Rather, $k_{\parallel}^{\text{cb}}$ is the upper limit of parallel wavenumber, and thus generally also implies an upper limit on the linear wave frequency (since $\omega \propto k_{\parallel}$ for Alfvénic fluctuations with $\omega \ll \Omega_i$). Rather, the turbulent fluctuation power extends over the range $0 \leq k_{\parallel} \leq k_{\parallel}^{\text{cb}}$ (Goldreich & Sridhar 1995; Maron & Goldreich 2001). Accounting for how the turbulent energy is distributed over this k_{\parallel} range would lead to order-unity or less quantitative changes in the heating rates. Since the goal of predictive turbulent heating models is generally to calculate the lowest-order, order-of-magnitude quantities for species heating rates, any effects due to the distribution of turbulent energy over $0 \leq k_{\parallel} \leq k_{\parallel}^{\text{cb}}$ are likely to yield only higher-order corrections to these predictions; thus, the effect of this range of turbulent energy in k_{\parallel} is neglected in the first generation of turbulent heating models addressed here.

In closing, note that these theories for MHD turbulence are largely focused on the transport of energy in Alfvénic fluctuations, so if significant energy is driven or transferred nonlinearly into other (non-Alfvénic) wave modes, this may significantly alter the energy transport from the predictions shown here, with the potential for qualitatively different predictions for the damping mechanisms of these non-Alfvénic turbulent fluctuations.

3.1. Exploiting turbulent scaling theories to reduce the number of fundamental dimensionless parameters

Given the large number of fundamental dimensionless parameters that characterize weakly collisional plasma turbulence, shown in table 3, it is imperative to reduce the number of important parameters to make progress in developing predictive models of turbulent

heating. Adopting idealized approximations, such as maintaining isotropic equilibrium velocity distributions for the plasma, enables one to eliminate some of the parameters in [table 3](#). Another approach is to exploit the MHD turbulent scaling theories described in [§ 3](#) to combine several parameters into a new single parameter, an approach presented here.

In general, the driving of the plasma turbulence depends on at least three independent parameters: (i) the perpendicular wavenumber at which the turbulence is driven $k_{\perp 0} \rho_i$, (ii) the anisotropy of the driven fluctuations with respect to the local magnetic field direction $k_{\parallel 0}/k_{\perp 0}$ and (iii) the nonlinearity parameter which characterizes the strength of the driving, $\chi_0 \equiv k_{\perp 0} \delta B_{\perp 0} \theta_0 / (k_{\parallel 0} B_0)$. Recall that quantities evaluated at the driving scale are given the subscript ‘0’. Fortunately, for turbulence driven at large scales (relative to the ion kinetic scales), as is typical in most space or astrophysical plasma environments, MHD scaling theory can be used to predict the properties of the turbulence upon reaching the kinetic scales, where kinetic plasma processes act to dissipate the turbulence. In fact, as detailed here, it is possible to combine these three dimensionless parameters into a new, single dimensionless parameter: the isotropic driving wavenumber, $k_0 \rho_i$.

MHD turbulent scaling theories can be used, for a given set of driving parameters ($k_{\perp 0} \rho_i$, $k_{\parallel 0}/k_{\perp 0}$, χ_0), to predict the properties of the turbulent fluctuations (e.g. anisotropy, amplitude) upon reaching the ion kinetic scales, here taken to be the perpendicular wavenumber $k_{\perp} \rho_i = 1$. The isotropic driving wavenumber $k_0 \rho_i$ is the unique wavenumber that produces the same conditions at $k_{\perp} \rho_i = 1$ as if the turbulence were driven isotropically at that wavenumber with $k_{\perp 0} = k_{\parallel 0} \equiv k_0$ and in a condition of critical balance with $\chi_0 = 1$.

The key procedure for determining the isotropic driving wavenumber $k_0 \rho_i$ is illustrated in [figure 2](#). Panel (a) shows the perpendicular wavenumber magnetic-energy spectrum $E_{B_{\perp}}(k_{\perp})$ driven weakly with $\chi_0 = 0.1$ at perpendicular wavenumber $k_{\perp 0} \rho_i = 10^{-5}$, where a weak turbulent cascade leads to a steep weak MHD turbulence spectrum with $E_{B_{\perp}} \propto k_{\perp}^{-2}$ (Sridhar & Goldreich 1994; Galtier *et al.* 2000; Boldyrev & Perez 2009), followed by a flatter strong MHD turbulence spectrum with $E_{B_{\perp}} \propto k_{\perp}^{-(5+\alpha)/(3+\alpha)}$ (Goldreich & Sridhar 1995; Boldyrev 2006). The cascade reaches the perpendicular ion kinetic scale $k_{\perp} \rho_i = 1$, and at higher wavenumbers the cascade continues as strong kinetic Alfvén wave (KAW) turbulence with a significantly steeper magnetic-energy spectrum with $E_{B_{\perp}} \propto k_{\perp}^{-2.8}$ (Alexandrova *et al.* 2009; Kiyani *et al.* 2009; Sahraoui *et al.* 2009; Chen *et al.* 2010; Howes *et al.* 2011b; Sahraoui *et al.* 2013). When the collisionless damping of the KAW turbulent cascade begins to diminish the rate of nonlinear energy cascade, the spectrum begins to fall off exponentially in the weakly dissipating KAW turbulence (WDKT) regime (Howes, Tenborge & Dorland 2011a), ultimately terminating the turbulent cascade at scales $k_{\perp} \rho_e \gtrsim 1$.

In [figure 2\(b\)](#) is presented the characteristic path of the anisotropic cascade of energy through $(k_{\perp}, k_{\parallel})$ wavevector space for the different regimes of the turbulent cascade. There is no parallel cascade in the weak MHD turbulence regime (Sridhar & Goldreich 1994; Galtier *et al.* 2000), followed by a scale-dependent anisotropy given by $k_{\parallel} \propto k_{\perp}^{2/(3+\alpha)}$ in the strong MHD turbulence regime (Goldreich & Sridhar 1995; Boldyrev 2006). The turbulence transitions to the strong KAW regime at $k_{\perp} \rho_i \sim 1$, with the anisotropy becoming stronger at $k_{\perp} \rho_i > 1$, scaling as $k_{\parallel} \propto k_{\perp}^{1/3}$ (Cho & Lazarian 2004; Howes *et al.* 2008a, 2011a; TenBorge & Howes 2012; TenBorge, Howes & Dorland 2013). As the turbulence weakens due to collisionless damping of turbulent fluctuations in the WDKT regime, the parallel cascade is predicted to cease once again (Howes *et al.* 2011a).

The diagrams in [figure 2](#) provide guidance to understand how MHD turbulence scaling theories can be used to combine $(k_{\perp 0} \rho_i, k_{\parallel 0}/k_{\perp 0}, \chi_0)$ into a single new parameter, the isotropic driving wavenumber, $k_0 \rho_i$. If the turbulence is driven at critical balance ($\chi_0 = 1$) and isotropically ($k_{\parallel 0}/k_{\perp 0} = 1$), then the isotropic driving wavenumber is simply the same

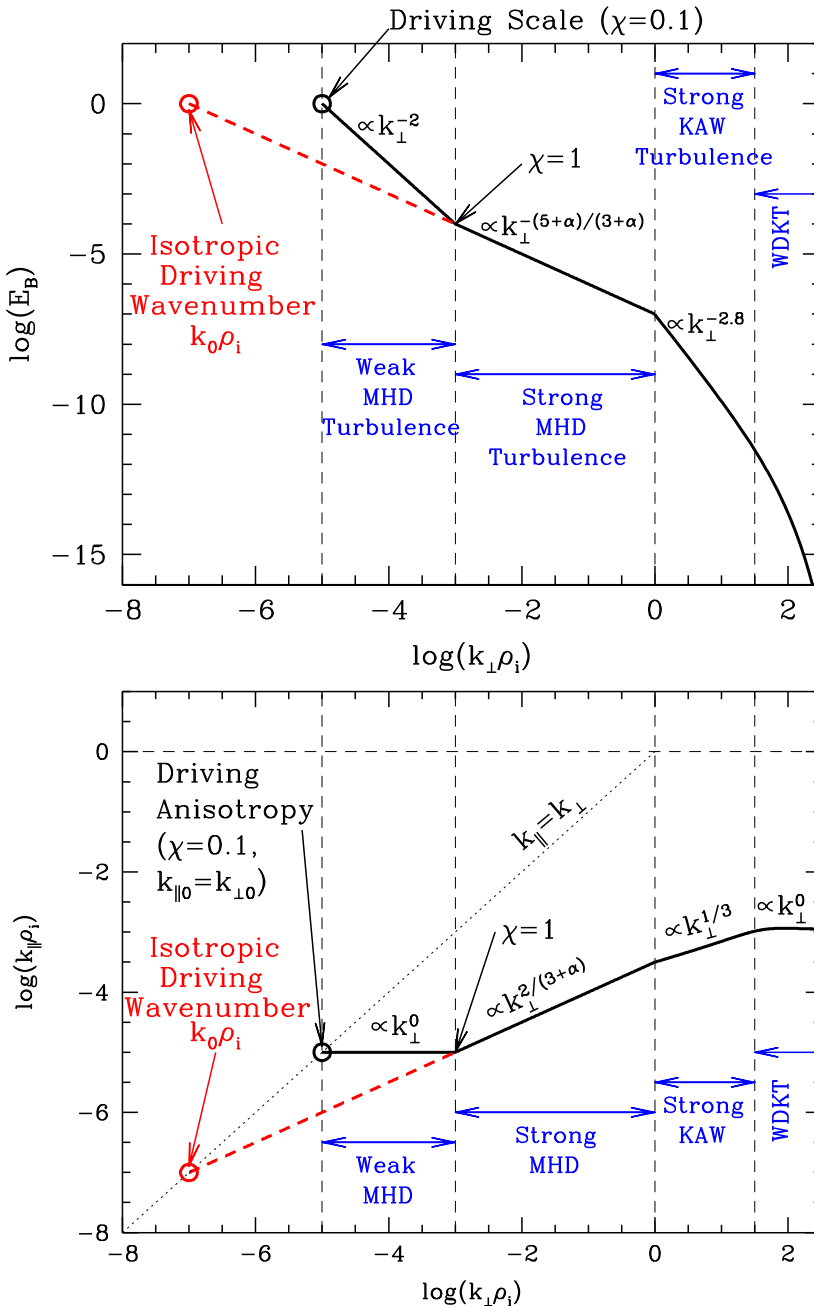


FIGURE 2. Diagram illustrating how to determine the isotropic driving wavenumber $k_0\rho_i$ in terms of the perpendicular driving wavenumber $k_{\perp}\rho_i$, the driving anisotropy $k_{\parallel 0}/k_{\perp 0}$ and the nonlinearity parameter of the driving, $\chi_0 = k_{\perp 0}\delta B_{\perp}\theta_0/(k_{\parallel 0}B_0)$.

as the perpendicular driving wavenumber, $k_0\rho_i = k_{\perp 0}\rho_i$. Therefore, it is necessary to use MHD turbulence scaling theory to determine $k_0\rho_i$ only in the case that the turbulence is driven weakly with $\chi_0 < 1$ or anisotropically with $k_{\parallel 0}/k_{\perp 0} \neq 1$.

For weakly driven turbulence with $\chi_0 < 1$, MHD turbulence theory predicts that the parallel cascade is inhibited and that the perpendicular wavenumber magnetic-energy spectrum of the turbulence scales as $E_{B_\perp} \propto (\delta B_\perp)^2/k_\perp \propto k_\perp^{-2}$. Therefore, in terms of the driving amplitude $\delta B_{\perp 0}$ and perpendicular driving wavenumber $k_{\perp 0}$, the amplitude of the turbulence as a function of k_\perp is given by $\delta B_\perp(k_\perp) = \delta B_{\perp 0}(k_{\perp 0}/k_\perp)^{1/2}$. Given the lack of parallel cascade in weak MHD turbulence, we fix $k_\parallel = k_{\parallel 0}$, and obtain the following scaling⁸ for the nonlinearity parameter as a function of k_\perp :

$$\chi(k_\perp) = \chi_0 \left(\frac{k_\perp \rho_i}{k_{\perp 0} \rho_i} \right)^{1/2}. \quad (3.8)$$

Magnetohydrodynamic turbulence theory predicts that the nonlinearity parameter will increase through the weak turbulent cascade until it reaches a value of unity, $\chi \sim 1$, at which point the turbulence has reached a state of critical balance in the strong turbulence regime. From that point, theory predicts that an anisotropic cascade will ensue (transferring energy to smaller scales more rapidly in the perpendicular than the parallel direction), with the parallel and perpendicular cascades balanced to maintain a nonlinearity parameter of unity, $\chi \sim 1$. Therefore, the key point in the cascade is the perpendicular wavenumber at which the turbulence first reaches $\chi = 1$, given by

$$k_\perp \rho_i|_{\chi=1} = \frac{1}{\chi_0^2} k_{\perp 0} \rho_i. \quad (3.9)$$

An example of this weakly turbulent, strictly perpendicular cascade in (k_\perp, k_\parallel) space is depicted in [figure 2\(b\)](#), where turbulence driven weakly with $\chi_0 = 0.1$, cascades to $k_\perp \rho_i = 100 k_{\perp 0} \rho_i$, at which point the turbulence becomes strong, with $\chi = 1$.

To obtain the isotropic driving wavenumber $k_0 \rho_i$ from this point in wavevector space $(k_\perp \rho_i|_{\chi=1}, k_{\parallel 0})$, we need to extend the cascade backward along the critical balance line (red dashed lines) until it intersects with isotropy $k_\parallel = k_\perp$ (dotted line). From the MHD scaling theories in § 3, for a critically balanced, strong turbulent cascade that is driven strongly and isotropically at $k_0 \rho_i$, the anisotropy as a function of k_\perp scales as

$$\frac{k_\parallel}{k_\perp} = \left(\frac{k_0 \rho_i}{k_\perp \rho_i} \right)^{(1+\alpha)/(3+\alpha)}. \quad (3.10)$$

The anisotropy at the point $(k_\perp \rho_i|_{\chi=1}, k_{\parallel 0})$ is given by $k_\parallel/k_\perp = (k_{\parallel 0}/k_{\perp 0})\chi_0^2$. Substituting this expression for k_\parallel/k_\perp on the left-hand side of (3.10) and substituting (3.9) into the denominator on the right-hand side of (3.10), we can solve for the isotropic driving wavenumber $k_0 \rho_i$, obtaining the results

$$k_0 \rho_i = k_{\perp 0} \rho_i \left(\frac{k_{\parallel 0}}{k_{\perp 0}} \right)^{(3+\alpha)/(1+\alpha)} \chi_0^{4/(1+\alpha)}. \quad (3.11)$$

In [figure 2\(b\)](#), the isotropic driving wavenumber $k_0 \rho_i$ (red circle) is the shown where the critical balance line (solid black and red dashed lines) intersects the isotropy line, $k_\parallel = k_\perp$ (dotted line). Note that this reduction of the three driving parameters to $k_0 \rho_i$ is valid only in the limit that the turbulent cascade becomes strong before it reaches the ion kinetic scales at $k_\perp \rho_i \sim 1$.

⁸Here we have assumed that the dynamic alignment angle θ_0 also does not evolve as a function of k_\perp in weak MHD turbulence, as there is no prediction in the literature for the scaling of dynamic alignment in weak turbulence.

The relation (3.11) provides the means to combine the three turbulence driving parameters ($k_{\perp 0} \rho_i$, $k_{\parallel 0}/k_{\perp 0}$, χ_0) into the single new effective parameter, the isotropic driving wavenumber $k_0 \rho_i$. The properties of the turbulent fluctuations at perpendicular scales smaller than the point where the turbulent cascade becomes strong, or $k_{\perp} \rho_i > k_{\perp} \rho_i|_{\chi=1}$, will be the same for the original case with driving parameterized by ($k_{\perp 0} \rho_i$, $k_{\parallel 0}/k_{\perp 0}$, χ_0) as for turbulence driven strongly and isotropically at $k_0 \rho_i$. In the development of a turbulent heating model, it is the properties of the turbulent fluctuations at the small, kinetic length scales that will determine the kinetic damping mechanism and the resulting particle energization, so reducing three turbulence driving parameters to a single parameter substantially reduces the dimensionality of the parameter space to be modelled.

It is worthwhile noting that the evolution of the dynamic alignment angle with perpendicular wavenumber $\theta(k_{\perp})$ is not well modelled by $k_0 \rho_i$. The development of current sheets at very small scales due to dynamic alignment, and the possibility for the interruption of the turbulent cascade by magnetic reconnection (Boldyrev & Loureiro 2017; Loureiro & Boldyrev 2017a, b; Mallet *et al.* 2017a, b; Walker *et al.* 2018), will depend on this scaling of $\theta(k_{\perp})$. But, from a practical point of view, this issue in modelling $\theta(k_{\perp})$ while reducing ($k_{\perp 0} \rho_i$, $k_{\parallel 0}/k_{\perp 0}$, χ_0) to $k_0 \rho_i$ is likely to be a problem only in rare cases, for the following reasons. First, the scaling of dynamic alignment angle $\theta \propto k_{\perp}^{-1/4}$ in B06 is rather weak, scaling as the $-1/4$ power, so only when the MHD inertial range spans many orders of magnitude in the perpendicular length scale will the development of current sheets likely have a significant impact on the turbulent dynamics. Second, dynamic alignment appears to arise only in strong MHD turbulence, so it seems reasonable to take $\theta_0 \sim 1$ rad (roughly equivalent to isotropy in the perpendicular plane) at the perpendicular scale $k_{\perp} \rho_i|_{\chi=1}$ where the turbulence becomes strong. One may then estimate the evolution of that dynamic alignment angle $\theta(k_{\perp})$ from that point for the cases in which it impacts the evolution. Finally, although the development of current sheets in plasma turbulence is well established (Matthaeus & Montgomery 1980; Meneguzzi *et al.* 1981; Borovsky 2008; Uritsky *et al.* 2010; Osman *et al.* 2011; Zhdankin *et al.* 2012, 2013), it is not clear that the scaling theory in B06 indeed properly describes this development; an alternative explanation for the development of current sheets arising self-consistently from Alfvén wave collisions exists (Howes 2015a, 2016; Verniero *et al.* 2018), although a specific scaling for this alternative mechanism has not yet been proposed.

3.2. Efficiently modelling the small-scale end of the turbulent inertial range

The multiscale physics of astrophysical plasma turbulence presents a particular challenge for numerical modelling that covers the entire dynamic range of the turbulent cascade while simultaneously capturing the kinetic mechanisms that govern the damping of the turbulence under weakly collisional plasma conditions, in particular since the physics of plasma turbulence is inherently three-dimensional (Howes 2015b). For the development of turbulent heating models, it is critical to investigate the physical mechanisms that remove energy from the turbulence and energize the plasma particles. Fortunately, since the inertial range of turbulence is defined as the range of scales over which the turbulent energy cascades to smaller scales but the dissipation is negligible, as depicted in figure 1(a), it is not strictly necessary to model the entire inertial range in order to capture the physics of the turbulent dissipation⁹.

⁹Exceptions to this simplification may occur when the turbulence involves compressible fluctuations that may collisionlessly damp at scales within the inertial range or when kinetic instabilities at the driving or inertial range scales lead to the non-local transfer of energy.

One less computationally costly approach to capture numerically the mechanisms of turbulent damping is to choose to model directly only the small-scale end of the inertial range, preserving as much of the resolved dynamic range of the simulation as possible to capture the dissipation mechanisms. To do so, one takes advantage of the scaling relations for turbulence in the MHD regime $k_{\perp}\rho_i \ll 1$, summarized in § 3, to ‘drive’ the turbulence at the domain scale of the simulation with turbulent fluctuations that have the properties dictated by the scaling theories.

As an example of how to set up simulations in this way, consider turbulence physically driven strongly and isotropically at an isotropic driving wavenumber of $k_0\rho_i = 10^{-4}$, as depicted in figure 3. For a hydrogenic plasma of protons and electrons with a realistic mass ratio $m_i/m_e = 1836$, the turbulent cascade extends at least down to the perpendicular scales of the electron Larmor radius $k_{\perp}\rho_e \sim 1$ (Sahraoui *et al.* 2010; Howes *et al.* 2011b; TenBarge *et al.* 2013; Kiyani, Osman & Chapman 2015). Thus, a dynamic range of $L_0/\rho_e = k_{\perp\max}/k_0 = [(k_{\perp\max}\rho_e)/(k_0\rho_i)](\rho_i/\rho_e) \propto (k_0\rho_i)^{-1}(T_i/T_e)^{1/2}(m_i/m_e)^{1/2} \sim 4.3 \times 10^5$ in each of the three spatial dimensions is necessary when $T_i/T_e \sim 1$, well beyond the capabilities of any kinetic simulation code. If the simulation code can resolve a dynamic range of 10^3 in each spatial dimension, we can choose a perpendicular domain scale in the middle of the physical inertial range at $k_{\perp D}\rho_i = 10^{-2}$ and use a reduced mass ratio $m_i/m_e = 100$ so that $k_{\perp}\rho_e = 1$ corresponds to $k_{\perp}\rho_i = 10$ for $T_i/T_e = 1$. Thus, the resolved perpendicular length scales of the simulation span $10^{-2} \leq k_{\perp}\rho_i \leq 10$, corresponding to $10^{-3} \leq k_{\perp}\rho_e \leq 1$ in terms of the electron Larmor radius ρ_e , as shown in figure 3.

To drive the turbulence at the perpendicular simulation domain scale $L_{\perp} = 2\pi/k_{\perp D}$ with $k_{\perp D}\rho_i = 10^{-2}$, corresponding to domain scale in the middle of the turbulent inertial range, we use the scaling relations (3.1)–(3.4) to determine the appropriate turbulent scale-dependent anisotropy and amplitude of the fluctuations at the numerical domain scale for a physical inertial range driven strongly ($\chi_0 = 1$) and isotropically ($k_{\perp 0} = k_{\parallel 0} = k_{i0} \equiv k_0$ and $\theta_0 = 1$ rad) at $k_0\rho_i = 10^{-4}$. For this example, we will adopt the B06 scaling, choosing $\alpha = 1$. The wavevector anisotropy and amplitude of the fluctuations at the domain scale can be expressed using scaling relations (3.1)–(3.4) to yield

$$k_{\parallel D}\rho_i = k_0\rho_i \left(\frac{k_{\perp D}\rho_i}{k_0\rho_i} \right)^{1/2} \quad (3.12)$$

$$k_{iD}\rho_i = k_0\rho_i \left(\frac{k_{\perp D}\rho_i}{k_0\rho_i} \right)^{3/4} \quad (3.13)$$

$$\theta_D = \theta_0 \left(\frac{k_{\perp D}\rho_i}{k_0\rho_i} \right)^{-1/4} \quad (3.14)$$

$$\frac{\delta B_{\perp D}}{B_0} = \left(\frac{k_{\perp D}\rho_i}{k_0\rho_i} \right)^{-1/4}. \quad (3.15)$$

The properties of the domain-scale fluctuations at $k_{\perp D}\rho_i = 10^{-2}$ determined by these scaling relations are illustrated in figure 3 for a turbulent cascade parameterized by dimensionless parameters $k_0\rho_i = 10^{-4}$ and $\theta_0 = 1$ rad. The normalized value of the energy spectrum at $k_{\perp D}\rho_i = 10^{-2}$ is $(k_0/B_0)^2 E_{B_{\perp}}(k_{\perp}) = 10^{-3}$, consistent with the solution $\delta B_{\perp D}/B_0 = 0.32$ of (3.15) at the domain scale, given by the red circle in figure 3(a). The three-dimensional anisotropy of the wavevector of the turbulent fluctuations at the perpendicular domain scale $k_{\perp D}\rho_i = 10^{-2}$ is characterized by: (i) $k_{\parallel D}\rho_i = 10^{-3}$ from (3.12), given by the blue circle in figure 3(b); and (ii) $k_{iD}\rho_i = 3.2 \times 10^{-3}$ from (3.13), given

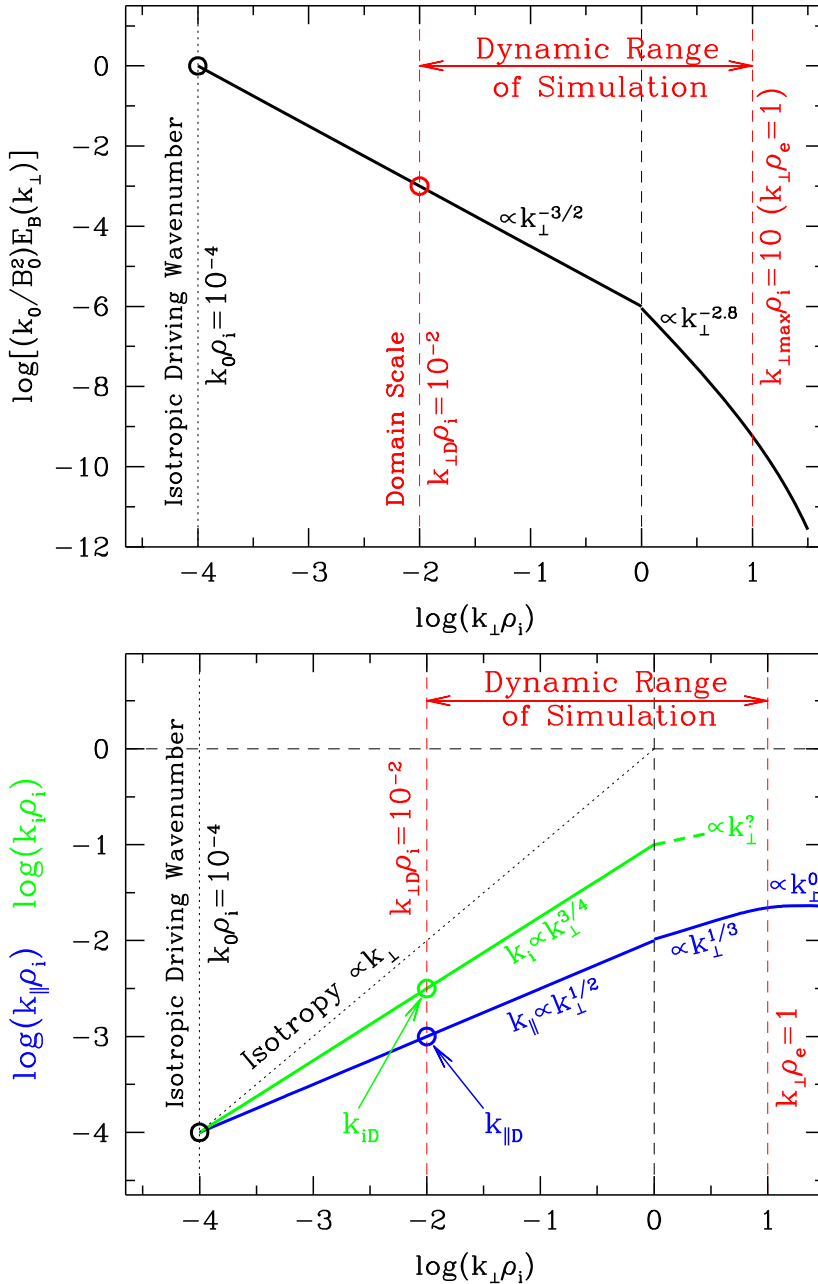


FIGURE 3. Modelling the small-scale end of the turbulent inertial range using MHD scaling relations, choosing B06 scaling with $\alpha = 1$, $m_i/m_e = 100$, $k_0 \rho_i = 10^{-4}$, $k_{\perp D} \rho_i = 10^{-2}$.

by the green circle in figure 3(b). The dynamic alignment of the velocity and magnetic field fluctuations at the domain scale is given by $\theta_D = 0.32$ rad from (3.14). Note that for these parameters, the scalings lead to a constant nonlinearity parameter as a function of perpendicular wavenumber $\chi(k_\perp) = \chi_0 = 1$ at all scales $k_\perp \rho_i < 1$, as dictated by the conjecture of critical balance in strong turbulence (Goldreich & Sridhar 1995; Mallet *et al.*

2015). These scaling calculations determine the nature of the turbulent fluctuations at the numerical domain scale, in the middle of the physical inertial range being modelled.

Since the largest perpendicular scale of the resolved dynamic range of the simulation at $k_{\perp D} \rho_i$ is constantly being fed turbulent cascade energy mediated by nonlinear interactions among turbulent fluctuations at scales slightly larger than the domain scale with $k_{\perp} < k_{\perp D}$, it is imperative that these turbulence simulations are driven, rather than simply simulating the decay of the energy turbulent fluctuations initialized at the domain scale. The nonlinear interactions among perpendicularly polarized, counterpropagating Alfvén waves drive the cascade of energy in Alfvénic plasma turbulence (Kraichnan 1965; Sridhar & Goldreich 1994; Goldreich & Sridhar 1995; Ng & Bhattacharjee 1996; Galtier *et al.* 2000; Howes *et al.* 2012b; Drake *et al.* 2013; Howes & Nielson 2013; Howes *et al.* 2013; Nielson *et al.* 2013; Howes 2016; Verniero & Howes 2018; Verniero *et al.* 2018). Exploiting this physical insight, driving counterpropagating Alfvén waves, polarized in both dimensions perpendicular to the equilibrium magnetic field, has been shown to generate successfully a steady-state plasma turbulent cascade (Howes *et al.* 2008b, 2011b; TenBarge *et al.* 2013; Told *et al.* 2015; Verniero & Howes 2018; Verniero *et al.* 2018). A finite-time correlated driving, such as an antenna driven by a Langevin equation (TenBarge *et al.* 2014), mimics the unsteady nature of the turbulent cascade from larger scales expected of turbulent driving at a chosen scale within the turbulent inertial range.

To set up the simulation to describe optimally the domain-scale fluctuations, it has become common practice to utilize a numerical domain that is elongated along the direction of the equilibrium magnetic field, consistent with the anisotropic scaling of turbulent fluctuations at small scales, $k_{\parallel}/k_{\perp} \ll 1$. For the example shown in figure 3, individual Alfvénic fluctuations are predicted to have a perpendicular plane anisotropy given by $k_{iD}/k_{\perp D} = 0.32$. But since these Alfvénic fluctuations can be polarized in either of the directions in the perpendicular plane, it is necessary for both perpendicular directions to be large enough to resolve the intermediate scale (the larger of the two perpendicular scales since $k_{iD}/k_{\perp D} < 1$). Thus, the simulation domain should be defined by $L_{\parallel} \times L_i^2$, where $L_{\parallel} = 2\pi\rho_i(k_{\parallel D}\rho_i)^{-1}$ and $L_i = 2\pi\rho_i(k_{iD}\rho_i)^{-1}$. Within this domain, counterpropagating Alfvénic fluctuations should be driven, polarized in both perpendicular directions, with wavevectors characterized by $(k_{\perp D}, k_{iD}, k_{\parallel D})$, with dynamic alignment characterized by θ_D , and with amplitudes $\delta B_{\perp D}$. Note that setting up properly dynamically aligned Alfvénic fluctuations at the domain scale is a challenging task that will depend on the particular numerical implementation of the simulation code. Nonetheless, by driving the simulation appropriately within the inertial range, this approach enables the efficient simulation of the small-scale end of the inertial range consistent with the scaling properties of MHD turbulence, enabling kinetic simulations to focus on the physical mechanisms damping the turbulent fluctuations.

3.3. A reduced parameter space for kinetic plasma turbulence

Although the physics of plasma turbulence, its dissipation, and the resulting heating of the plasma species formally depends on all ten of the general plasma and turbulence parameters $(\beta_{\parallel,i}, \tau_{\parallel}, A_i, A_e, k_{\parallel 0} \lambda_{\text{mfp},e}; k_{\perp 0} \rho_i, k_{\parallel 0}/k_{\perp 0}, \chi_0, Z_0^+/Z_0^-, E_{\text{comp}}/E_{\text{inc}})$ listed in table 3, focusing initially on the development of completely general turbulent heating models on a ten-dimensional parameter space is unlikely to be successful. Instead, first developing predictive turbulent heating models over a reduced parameter space is almost certainly a better strategy. As an initial exploration of Alfvénic turbulence and its kinetic damping mechanisms, we choose to focus on the simplified limit of isotropic temperatures, modifying our approach as needed for cases that violate these conditions.

For many of the calculations in this study, a reduced isotropic temperature case is adopted, assuming that the equilibrium velocity distribution for each species remains well described as an isotropic Maxwellian distribution. Note that kinetic temperature anisotropy instabilities generally bound the species temperature anisotropies in the vicinity of isotropy $A_s \sim 1$ (Kasper, Lazarus & Gary 2002; Hellinger *et al.* 2006; Štverák *et al.* 2008; Bale *et al.* 2009; Štverák *et al.* 2009; Verscharen *et al.* 2016), although if these instabilities are triggered, particularly at $\beta_i \gg 1$, they can impact both the linear wave physics at play in the turbulent dynamics of critically balanced turbulence (Squire, Quataert & Schekochihin 2016; Squire *et al.* 2017a; Squire, Schekochihin & Quataert 2017b) and mediate the non-local transfer of energy directly from the large driving scales to the kinetic length scales (Arzamasskiy *et al.* 2023).

To define a reduced parameter space, we first restrict the temperature anisotropies for ions and electrons to unity, $A_i = 1$ and $A_e = 1$, so that $T_{\perp,i} = T_{\parallel,i} \equiv T_i$ and $T_{\perp,e} = T_{\parallel,e} \equiv T_e$. With this idealization, the ion plasma beta and ion-to-electron temperature ratio are redefined in terms of these isotropic temperatures T_i and T_e , yielding the isotropic parameters $\beta_i = 8\pi n_i T_i / B^2$ and $\tau = T_i / T_e$. In addition, for this reduced parameter space, we will also assume that the turbulent inertial range is sufficiently large, or the driving is sufficiently strong, that the dynamics at the perpendicular ion kinetic length scales $k_{\perp} \rho_i \sim 1$ is in a state of strong plasma turbulence with a nonlinearity parameter $\chi \sim 1$. Under these conditions, we can replace the three turbulent driving parameters ($k_{\perp 0} \rho_i$, $k_{\parallel 0} / k_{\perp 0}$, χ_0) by the single isotropic driving wavenumber $k_0 \rho_i$, as detailed in § 3.1.

We will also make two other simplifying assumptions for this reduced, isotropic temperature case. We will assume that the turbulence is balanced, with approximately equal wave energy fluxes up and down the local magnetic field $Z_0^+ / Z_0^- \sim 1$, which is a necessary condition to apply the MHD turbulence scaling relations given by (3.1)–(3.4). Additionally, based on direct spacecraft measurements of turbulence in the heliosphere which find that incompressible Alfvénic fluctuations appear to dominate turbulent dynamics in space plasmas (Belcher & Davis 1971; Tu & Marsch 1995; Alexandrova *et al.* 2008; Bruno & Carbone 2013), as well as theoretical considerations that suggest that the dynamics of Alfvén waves dominates the turbulent cascade (Lithwick & Goldreich 2001; Maron & Goldreich 2001; Cho & Lazarian 2003; Schekochihin *et al.* 2009; Howes 2015a), we will also assume a negligible amount of energy in compressible turbulent fluctuations at the driving scale, $E_{\text{comp}} / E_{\text{inc}} \ll 1$.

Therefore, we propose the isotropic temperature case, a reduced parameter space for weakly collisional plasma turbulence in the limit of strong, balanced, Alfvénic turbulence, with a governing set of three dimensionless parameters, $(\beta_i, \tau; k_0 \rho_i)$, as shown in table 4. Although the isotropic temperature case eliminates a number of important physical effects such as temperature anisotropy instabilities, imbalanced turbulent wave energy fluxes and compressible fluctuations, it nonetheless represents an excellent starting point for the development of refined turbulent heating models. Such models can produce theoretical predictions that can be compared with kinetic numerical simulations and spacecraft observations of weakly collisional plasma turbulence, exemplified by the phase diagram for turbulent damping mechanisms shown in figure 12.

In terms of the fundamental parameters of the isotropic temperature case, the MHD turbulent scaling relations (3.1)–(3.4) simplify to the following easy-to-use forms:

$$k_{\parallel} \rho_i = (k_0 \rho_i)^{(1+\alpha)/(3+\alpha)} (k_{\perp} \rho_i)^{2/(3+\alpha)} \quad (3.16)$$

$$k_i \rho_i = (k_0 \rho_i)^{\alpha/(3+\alpha)} (k_{\perp} \rho_i)^{3/(3+\alpha)} \quad (3.17)$$

Plasma Parameters	
Parameter	Symbol and Definition
Ion Plasma Beta	$\beta_i = 8\pi n_i T_i / B^2$
Ion-to-Electron Temperature Ratio	$\tau = T_i / T_e$
Ion-to-Electron Mass Ratio	$\mu = m_i / m_e$
Turbulence Parameters	
Parameter	Symbol and Definition
Isotropic Driving Wavenumber	$k_0 \rho_i$

TABLE 4. Isotropic temperature case: reduced set of fundamental dimensionless parameters for isotropic Maxwellian equilibrium velocity distributions with $A_i = A_e = 1$, collisionless conditions $k_{\parallel 0} \lambda_{mfpe} \gg 1$, strong turbulence assumed at the ion kinetic scales, balanced turbulence $Z_0^+ / Z_0^- \sim 1$, and negligible energy in compressible fluctuations $E_{comp} / E_{inc} \ll 1$. This results in a reduced set of plasma and turbulence parameters ($\beta_i, \tau; k_0 \rho_i$).

$$\theta = \theta_0 \left(\frac{k_0 \rho_i}{k_{\perp} \rho_i} \right)^{\alpha / (3 + \alpha)} \tag{3.18}$$

$$\frac{\delta B_{\perp}}{B_0} = \left(\frac{k_0 \rho_i}{k_{\perp} \rho_i} \right)^{1 / (3 + \alpha)} \tag{3.19}$$

4. Review of previous turbulent heating models

Several previous studies have constructed turbulent heating models that attempt to quantify how the energy removed from the turbulent cascade is partitioned between protons and electrons and between parallel and perpendicular degrees of freedom. Here, we briefly summarize these existing turbulent heating models, including the dissipation mechanisms considered, the assumptions of how that energy is removed from the turbulence and the stated limitations of each model.

One of the earliest efforts to estimate the proton and electron energization rates by turbulence due to collisionless damping mechanisms was carried out by Quataert & Gruzinov (1999) (hereafter QG99), following earlier results by each of these authors to determine the collisionless damping rates under astrophysically relevant conditions (Gruzinov 1998; Quataert 1998). This study adopted the GS95 scaling for dominantly Alfvénic turbulence at perpendicular scales restricted to the MHD limit, $k_{\perp} \rho_i \lesssim 1$. The turbulent fluctuations upon reaching the end of the MHD limit at the perpendicular scale of the ion Larmor radius $k_{\perp} \rho_i \sim 1$ are predicted to be significantly anisotropic with $k_{\perp} \gg k_{\parallel}$; since the MHD Alfvén wave frequency $\omega = k_{\parallel} v_A$ is proportional to k_{\parallel} , this yields turbulent fluctuations at this perpendicular ion scale with low frequencies relative to the ion cyclotron frequency, $\omega \ll \Omega_i$. Thus, all collisionless damping is provided by the $n = 0$ Landau resonance, specifically Landau damping and transit-time damping. In addition, this model assumed that all turbulent energy at a given perpendicular wavenumber $k_{\perp} \rho_i$ was concentrated at the parallel wavenumber given by the conjecture of critical balance (Goldreich & Sridhar 1995; Quataert & Gruzinov 1999). They constructed a simple cascade model that balanced the collisionless damping by ions and electrons given by the Vlasov–Maxwell linear dispersion relation (Stix 1992) over the MHD range of scales, $k_{\perp} \rho_i \lesssim 1$. Beyond these scales at $k_{\perp} \rho_i \gtrsim 1$ in the kinetic regime, uncertainty about the nature of the turbulence at these sub-ion length scales led them to assume simply that

any energy reaching $k_{\perp}\rho_i \gtrsim 1$ ultimately heated the electrons. They calculated the fraction of the turbulent energy that heats the electrons, Q_e/Q , as function of total plasma beta $\beta = \beta_i + \beta_e = \beta_i(1 + T_i/T_e)$, yielding a numerical result for $Q_e/Q(\beta)$. Their resulting energy partition depended strongly on a constant assumed in the model that characterized the balance of the nonlinear turbulent cascade rate to the linear collisionless damping rate; uncertainty in the value of this constant (by a factor from 1/4 to 4) led the resulting prediction of $Q_e/Q(\beta)$ to vary by more than one order of magnitude over the range of $3 \lesssim \beta \lesssim 100$.

The Howes 2010 (hereafter H10) turbulent heating model (Howes 2010) was based on a turbulent cascade model (Howes *et al.* 2008a) that extended the GS95 turbulence scaling from MHD scales at $k_{\perp}\rho_i \lesssim 1$ into the kinetic regime at $k_{\perp}\rho_i \gtrsim 1$, generalizing the conjecture of critical balance to account for the dispersive nature of kinetic Alfvén waves at these sub-ion length scales (Biskamp *et al.* 1999; Cho & Lazarian 2004; Krishan & Mahajan 2004; Shaikh & Zank 2005; Schekochihin *et al.* 2009). The H10 model was based on three primary assumptions: (i) the Kolmogorov hypothesis that the energy cascade is determined by local interactions (Kolmogorov 1941); (ii) the conjecture that turbulence maintains a state of critical balance at all scales (Goldreich & Sridhar 1995); and (iii) the speculation that linear collisionless damping rates are applicable even in the presence of the strong nonlinear interactions that mediate the turbulent cascade to small scales. The cascade model used by H10 balanced at each perpendicular wavenumber $k_{\perp}\rho_i$ the nonlinear energy cascade rate given by the extended turbulent scaling theories with the linear collisionless damping rates at that value of $k_{\perp}\rho_i$ (as illustrated in figure 4). Similar to QG99, it assumed all turbulent energy at a given value of $k_{\perp}\rho_i$ resided at the parallel wavenumber governed by the extended critical balance. The H10 model assumed turbulence under non-relativistic conditions $v_{te}/c \ll 1$ with isotropic ion and electron temperatures, strictly Alfvénic turbulence with $E_{\text{comp}}/E_{\text{inc}} = 0$, balanced turbulence with $Z_0^+/Z_0^- = 1$, and strongly and isotropically driven turbulence with $\chi_0 = 1$ and $k_{\parallel 0}/k_{\perp 0} = 1$ (the driving was therefore characterized by the isotropic driving wavenumber, $k_0\rho_i$). Furthermore, adopting the same argument as the QG99 model, the model assumed that the inertial range of the turbulence is sufficiently large that the anisotropic fluctuations predicted by the turbulent scaling relations remain at a low enough frequency relative to the ion cyclotron frequency, $\omega \ll \Omega_i$, that the cyclotron resonance plays a negligible role; the H10 model calculated an estimate of the maximum value of $k_0\rho_i$ as a function of $(\beta_i, T_i/T_e)$ for this assumption to be satisfied. Thus, the H10 turbulent heating model predicted the damping of the turbulent cascade due to Landau damping and transit-time damping over the full range of the turbulent cascade, including MHD scales at $k_{\perp}\rho_i \lesssim 1$ and kinetic scales at $k_{\perp}\rho_i \gtrsim 1$. The H10 model predicted the partitioning of energy between ions and electrons as a function of the ion plasma beta β_i and the ion-to-electron temperature ratio T_i/T_e , providing a simple analytical fit to the numerically calculated predictions, $Q_i/Q_e(\beta_i, T_i/T_e)$. In short, the model found that Q_i/Q_e is a monotonically increasing function of β_i with weak dependence on T_i/T_e , where the transition from $Q_i/Q_e < 1$ to $Q_i/Q_e > 1$ happens at approximately $\beta_i \sim 1$.

The Chandran *et al.* (2011) (hereafter C11) turbulent heating model (Chandran *et al.* 2011) looked to incorporate the recently quantified damping rate due to nonlinear ion stochastic heating (Chandran 2010; Chandran *et al.* 2010) into a model that also accounted for ion and electron Landau damping and transit-time damping. Similar to QG99 and H10, it assumed a sufficiently large inertial range that no significant cyclotron damping would occur since the anisotropic cascade would lead to turbulent fluctuations with low frequencies, $\omega \ll \Omega_i$. Focusing also on Alfvénic turbulence that transitions from an MHD Alfvén wave cascade at $k_{\perp}\rho_i \lesssim 1$ and to a KAW cascade at $k_{\perp}\rho_i \gtrsim 1$, the C11 model

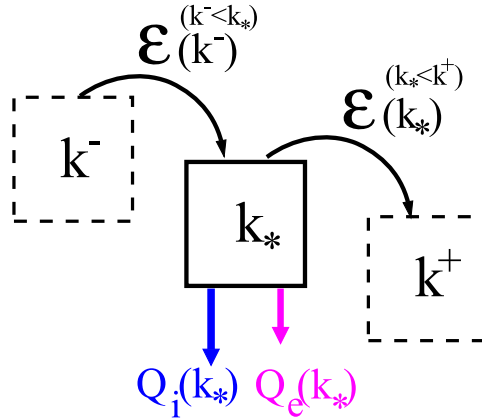


FIGURE 4. Diagram of the balance of the energy transfer rates in a steady-state turbulent cascade at a local wavenumber k_* , where the combination of three terms must balance to zero: (i) the turbulent nonlinear energy transfer rate from lower wavenumbers $\mathcal{E}(k^-)^{(k^- < k_*)}$; (ii) the turbulent nonlinear energy transfer rate to higher wavenumbers $\mathcal{E}(k_*)^{(k_* < k^+)}$; and (iii) the local (in scale) kinetic damping rates of the turbulent energy, due to the sum of ion energization rate $Q_i(k_*)$ (blue) and electron energization rate $Q_e(k_*)$ (magenta).

assumed that dissipation occurred dominantly in two distinct wavenumber ranges: (i) at $k_\perp \rho_i \sim 1$, where collisionless damping via the Landau ($n = 0$) resonance can lead to parallel energization of the ions and electrons and also where nonlinear stochastic heating can lead to perpendicular energization of the ions; and (ii) at $k_\perp \rho_i \gg 1$, where all remaining energy in the turbulent cascade is ultimately deposited with the electrons. The model used fitting forms for the Landau-resonant collisionless damping rates for the ions and electrons at $k_\perp \rho_i = 1$ over $10^{-3} < \beta_i < 10$ and $1 < T_i/T_e < 5$. It also included an empirically derived formula for the ion stochastic heating rate at $k_\perp \rho_i = 1$ (Chandran *et al.* 2010). This empirical prescription for the ion stochastic heating depended on two dimensionless constants: one governed the scaling of the stochastic heating rate relative to the turbulent frequencies; and the other, which appeared as a factor in the argument of the exponential function, effectively established a threshold amplitude below which ion stochastic heating was negligible. Thus, the C11 model calculated how the turbulent cascade rate at $k_\perp \rho_i = 1$ is partitioned among ion Landau and transit-time damping, electron Landau and transit-time damping, ion stochastic heating and nonlinear transfer to smaller scales with $k_\perp \rho_i > 1$. The model provided a partitioning of the total turbulent heating rate into parallel ion heating by ion Landau and transit-time damping $Q_{\parallel,i}/Q$, perpendicular ion stochastic heating $Q_{\perp,i}/Q$, and electron heating Q_e/Q , each as a function of ion plasma beta β_i , the ion-to-electron temperature ratio T_i/T_e , and the amplitude of the turbulent fluctuations at the ion Larmor-radius scale determined using the B06 scaling for the amplitude in terms of the driving scale, as given here by (3.19), indicating that the amplitude dependence can be characterized by $k_0 \rho_i$.

Motivated by the desire to understand the partitioning of dissipated turbulent energy between ions and electrons in hot collisionless accretion flows, the Rowan 2017 (hereafter R17) heating model (Rowan *et al.* 2017) took a fundamentally different approach from that adopted in the QG99, H10 and C11 turbulent heating models by focusing instead on the heating arising from transrelativistic magnetic reconnection. In this case, the protons are nonrelativistic, but the electrons can be ultrarelativistic. Utilizing a large suite of

two-dimensional particle-in-cell simulations of anti-parallel reconnection, the R17 model studied the irreversible particle energization over a range of ion plasma beta $10^{-4} \lesssim \beta_i \leq 2$ and magnetization $0.1 \leq \sigma_w \leq 10$, where σ_w is defined as the ratio of the magnetic-energy density to the enthalpy density. Starting with a Harris current sheet (Harris 1962) of the antiparallel magnetic field (given by a tanh profile) with width $a \sim 40d_e$, they carefully separated the irreversible heating associated with an increase in the entropy from the reversible heating associated with adiabatic compression. From their synthesis of the results of a large suite of simulations varying different parameters, they fit a formula to their numerical results that provided to electron-to-total heating ratio Q_e/Q as a function of the ion plasma beta β_i and magnetization σ_w .

The numerical study by Kawazura *et al.* (2019) (hereafter K19) used a large suite of hybrid gyrokinetic simulations to determine directly the ion-to-electron heating ratio Q_i/Q_e over a broad range of ion plasma beta $0.1 \leq \beta_i \leq 100$ and ion-to-electron temperature ratio $0.05 \leq T_i/T_e \leq 100$. Using a hybrid code (Kawazura & Barnes 2018) that evolves the ions gyrokinetically and the electrons as an isothermal fluid, this study adopted many of the same assumptions as the H10 model: (i) the anisotropic ($k_\perp \gg k_\parallel$) Alfvénic turbulence was driven in a statistically balanced manner with $Z_0^+/Z_0^- = 1$; (ii) the equilibrium ion and electron temperatures were assumed to be isotropic; (iii) the gyrokinetic approximation eliminated the physics of the ion cyclotron resonances, leaving the Landau resonances and collisionless magnetic reconnection in the large-guide-field limit as potential damping mechanisms; and (iv) the strategy explained in § 3.2 was exploited to model numerically only the small-scale end of the inertial range, where the isotropic driving wavenumber $k_0\rho_i$, characterizing the physical driving scale, was assumed to be sufficiently small that the amplitudes of the turbulent fluctuations at $k_\perp\rho_i \sim 1$ were small enough that ion stochastic heating was inhibited (Chandran *et al.* 2010, 2011). The K19 model provides a numerically validated prescription for Q_i/Q_e as a function of β_i and T_i/T_e , presenting a simple analytical formula that fit the numerical results well. The numerical results largely validated the qualitative predictions of the H10 turbulent heating model that Q_i/Q_e is a monotonic function of β_i with little dependence on T_i/T_e , with a couple of minor quantitative differences: the K19 model found a ceiling of $Q_i/Q_e \simeq 30$ at $\beta_i \gg 1$, cutting off at lower values than the H10 model; and the numerical results did not find the drop in the heating rate $Q_i/Q_e \ll 0.1$ predicted by the H10 model at $\beta_i \ll 1$.

The first of the two disagreements above between the H10 model and the K19 model – where the numerical simulations found an effective ceiling at $Q_i/Q_e \simeq 30$ at $\beta_i \gg 1$ – was recently addressed by Gorman & Klein (2024). They examined in detail the small range of perpendicular wavenumber scales around $k_\perp\rho_i \sim 1$ where the linear dispersion relation predicts that the Alfvén wave solution becomes non-propagating at $\beta_i \gg 1$. For turbulent cascade models assuming critical balance and strictly local (in scale space) interactions mediating the turbulent cascade, this gap in the Alfvén wave propagation leads to the turbulent cascade being terminated at the onset of the gap with the bulk of the turbulent energy transferred to the ions, leading to the potential overestimation of Q_i/Q_e in the $\beta_i \gg 1$ limit. Gorman & Klein (2024) (hereafter GK24) tested the local cascade model underlying the H10 model against a more refined cascade model, the weakened cascade model (Howes *et al.* 2011a). The weakened cascade model is a non-local cascade model that accounts both for the weakening of the local nonlinear interactions as damping taps the turbulent energy and for nonlocal interactions by large-scale shearing and small-scale diffusion. It was found that the inclusion of non-local interactions to the nonlinear energy transfer prevents the termination of the cascade at the ion scales, leading to predictions for Q_i/Q_e at $\beta_i \gg 1$ (Gorman & Klein 2024) that agree much more closely

with the results of the suite of simulations by Kawazura *et al.* (2019): the resulting GK24 model produced by this study includes updated coefficients for the H10 formula for $Q_i/Q_e(\beta_i, T_i/T_e)$.

Relaxing the limitation of their simulations to driving by strictly Alfvénic turbulent fluctuations, Kawazura *et al.* (2020) used the same hybrid gyrokinetic code (Kawazura & Barnes 2018) to explore the effect of compressible driving $E_{\text{comp}}/E_{\text{inc}} > 0$ on the ion-to-electron heating ratio Q_i/Q_e (hereafter K20). The turbulence was driven at MHD scales $k_{\perp}\rho_i \ll 1$ with an adjustable mixture of incompressible Alfvénic fluctuations and compressible slow magnetosonic fluctuations (fast magnetosonic wave modes are ordered out of gyrokinetic simulations by the perpendicular pressure balance that is maintained under the gyrokinetic approximation, as explained in Howes *et al.* 2006). At $\beta_i \ll 1$, they found that $Q_i/Q_e = E_{\text{comp}}/E_{\text{inc}}$, confirming a previous theoretical prediction that compressive energy strictly heats ions at low ion plasma beta $\beta_i \ll 1$ (Schekochihin, Kawazura & Barnes 2019). Surprisingly, the K20 model also found that $Q_i/Q_e = E_{\text{comp}}/E_{\text{inc}}$ when the compressible driving dominates, $E_{\text{comp}}/E_{\text{inc}} \gg 1$. A simple fitting formula was constructed that simply added the term $E_{\text{comp}}/E_{\text{inc}}$ to the previous prescription for Q_i/Q_e due to Alfvénic turbulence in the K19 model. Thus, the K20 model provided a simple analytical formula for $Q_i/Q_e(\beta_i, T_i/T_e, E_{\text{comp}}/E_{\text{inc}})$.

The application of the K20 model to understand the ion-to-electron heating ratio in accretion disks where the magnetorotational instability (MRI) (Balbus & Hawley 1991; Hawley & Balbus 1991; Balbus & Hawley 1998) drives the turbulence requires a determination of the ratio of the compressible-to-incompressible driving $E_{\text{comp}}/E_{\text{inc}}$. The application of a rotating reduced MHD model to simulate the collisional MRI turbulence threaded by a nearly azimuthal magnetic field in a three-dimensional pseudo-spectral, shearing reduced MHD code (Kawazura 2022) found a ratio of compressible-to-incompressible turbulent energy of $2 \lesssim E_{\text{comp}}/E_{\text{inc}} \lesssim 2.5$ (Kawazura *et al.* 2022), providing a solid foundation for the application of the K20 model to astrophysical accretion disks.

5. Dependence of dissipation mechanisms on fundamental parameters

The development of turbulent heating models for weakly collisional space and astrophysical plasmas requires two fundamental steps: (i) identifying the mechanisms that play a role in the damping of the turbulence; and (ii) determining upon which of the fundamental dimensionless parameters of turbulence each mechanism depends and approximating a functional form for those dependencies.

It is worthwhile first noting an important subtlety regarding irreversible plasma heating in the thermodynamic picture of turbulent dissipation in weakly collisional plasmas (Howes 2017). In the strongly collisional limit of fluid plasma turbulence, the dissipation of turbulence is fundamentally collisional on a microscopic level. For example, in an MHD plasma, the physical mechanisms of viscosity and resistivity arise in the limit of a non-negligible collisional mean free path of the plasma particles. These two dissipative mechanisms may be derived rigorously beginning with kinetic theory through a hierarchy of moment equations derived in the limit of small mean free path by the Chapman–Enskog procedure (Chapman & Cowling 1970) for neutral gases, or an analogous procedure for plasma systems (Spitzer 1962; Grad 1963; Braginskii 1965). Because viscosity and resistivity are ultimately collisional in nature, the resulting energy transfer from the turbulent fluctuations to the particles is irreversible, leading to an increase in the entropy of the system.

Under the weakly collisional conditions typical of many space and astrophysical plasmas, the collisionless removal of energy from the turbulent fluctuations and the

ultimate conversion of that removed energy into plasma heat is a two-step process (Howes *et al.* 2006; Howes 2008; Schekochihin *et al.* 2009; Navarro *et al.* 2016; Howes 2017; Howes, McCubbin & Klein 2018). First, collisionless damping mechanisms remove energy from the turbulent fluctuations, transferring that energy into non-thermal internal energy contained in non-Maxwellian fluctuations of the particle velocity distributions, an energy transfer that is reversible in principle. That free energy in the fluctuations of the velocity distribution about the equilibrium may be transferred to smaller scales in velocity space – e.g. via linear phase mixing by the ballistic term of the Boltzmann equation (Landau 1946; Hammett, Dorland & Perkins 1992; Snyder, Hammett & Dorland 1997; Schekochihin *et al.* 2009) or via nonlinear phase mixing, a process often denoted the entropy cascade (Dorland & Hammett 1993; Schekochihin *et al.* 2009; Tatsuno *et al.* 2009; Plunk *et al.* 2010; Plunk & Tatsuno 2011; Kawamori 2013) – until it reaches sufficiently small velocity-space scales that an arbitrarily weak collisionality is sufficient to smooth out those fluctuations, providing an irreversible conversion of that energy to plasma heat and thereby increasing the entropy of the system (Howes *et al.* 2006; Howes 2008; Schekochihin *et al.* 2009).

The subtleties of energy conversion and plasma heating in weakly collisional plasmas that are not in a state of local thermodynamic equilibrium remains a topic of vigorous investigation, with many recent developments that will not be reviewed in detail here (Parker *et al.* 2016; Schekochihin *et al.* 2016; Yang *et al.* 2016, 2017*a, b*; Howes *et al.* 2018; Kawazura *et al.* 2019; Meyrand *et al.* 2019, 2021; Barbhuiya & Cassak 2022; Cassak & Barbhuiya 2022; Cassak, Barbhuiya & Weldon 2022; Squire *et al.* 2022; Cassak *et al.* 2023). In this paper, we use the term turbulent dissipation to mean the entire process of removing energy from the turbulent fluctuations and subsequently thermalizing that energy via collisions to realize irreversible heating of the plasma and an increase in the entropy of the system. When we refer to only the first step of the process, the collisionless removal of energy from the turbulent fluctuations, we denote those specific processes as turbulent damping mechanisms.

A primary aim of this study is to provide a unified framework for characterizing the dependence of the turbulence and its dissipation on a common set of dimensionless parameters. The first step pursued here is to identify the fundamental dimensionless parameters upon which each proposed turbulent damping mechanism primarily depends, where the set of dimensionless parameters for the general case is presented in [table 3](#) and for the isotropic temperature case in [table 4](#). The key parameter dependencies for each proposed damping mechanism found here are summarized in [table 5](#). Although, for any single particular mechanism, different choices of dimensionless parameters may be more natural (e.g. taking β_e instead of β_i/τ in the case of magnetic reconnection), the particular sets of dimensionless parameters in [tables 3](#) and [4](#) are proposed here as a useful framework for describing all of the proposed turbulent damping mechanisms, thereby simplifying the task of determining how different mechanisms compete with each other throughout the full parameter space.

5.1. Proposed damping mechanisms for kinetic turbulence

In weakly collisional space and astrophysical plasmas, the proposed kinetic damping mechanisms that remove energy from the turbulent fluctuations and transfer it to the particle species fall into three broad categories: (i) resonant wave-particle interactions, (ii) non-resonant wave-particle interactions and (iii) damping occurring in coherent structures.

Resonant mechanisms for the damping of the turbulent fluctuations in a magnetized plasma transfer energy to particles in regions of the velocity distribution that satisfy the

Category	Abbrev	Mechanism	Key Parameters
Resonant	iLD	Ion Landau Damping	β_i
	eLD	Electron Landau Damping	$\beta_i, T_i/T_e, (\mu)$
	iTTD	Ion Transit-Time Damping	β_i
	eTTD	Electron Transit-Time Damping	$\beta_i, T_i/T_e, (\mu)$
	iCD	Ion Cyclotron Damping	$k_0 \rho_i, \beta_i$
Non-Resonant	iSH	Ion Stochastic Heating	$k_0 \rho_i, \beta_i$
	iMP	Ion Magnetic Pumping	$E_{\text{comp}}/E_{\text{inc}}, \beta_i, T_i/T_e, k_{\parallel 0} \lambda_{\text{mf},e}, k_{\parallel 0}/k_{\perp 0}, \chi_0$
	eMP	Electron Magnetic Pumping	$\beta_i, T_i/T_e, k_{\parallel 0} \lambda_{\text{mf},e}, k_{\parallel 0}/k_{\perp 0}, \chi_0, E_{\text{comp}}/E_{\text{inc}}, (\mu)$
	iVH	Ion Kinetic Viscous Heating	$\beta_i, k_{\perp 0}/k_{\parallel 0}, \chi_0$
Coherent	iRXN	Ion Magnetic Reconnection	$k_0 \rho_i, \beta_i, T_i/T_e, (\mu)$
Structures	eRXN	Electron Magnetic Reconnection	$k_0 \rho_i, \beta_i, T_i/T_e, (\mu)$

TABLE 5. Proposed turbulent damping mechanisms and their key dimensionless parameter dependencies for the case of a fully ionized hydrogenic plasma. The ion-to-electron mass ratio μ is listed in parentheses since it is not a physically variable parameter, but it is often adjusted in numerical studies for computational efficiency.

resonance condition

$$\omega - k_{\parallel} v_{\parallel} - n\Omega_s = 0, \tag{5.1}$$

where Ω_s is the cyclotron frequency for species s and $|n| > 1$ indicates the harmonics of the cyclotron frequency. The $n = 0$ resonance is often denoted the Landau resonance and includes two damping mechanisms: (i) Landau damping is mediated by the parallel component of the electric field E_{\parallel} doing work on the charged particles (Landau 1946; Leamon *et al.* 1998*a, b*; Quataert 1998; Leamon *et al.* 1999; Quataert & Gruzinov 1999; Leamon *et al.* 2000; Howes *et al.* 2008*a*; Schekochihin *et al.* 2009; TenBarge & Howes 2013; Howes 2015*a*; Li *et al.* 2016; Chen, Klein & Howes 2019; Afshari *et al.* 2021; Zhou, Liu & Loureiro 2023); and (ii) transit-time damping, also known as Barnes damping, is mediated by the magnetic mirror force associated with magnetic field magnitude fluctuations doing work on the magnetic moment of the charged particle gyromotion (Barnes 1966; Quataert 1998; Quataert & Gruzinov 1999; Howes *et al.* 2008*a*; Howes, Huang & Felix 2024). Both of these Landau-resonant collisionless damping mechanisms energize particles in the degree of freedom parallel to the local magnetic field. The $n \neq 0$ resonances yield cyclotron damping of the turbulent fluctuations by E_{\perp} , generally energizing particles in the two perpendicular degrees of freedom (Coleman 1968; Denskat, Beinroth & Neubauer 1983; Isenberg & Hollweg 1983; Goldstein, Roberts & Fitch 1994; Leamon *et al.* 1998*a*; Gary 1999; Isenberg, Lee & Hollweg 2001; Hollweg & Isenberg 2002; Isenberg & Vasquez 2019; Afshari *et al.* 2024).

Non-resonant damping mechanisms can remove energy from turbulent fluctuations through wave-particle interactions that do not require satisfying a particular resonance condition. Stochastic heating can arise when sufficiently large-amplitude turbulent electromagnetic fluctuations can effectively scatter the otherwise organized gyromotion of particles, leading to a heating of the particles in the perpendicular degrees of freedom (McChesney, Stern & Bellan 1987; Chen, Lin & White 2001; Johnson & Cheng 2001;

White, Chen & Lin 2002; Voitenko & Goossens 2004; Bourouaine, Marsch & Vocks 2008; Chandran 2010; Chandran *et al.* 2010, 2011; Bourouaine & Chandran 2013; Chandran *et al.* 2013; Klein & Chandran 2016; Arzamasskiy *et al.* 2019; Martinović *et al.* 2020; Cerri, Arzamasskiy & Kunz 2021). Magnetic pumping energizes particles through a combination of two effects: (i) particles undergo the reversible, double-adiabatic evolution of their perpendicular and parallel velocities in a magnetic field with a time varying magnitude; and (ii) those particles are scattered by collisions during this evolution, introducing irreversibility and leading to a small net transfer of energy to the particles over a full oscillation cycle (Spitzer & Witten 1953; Berger *et al.* 1958; Lichko *et al.* 2017; Lichko & Egedal 2020; Montag & Howes 2022). One final proposed non-resonant damping mechanism is the recently identified kinetic ‘viscous’ heating mediated by the effective collisionality associated with temperature anisotropy instabilities driven by large-scale fluctuations of the magnetic field magnitude in high beta plasmas (Arzamasskiy *et al.* 2023).

The final category involves the removal of turbulent fluctuation energy in coherent structures, such as particle energization arising from collisionless magnetic reconnection in current sheets that are found to arise naturally in plasma turbulence (Ambrosiano *et al.* 1988; Dmitruk, Matthaeus & Seenu 2004; Markovskii & Vasquez 2011; Matthaeus & Velli 2011; Osman *et al.* 2011; Servidio *et al.* 2011; Osman *et al.* 2012a, b; Wan *et al.* 2012; Karimabadi *et al.* 2013; Zhdankin *et al.* 2013; Dalena *et al.* 2014; Osman *et al.* 2014a, b; Zhdankin, Uzdensky & Boldyrev 2015a, b; Loureiro & Boldyrev 2017b; Mallet *et al.* 2017a, b). It has also been argued that stochastic heating can also play a role in energizing particles in intermittent turbulence at the location of coherent structures where the fluctuation amplitudes are unusually large (Chandran *et al.* 2010; Xia *et al.* 2013; Mallet *et al.* 2019).

Each of the kinetic damping mechanisms in these three categories (with helpful abbreviations) are summarized in table 5. Also included in table 5 are the primary dimensionless parameters upon which each damping mechanism depends, as explored in more detail in the following subsections.

5.2. A competition between turbulent cascade rates and damping rates

One of the most challenging aspects of modelling the damping of plasma turbulence is that the net energy transfer to each species arises from the competition between the turbulent cascade rate and the kinetic damping rates as a function of scale, as depicted by the arrows in figure 1(a). Nonlinear interactions among turbulent fluctuations – denoted Alfvén wave collisions (Howes & Nielson 2013) in the case of Alfvénic turbulence – mediate the transfer of energy from large to small scales that is dominantly local in scale space (Howes *et al.* 2011a; Told *et al.* 2015), where energy is transferred locally from a wavenumber k to a wavenumber $2k$, then on to $4k$ and so on. This is indicated by the black curved arrows in the figure. Because the physics of the cascade is dominantly local in nature (Howes *et al.* 2011a; Told *et al.* 2015), scaling theory implies that the energy transfer rate at a given wavenumber k is determined solely by the conditions at that scale. Note that, when analysed in Fourier space, the energy transfer to small scales in the turbulent cascade is the sum of the nonlinear interactions among many triads of plane-wave modes, with a wide spread of energy transfer rates about zero; the net energy transfer given by this sum at a given scale is much smaller in amplitude than the spread of all of the individual three-wave interaction rates, and the sum typically indicates a forward cascade of energy to small scales for turbulence in three spatial dimensions (Coburn *et al.* 2014, 2015). The turbulent cascade rate ε used here specifically refers to this net energy

transfer rate obtained by integrating over all contributing nonlinear interactions involving that scale¹⁰.

Competing with the turbulent cascade rate at each scale is the damping rate due to collisionless interactions between the electromagnetic fields and the plasma particles, as shown by the blue arrows for the transfer of energy to ions and the magenta arrows for the transfer of energy to electrons in [figure 1\(a\)](#). The net damping rate of the entire turbulent cascade, resulting from the sum of the energization rates for each particle species s , can be computed by integration over all scales of the turbulent cascade. In a steady state, at each wavenumber k_* , the combination of three terms representing energy transfer into and out of wavenumber k_* must balance to zero, as illustrated in [figure 4](#): (i) the energy transfer from lower wavenumbers $k^- < k_*$ (larger scales), denoted by $\varepsilon(k^-)^{(k^- < k_*)}$; (ii) the energy transfer to higher wavenumbers $k^+ > k_*$ (smaller scales), denoted by $\varepsilon(k_*)^{(k_* < k^+)}$; and (iii) the kinetic damping of the fluctuations at wavenumber k_* , given by $Q(k_*)$, which is the sum of the local (in scale) ion energization rate $Q_i(k_*)$ (blue) and electron energization rate $Q_e(k_*)$ (magenta). Complicating the determination of the partitioning of damped turbulent energy between ions and electrons Q_i/Q_e is the fact that the kinetic damping rates due to ions and electrons may overlap as a function of scale (Howes *et al.* 2011b, a; Told *et al.* 2015).

Determining this balance of cascade and damping rates as a function of scale, and ultimately using the terms in that balance to determine the partitioning of turbulent energy among species and degrees of freedom – parameterized by Q_i/Q_e , $Q_{\perp,i}/Q_i$ and $Q_{\perp,e}/Q_e$ – has been attempted in empirical turbulent cascade models (Pao 1965; Howes *et al.* 2008a; Podesta, Borovsky & Gary 2010; Howes *et al.* 2011a; Zhao, Wu & Lu 2013; Schreiner & Saur 2017). An example of the modelling of the turbulent energy cascade and its kinetic dissipation is presented in [figure 5](#) from the results of the weakened cascade model by Howes *et al.* (2011a). In addition to balancing the physics of the local cascade rate $\varepsilon(k_{\perp})$ with the kinetic damping rates due to ions $Q_i(k_{\perp})$ and electrons $Q_e(k_{\perp})$ via the Landau resonance, this cascade model also includes the contributions to the local cascade rate from non-local interactions by large-scale shearing and small-scale diffusion. The model results shown here in [figure 5](#) are from the same calculation as presented in [figure 8](#) of Howes *et al.* (2011a), where we reproduce (a) the one-dimensional perpendicular magnetic-energy spectrum $E_{B_{\perp}}(k_{\perp})$ and (b) the anisotropic cascade through wavevector space characterized by the characteristic parallel wavenumber as a function of the perpendicular wavenumber, $k_{\parallel}(k_{\perp})$. This model for a plasma with $\beta_i = 1$ and isotropic equilibrium Maxwellian velocity distributions with $T_i/T_e = 9$ is driven weakly with $\chi(k_{\perp 0}) = 0.1$ at $k_{\perp 0}\rho_i = k_{\parallel}\rho_i = 10^{-5}$, taking the model Kolmogorov constants to be $C_1 = 1.4$ and $C_2 = 1.0$. Note that an important avenue of research is to use kinetic numerical simulations or spacecraft observations to constrain the values of these Kolmogorov constants, as recently done by Shankarappa, Klein & Martinović (2023) using observations in the inner heliosphere by the Parker Solar Probe (Fox *et al.* 2016).

In [figure 5\(c\)](#) is plotted the rate of energy density transfer to the ions $Q_i(k_{\perp})$ (blue) and to the electrons $Q_e(k_{\perp})$ (magenta) as a function of $k_{\perp}\rho_i$, both normalized by the turbulent energy cascade rate at the driving scale ε_0 . This shows that the ion kinetic damping occurs at the ion kinetic scales $k_{\perp}\rho_i \sim 1$, whereas the electron damping rises monotonically from the ion scales, peaking around $k_{\perp}\rho_i \sim 30$ for this case. To obtain the net partitioning of energy between ions and electrons Q_i/Q_e , it is necessary to integrate these energy damping

¹⁰Because the net energy transfer rate at a given scale fundamentally involves the integration over all possible nonlinear triads, it can in principle include a non-negligible contribution from non-local interactions, such as those incorporated in the weakened cascade model of the turbulent cascade (Howes *et al.* 2011a).

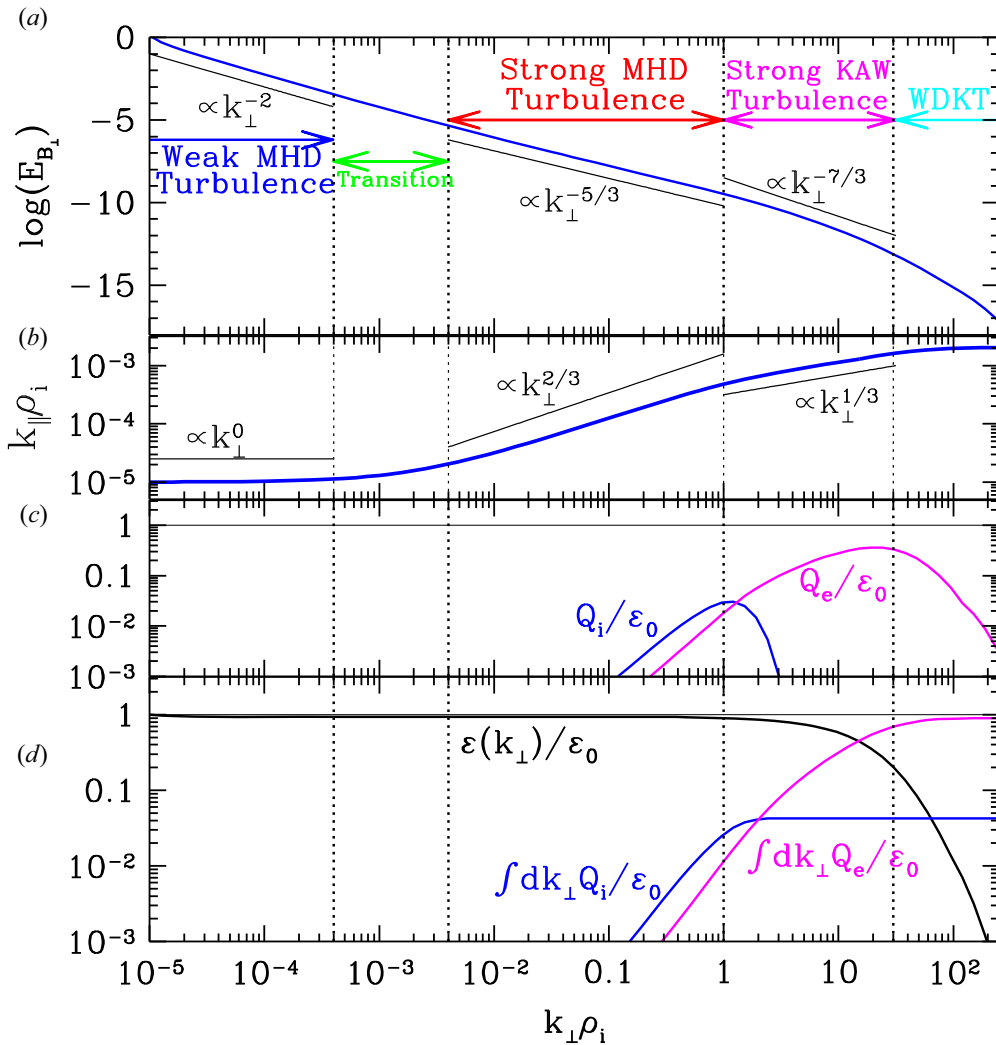


FIGURE 5. Weakened cascade model results for a turbulent cascade driven weakly at $k_{\perp 0}\rho_i = k_{\parallel 0}\rho_i = 10^{-5}$ with nonlinearity parameter $\chi(k_{\perp 0}) = 0.1$ in a plasma with isotropic equilibrium Maxwellian velocity distributions with $T_i/T_e = 9$ and $\beta_i = 1$. (a) One-dimensional perpendicular magnetic-energy spectrum $E_{B_{\perp}}(k_{\perp})$, (b) anisotropic cascade through wavevector space given by $k_{\parallel}(k_{\perp})$, (c) energy transfer rates to the ions $Q_i(k_{\perp})$ (blue) and electrons $Q_e(k_{\perp})$ (magenta) and (d) integrated energy damping rates by ions $\int_0^{k_{\perp}} dk'_{\perp} Q_i(k'_{\perp})$ (blue) and by electrons $\int_0^{k_{\perp}} dk'_{\perp} Q_e(k'_{\perp})$ (magenta), all plotted as a function of the perpendicular wavenumber $k_{\perp}\rho_i$. The ranges of $k_{\perp}\rho_i$ of the full turbulent cascade include weak MHD turbulence (blue), the transition from weak to strong MHD turbulence (green), strong MHD turbulence (red), strong KAW turbulence (magenta) and WDKT (cyan) (Howes *et al.* 2011a).

rates over the entire cascade, as shown in figure 5(d): the turbulent energy cascade rate $\epsilon(k_{\perp})$ (black) is ultimately terminated at $k_{\perp}\rho_i \gg 1$ by the integrated energy damping rates by ions $\int_0^{k_{\perp}} dk'_{\perp} Q_i(k'_{\perp})$ (blue) and by electrons $\int_0^{k_{\perp}} dk'_{\perp} Q_e(k'_{\perp})$ (magenta).

The energy density transfer rates $Q_i(k_{\perp})$ and $Q_e(k_{\perp})$ that remove energy from the turbulent fluctuations and transfer it to the plasma particles in turbulent cascade models

require as input the kinetic damping rates due to ions $\gamma_i(k_\perp)$ and electrons $\gamma_e(k_\perp)$. In the case of the weakened cascade model shown in figure 5 (Howes *et al.* 2011a), the damping rates used are collisionless damping rates via the Landau ($n = 0$) resonance for the Alfvén wave mode (and its extension as a KAW at scales $k_\perp \rho_i \gtrsim 1$) from the Vlasov–Maxwell linear dispersion relation (Stix 1992). Previous studies have called into question whether resonant collisionless wave–particle interactions, such as Landau damping, can effectively damp turbulent fluctuations in the presence of the strong nonlinear interactions that mediate the turbulent cascade (Plunk 2013; Schekochihin *et al.* 2016). Using the field–particle correlation technique (Klein & Howes 2016; Howes, Klein & Li 2017; Klein, Howes & TenBarge 2017), several recent analyses of kinetic simulations (Klein *et al.* 2017; Howes *et al.* 2018; Klein *et al.* 2020) and spacecraft observations (Chen *et al.* 2019; Afshari *et al.* 2021) of plasma turbulence find clear velocity–space signatures of Landau damping. These findings indicate indeed that resonant wave–particle interactions do play a role, and possibly a dominant role (Afshari *et al.* 2021), in the damping of space and astrophysical plasma turbulence, settling the question of whether Landau damping can effectively damp strong plasma turbulence¹¹.

In quantifying how a particular damping mechanism competes with the nonlinear turbulent cascade, the key dimensionless quantity to evaluate is the ratio of linear damping rate due to nonlinear cascade rate γ/ω_{nl} (Howes *et al.* 2008a, 2011a). Adopting the conjecture of critical balance between linear and nonlinear time scales in strong plasma turbulence $\omega \sim \omega_{nl}$ (Goldreich & Sridhar 1995; Howes *et al.* 2008a, 2011a; Mallet *et al.* 2015), the key dimensionless measure of the importance of any particular mechanism is the ratio γ/ω , which can be estimated using the linear theory for each of the different damping mechanisms. Nonlinear kinetic simulations and spacecraft observations of weakly collisional plasma turbulence present opportunities to test whether the linear collisionless damping rates provide a quantitatively accurate, lowest-order estimate of the turbulent damping rates as a function of wavenumber. It is clear from the numerical and observational evidence, however, that Landau damping (Klein *et al.* 2017; Howes *et al.* 2018; Chen *et al.* 2019; Klein *et al.* 2020; Afshari *et al.* 2021; Zhou *et al.* 2023) and cyclotron damping (Afshari *et al.* 2024) can play a significant role in the damping of astrophysical plasma turbulence.

5.3. The relevance of linear physics to strong plasma turbulence

The concept of critical balance in plasma turbulence (Goldreich & Sridhar 1995; Howes *et al.* 2008a, 2011a; Mallet *et al.* 2015) – which suggests that the nonlinear time scales of the turbulent cascade remain in approximate balance with the time scales of the linear wave physics, $\omega_{nl} \sim \omega$ – implies that the physics of the linear plasma response remains valid even in strong plasma turbulence. But, perhaps in analogy with the case of incompressible hydrodynamic turbulence in which no linear response exists (Howes 2015a), the validity of linear physics has been called into question in the presence of strong plasma turbulence (Matthaeus *et al.* 2014). Although there exist numerous counterexamples in which linear physics properties have been shown to be relevant to strong plasma turbulence (Maron & Goldreich 2001; Cho & Lazarian 2003; Alexandrova *et al.* 2008; Howes *et al.* 2008a, b; Svidzinski *et al.* 2009; Sahraoui *et al.* 2010; Howes *et al.* 2011b; Hunana *et al.* 2011; TenBarge *et al.* 2012; Chen *et al.* 2013), the question has persisted. A more recent careful study of kinetic numerical simulations and spacecraft observations

¹¹Note that recent work found that an anti-phase-mixing process can inhibit the process of the linear phase mixing that transfers non-thermal internal energy to small parallel velocity–space scales, thereby shutting down the effect of Landau damping of compressible turbulent fluctuations within the inertial range under sufficiently collisionless conditions (Parker *et al.* 2016; Schekochihin *et al.* 2016; Meyrand *et al.* 2019).

has shown clearly that both small-amplitude and large-amplitude fluctuations, including variations interpreted to be coherent structures, preserve the linear properties of Alfvénic fluctuations (Grošelj *et al.* 2019), hopefully providing sufficient evidence to establish definitively the relevance of linear physics to strong plasma turbulence.

The key to predicting qualitatively which kinetic damping mechanisms are likely to dominate for a given instance of turbulence is to determine how the various collisionless damping mechanisms in § 5.1 depend on the fundamental dimensionless plasma and turbulence parameters. For a fully ionized proton and electron plasma with anisotropic (bi-Maxwellian) equilibrium velocity distribution functions (Stix 1992; Quataert 1998; Quataert & Gruzinov 1999; Swanson 2003; Klein & Howes 2015), the complex eigenfrequencies determined by the linear Vlasov–Maxwell dispersion relation depend on the dimensionless parameters that characterize the nature of the turbulent fluctuations through the typical wavevector components in a plane-wave decomposition of the turbulent fluctuations, $k_{\perp}\rho_i$ and $k_{\parallel}\rho_i$, and on the plasma parameters through the parallel ion plasma beta $\beta_{\parallel,i}$, the parallel ion-to-electron temperature ratio $\tau_{\parallel} = T_{\parallel,i}/T_{\parallel,e}$, the temperature anisotropies of each species $A_i = T_{\perp,i}/T_{\parallel,i}$ and $A_e = T_{\perp,e}/T_{\parallel,e}$, and the ratio $v_{t\parallel,i}/c$. Thus, these dependencies can be expressed through the general relation

$$\omega = \omega_{\text{VM}}^{\text{aniso}}(k_{\perp}\rho_i, k_{\parallel}\rho_i, \beta_{\parallel,i}, \tau_{\parallel}, A_i, A_e, v_{t\parallel,i}/c). \quad (5.2)$$

In the limit of isotropic equilibrium velocity distributions for the ions and electrons – leading to the simplifications $A_i = 1, A_e = 1$ and $\tau_{\parallel} = \tau \equiv T_i/T_e$ – this set of dependencies is reduced to

$$\omega = \omega_{\text{VM}}(k_{\perp}\rho_i, k_{\parallel}\rho_i, \beta_i, \tau, v_{ii}/c). \quad (5.3)$$

For both the isotropic and anisotropic equilibrium temperatures, in the non-relativistic limit $v_{ii}/c \ll 1$ typical of many space and astrophysical plasmas of interest, the linear Vlasov–Maxwell dispersion relation is practically independent of v_{ii}/c , so this parameter may effectively be dropped for the case of non-relativistic plasma turbulence.

In the limit of a sufficiently large inertial range of turbulence, the MHD turbulence scaling parameters given by (3.1)–(3.4) predict that turbulent fluctuations at the small-scale end of the inertial range – where most of the kinetic damping mechanisms are believed to become significant – will be anisotropic with $k_{\parallel} \ll k_{\perp}$ and small amplitude relative to the equilibrium magnetic field $|\delta B| \ll B_0$ (Howes *et al.* 2006, 2008a; Schekochihin *et al.* 2009). In this limit, the turbulent frequencies of the incompressible Alfvénic fluctuations directly observed to dominate turbulence in space plasmas (Belcher & Davis 1971; Tu & Marsch 1995; Alexandrova *et al.* 2008; Howes *et al.* 2012a; Bruno & Carbone 2013) have frequencies much smaller than the ion cyclotron frequency, $\omega/\Omega_i = k_{\parallel}d_i \ll 1$, where $d_i = v_A/\Omega_i = \rho_i/\sqrt{\beta_i}$ is the ion inertial length. In this limit, the turbulent fluctuations at the small-scale end of the inertial range satisfy the conditions for the applicability of gyrokinetic theory (Rutherford & Frieman 1968; Taylor & Hastie 1968; Catto 1978; Antonsen & Lane 1980; Catto, Tang & Baldwin 1981; Frieman & Chen 1982; Dubin *et al.* 1983; Hahm, Lee & Brizard 1988; Brizard 1992; Howes *et al.* 2006; Brizard & Hahm 2007; Schekochihin *et al.* 2009). Gyrokinetic theory can be rigorously derived from plasma kinetic theory under the limits of low frequency ($\omega/\Omega_i \ll 1$) and anisotropic ($k_{\parallel} \ll k_{\perp}$) fluctuations in the non-relativistic limit ($v_{ii}/c \ll 1$). In the gyrokinetic approximation, the physics of the the cyclotron resonances and of the fast magnetosonic fluctuations – and their kinetic extension to whistler fluctuations (Howes, Klein & TenBarge 2014) – are ordered out of the system. Gyrokinetics retains the physics of the $\mathbf{E} \times \mathbf{B}$ nonlinearity that mediates the turbulent cascade to small scales, full finite-Larmor-radius effects, and the collisionless damping associated with the $n = 0$ Landau resonance. In this reduced limit,

the complex eigenfrequencies of the linear gyrokinetic dispersion relation for isotropic equilibrium velocity distributions are linearly dependent on the parallel wavenumber, and have the significantly reduced dimensionless parameter dependency given by (Howes *et al.* 2006)

$$\bar{\omega} \equiv \frac{\omega}{k_{\parallel} v_A} = \bar{\omega}_{GK}(k_{\perp} \rho_i, \beta_i, \tau). \quad (5.4)$$

Although the ion-to-electron mass ratio $\mu = m_i/m_e$ is not a parameter that varies in the physical world, many numerical studies of plasma turbulence choose to employ a reduced mass ratio for computational efficiency. Therefore, we choose to include the μ dependence of different proposed turbulent damping mechanisms in our calculations below to determine how the use of a reduced mass ratio may impact the partitioning of turbulent energy removed by different damping mechanisms. Note also that it is important to employ a sufficiently large mass ratio to achieve a separation between the ion and electron scales, with a previous study suggesting $m_i/m_e \geq 32$ is necessary to model with qualitative fidelity the distinct ion and electron responses to the electromagnetic fluctuations due to this scale separation (Howes *et al.* 2018).

5.4. Landau damping and transit-time damping

To explore the two Landau-resonant collisionless damping mechanisms – Landau damping and transit-time damping – we take $n = 0$ in the resonance condition in (5.1), obtaining the condition that particles with parallel velocities equal to the parallel phase velocity of the waves, $v_{\parallel} = \omega/k_{\parallel}$, may resonantly exchange energy with the electromagnetic waves.

For simplicity in this analysis, we will assume the isotropic temperature case for a proton–electron plasma with linear wave properties given by the isotropic linear Vlasov–Maxwell dispersion relation (5.3); extending these calculations to allow for anisotropic temperatures can be done simply following the same logical procedure and using the linear Vlasov–Maxwell dispersion relation for anisotropic temperatures given by (5.2). Furthermore, justified by observations in solar wind turbulence that incompressible Alfvénic fluctuations energetically dominate the turbulence (Belcher & Davis 1971; Tu & Marsch 1995; Alexandrova *et al.* 2008; Bruno & Carbone 2013), we will focus on the linear collisionless damping rates of the Alfvénic fluctuations, including both Alfvén waves in the MHD limit at $k_{\perp} \rho_i \ll 1$, and KAWs at $k_{\perp} \rho_i \gtrsim 1$. Consideration of the damping of compressible turbulent fluctuations, specifically fast and slow magnetosonic fluctuations at $k_{\perp} \rho_i \ll 1$ (Howes *et al.* 2012a), is easily performed using the same procedure with the linear dispersion relations for these alternative wave modes¹².

Normalizing the resonant parallel velocity by the thermal velocity for both species in turn and converting the result into our dimensionless parameters for the isotropic temperature case, we obtain the key relations

$$\frac{v_{\parallel}}{v_{ti}} = \frac{\omega}{k_{\parallel} v_{ti}} = \bar{\omega} \beta_i^{-1/2}, \quad \frac{v_{\parallel}}{v_{te}} = \frac{\omega}{k_{\parallel} v_{te}} = \bar{\omega} \left(\frac{\tau}{\beta_i \mu} \right)^{1/2}, \quad (5.5a, b)$$

where we define the dimensionless wave frequency normalized by the Alfvén wave frequency in the MHD limit

$$\bar{\omega} \equiv \frac{\omega}{k_{\parallel} v_A}. \quad (5.6)$$

¹²Although, it is important to keep in mind that the recently identified nonlinear effect of anti-phase mixing in turbulent plasmas can suppress the collisionless damping predicted by linear kinetic theory for the compressible wave modes in the inertial range of scales at $k_{\perp} \rho_i \ll 1$ (Parker *et al.* 2016; Schekochihin *et al.* 2016; Meyrand *et al.* 2019).

For Alfvén waves, this normalized frequency $\bar{\omega}$ is well approximated by (Howes *et al.* 2014)

$$\bar{\omega}(k_{\perp}\rho_i, \beta_i, \tau) = \sqrt{1 + \frac{(k_{\perp}\rho_i)^2}{\beta_i + 2/(1 + 1/\tau)}}, \quad (5.7)$$

an expression that is valid in the limits that the ion plasma beta is not very low $\beta_i \gg \mu^{-1}$ and that the wave frequency remains smaller than the ion cyclotron frequency $\omega/\Omega_i \ll 1$, equivalent to the condition $k_{\parallel}d_i \ll 1$, or $k_{\parallel}\rho_i \ll \beta_i^{1/2}$.

Whether damping by the Landau-resonant mechanisms is weak or strong primarily depends on where the parallel wave phase velocity falls within the equilibrium particle velocity distribution, as quantified by the expressions in (5.5a,b). The application of the weak-growth-rate approximation to the kinetic theory for Landau damping (Krall & Trivelpiece 1973) indicates that the linear damping rate is proportional to the slope of the distribution function at the resonant velocity, as depicted in figure 6. For phase velocities that fall deep in the core of the velocity distribution $\omega/k_{\parallel} \ll v_{ts}$ (blue dotted) where the slope of $f_s(v_{\parallel})$ is relatively flat, the damping is weak because nearly equal numbers of particles with $v_{\parallel} < \omega/k_{\parallel}$ are accelerated by the wave as particles with $v_{\parallel} > \omega/k_{\parallel}$ are decelerated by the wave, leading to little net energy exchange. Similarly, for phase velocities far out in the tail of the velocity distribution $\omega/k_{\parallel} \gg v_{ts}$ (black dashed), there are few particles to resonate with the waves and the slope of $f_s(v_{\parallel})$ is also quite flat, so the damping is weak. Only if the parallel phase velocity falls in the steep region of the velocity distribution at $\omega/k_{\parallel} \sim v_{ts}$ (red solid) is there a significant net energy transfer to the particles: more particles with $v_{\parallel} < \omega/k_{\parallel}$ are accelerated by the wave than those particles with $v_{\parallel} > \omega/k_{\parallel}$ are decelerated by the wave, so that particles gain net energy at the expense of the wave. Note that this qualitative picture of collisionless damping by the Landau resonance being controlled by where the parallel wave phase velocity falls within the distribution function is independent of the form of the equilibrium velocity distribution; thus, one can apply the same reasoning to estimate the strength of the Landau-resonant damping for other non-Maxwellian forms of the equilibrium velocity distribution, such as the kappa distributions often applied to model *in situ* measurements in space plasmas (Vasyliunas 1968; Abraham-Shrauner & Feldman 1977; Gosling *et al.* 1981; Lui & Krimigis 1981; Armstrong *et al.* 1983; Summers & Thorne 1991; Thorne & Summers 1991; Summers, Xue & Thorne 1994; Livadiotis & McComas 2013; Livadiotis, Desai & Wilson 2018).

The ultimate goal is to characterize the turbulent plasma heating – specifically Q_i/Q_e , $Q_{\perp,i}/Q_i$ and $Q_{\perp,e}/Q_e$ – due to Landau damping and transit-time damping as a function of the fundamental dimensionless parameters of turbulence. To accomplish this goal, it is necessary to integrate the damping rates over the full range of the turbulent cascade, as discussed in § 5.2 and illustrated in figures 4 and 5. This integration over all scales effectively eliminates the dependence of the damping mechanisms on the components of the wavevector $k_{\perp}\rho_i$ and $k_{\parallel}\rho_i$, leaving only the desired dependence on the plasma and turbulence parameters enumerated in tables 3 and 4.

With the scale dependence on $k_{\perp}\rho_i$ eliminated, the ion Landau damping (iLD) and ion transit-time damping (iTDD) rates depend primarily on β_i , and the electron Landau damping (eLD) and electron transit-time damping (eTTD) rates depend on β_i , τ and μ , as shown by (5.5a,b). Note that the dependence of eLD and eTTD on τ and μ primarily arises from those two parameters controlling the scale separation of the ion and electron Larmor-radius scales, $\rho_i/\rho_e = (\tau\mu)^{1/2}$.

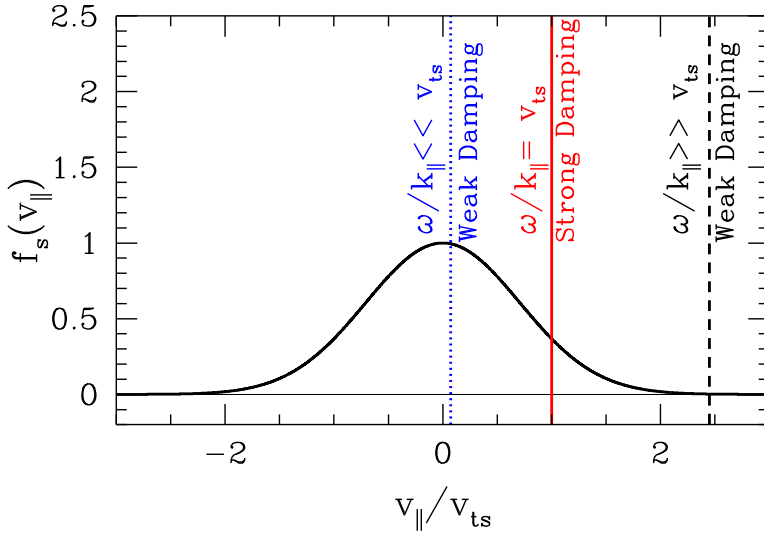


FIGURE 6. Diagram demonstrating how Landau-resonant damping qualitatively depends on where the parallel phase velocity ω/k_{\parallel} of the wave falls within the velocity distribution of particle species s , with weak damping for $\omega/k_{\parallel} \ll v_{ts}$ or $\omega/k_{\parallel} \gg v_{ts}$, and strong damping for $\omega/k_{\parallel} \sim v_{ts}$.

It is worthwhile pointing out that the physics of collisionless damping via the Landau resonance is fully captured in the gyrokinetic approximation, with the linear wave frequencies and damping rates both linearly proportional to k_{\parallel} , as shown in (5.4). Thus, the ratio of the damping-to-cascade rate¹³, $\gamma/\omega_{nl} \simeq \gamma/\omega$, is effectively independent of k_{\parallel} , leaving the expected parameter dependence on the plasma parameters β_i and τ , along with the mass ratio μ , once the cascade is integrated over the perpendicular scales of the cascade.

In addition to the fact that the dependence of the linear gyrokinetic dispersion relation on $(k_{\perp}\rho_i, \beta_i, \tau)$ in (5.4) is consistent with the results of our analysis of the parameter dependence of the Landau-resonant damping mechanisms, the linear gyrokinetic dispersion relation also determines the amplitudes and phases of the key electromagnetic fields E_{\parallel} and δB_{\parallel} that mediate the particle energization by Landau damping and transit-time damping. As done in the H10 turbulent heating model (see §4), the linear dispersion relation can simply be used to calculate directly the linear collisionless damping rates as a function of $(k_{\perp}\rho_i, \beta_i, \tau)$. It is possible, of course, that these linear damping rates may be modified under strongly turbulent plasma conditions, but modest quantitative changes to the effective damping rates are typically absorbed into the adjustable constant typically used in cascade models to specify the balance between the nonlinear cascade rate and collisionless damping rate (Howes *et al.* 2008a, 2011a). However, field-particle correlation analyses of numerical simulations (Klein *et al.* 2017, 2020; Horvath, Howes & McCubbin 2020; Conley, Howes & McCubbin 2023; Huang, Howes & McCubbin 2024) and spacecraft observations (Chen *et al.* 2019; Afshari *et al.* 2021) of plasma turbulence have clearly shown that Landau damping and transit-time damping do indeed play a role in the damping of strong plasma turbulence.

¹³Here, we have adopted the condition of critical balance for strong plasma turbulence $\omega_{nl} \simeq \omega$ (Goldreich & Sridhar 1995; Mallet *et al.* 2015).

One final step is to estimate how the ion-to-electron heating ratio Q_i/Q_e depends on the remaining key parameters β_i , τ and μ . As illustrated in figure 5(c) and 7, the ion damping rate γ_i peaks at scales $k_\perp \rho_i \sim 1$, and numerical solutions of the Vlasov–Maxwell dispersion relation (not presented here) show that this Landau-resonant damping onto the ions is essentially independent of the ion-to-electron temperature ratio. The electron damping rate γ_e , on the other hand, increases monotonically as the perpendicular wavevector increases to the electron Larmor-radius scale $k_\perp \rho_e \rightarrow 1$, eventually yielding a normalized collisionless damping rate that is believed to be sufficiently strong to terminate the turbulent cascade with $\gamma_e/\omega \rightarrow 1$, as shown in figure 7. Thus, it is expected that any energy in the turbulent cascade that passes beyond the ion kinetic scales at $k_\perp \rho_i \sim 1$ will ultimately be transferred to the electrons. Since the ion damping rate depends dominantly on β_i with very weak dependence on τ , yielding $Q_i(\beta_i)$ to lowest order, this means that the ratio Q_i/Q_e is effectively determined by the ion plasma beta alone. This simplification arises because the total turbulent damping rate must eventually balance the total cascade rate, $Q = Q_i + Q_e \sim \varepsilon_0$, so it can be shown that $Q_e/Q_i = \varepsilon_0/Q_i(\beta_i) - 1$. This dominant dependence of the Landau-resonant collisionless damping mechanisms on β_i is consistent with existing turbulent heating models (Howes 2010) and kinetic numerical simulations (Kawazura *et al.* 2019) of Alfvénic turbulence.

One final unexpected physical behaviour of Landau damping and transit-time damping is also illustrated in figure 7. For isotropic Maxwellian velocity distributions of the ions and electrons, the imaginary component of the complex frequency, $\omega_c \equiv \omega - i\gamma$, determined by the linear dispersion relation is always negative (solid black curve), corresponding to a damping of the wave with damping rate $\gamma > 0$. However, for the particular plasma parameter choices in figure 7 of $\beta_i = 3$, $T_i/T_e = 1$, and $m_i/m_e = 1836$, the individual energy transfer rates to the ions through Landau damping¹⁴ mediated by E_\parallel are actually negative over the range $k_\perp \rho_i \lesssim 2$ (red dotted), indicating a net transfer of energy from the ions to the wave fields when averaged over the full period (or, alternatively, over 2π in phase) of the Alfvén wave. But the contribution from transit-time damping mediated by E_\perp (Howes *et al.* 2024) is positive and much larger (green long dashed), leading to a net damping of the wave ($\gamma_i > 0$, thin blue) by the sum of the Landau-resonant ($n = 0$) interactions of ions with the Alfvén wave. Whether the wave-period-averaged energy transfer to ions is positive or negative depends on the relative phases of E_\parallel and E_\perp to the self-consistently determined components of the ion current density \mathbf{j}_i . For the case of $\beta_i = 3$ pictured in figure 7, at scales $k_\perp \rho_i \lesssim 2$ (red dotted), this relative phase $\delta\phi$ between E_\parallel and $j_{\parallel,i}$ must fall in the range $\pi/2 \leq \delta\phi \leq 3\pi/2$ (corresponding to wave growth at the expense of ion energy), while the relative phase between E_\perp and $j_{\perp,i}$ must fall in the range $-\pi/2 \leq \delta\phi \leq \pi/2$ (corresponding to wave damping and ion energy gain). Because each individual mechanism can possibly lead to negative energy transfer while the sum always leads to damping for an isotropic Maxwellian distribution, it suggests that perhaps a separation of the particle energization rates by Landau damping and transit-time damping is not particularly important in unravelling the turbulent heating of the plasma (especially since both of these mechanisms ultimately lead to energization of the parallel degree of freedom of the particles), so that only the summed effect of the Landau-resonant collisionless damping rates is important.

Summarizing our results for Landau-resonant collisionless damping of the turbulent cascade, the resulting ion-to-electron heating is predicted to be dominantly a function of the ion plasma beta, $Q_i/Q_e(\beta_i)$, with a weak dependence on the ion-to-electron

¹⁴The separation of the contributions of Landau damping and transit-time to the total collisionless damping rate for the Vlasov–Maxwell dispersion relation is detailed in Huang *et al.* (2024).

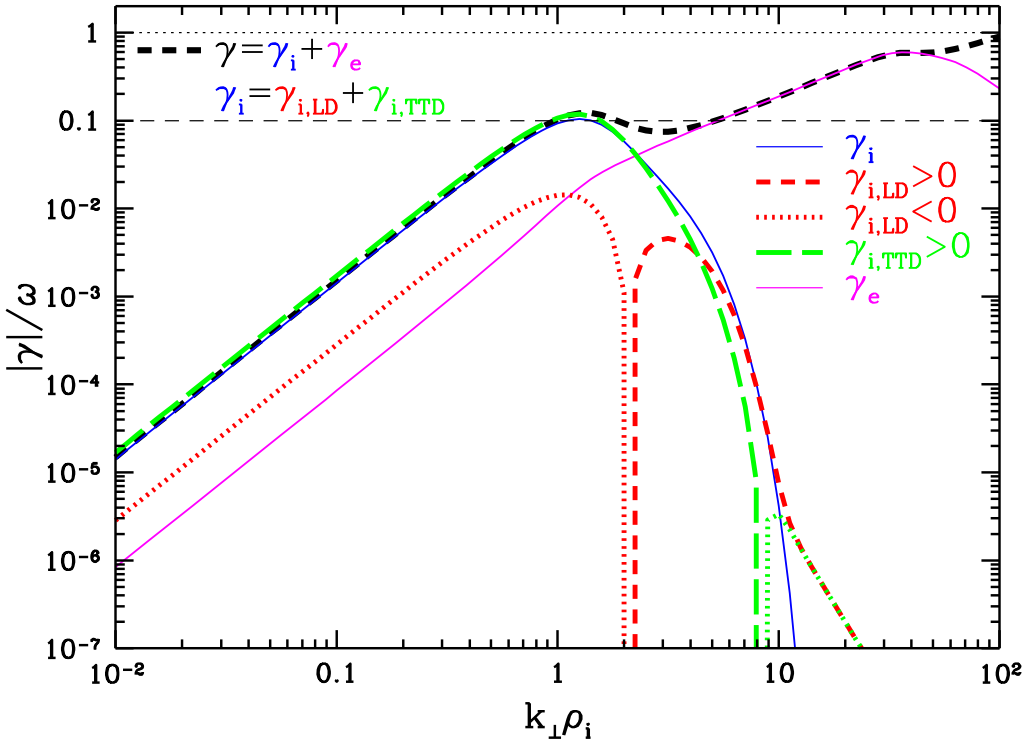


FIGURE 7. Plot of the normalized damping rate γ/ω (black dashed) for the Alfvén wave and KAW over the perpendicular wavenumber range $10^{-2} \leq k_{\perp}\rho_i \leq 10^2$ for a plasma with $\beta_i = 3$, $T_i/T_e = 1$, and $m_i/m_e = 1836$, where the complex eigenfrequency is given by $\omega_c = \omega - i\gamma$, so that $\gamma > 0$ corresponds to wave damping and $\gamma < 0$ to wave growth. The contributions from the ion damping rate γ_i (thin blue) and electron damping rate γ_e (thin magenta) are separately plotted, with the decomposition by species failing at strong damping rates with $\gamma/\omega \gtrsim 0.5$, occurring for $k_{\perp}\rho_i \gtrsim 40$. Ion damping due to Landau damping $\gamma_{i,LD} > 0$ (red dashed) and transit-time damping $\gamma_{i,TTD} > 0$ (green long dashed) are separated, showing a region of net energy transfer from ions to the wave by the Landau resonance with the ions yielding $\gamma_{i,LD} < 0$ (red dotted) at $k_{\perp}\rho_i \leq 2$.

temperature ratio τ and mass ratio μ . Both Landau damping, mediated by the parallel component of the electric field E_{\parallel} , and transit-time damping, mediated by the perpendicular component of the electric field E_{\perp} , lead to energization of the degrees of freedom parallel to the magnetic field, so $Q_{\perp,i}/Q_i = 0$ and $Q_{\perp,e}/Q_e = 0$.

5.5. Cyclotron damping

For the fundamental ($n = 1$) cyclotron resonance, the resonance condition in (5.1) simplifies to $(\omega - k_{\parallel}v_{\parallel})/\Omega_s = 1$. The numerator involves the fluctuation frequency modified by the Doppler shift of the particle’s motion parallel to the magnetic field. When that Doppler-shifted frequency matches the ion cyclotron frequency, the perpendicular component of the electric field E_{\perp} can resonantly interact with the particles to energize the particles in the directions perpendicular to the magnetic field, yielding $Q_{\perp,s}/Q_s = 1$. To estimate the conditions required for cyclotron resonant damping, it is often sufficient to require the condition $\omega/\Omega_s \rightarrow 1$.

In typical space and astrophysical plasmas, the turbulent cascade can reach the ion cyclotron frequency $\omega/\Omega_i \rightarrow 1$ under the conditions derived below, but since the electron cyclotron frequency is higher by the mass ratio, $\Omega_e/\Omega_i = m_i/m_e$, there is typically little energy remaining in the cascade at the very high frequencies needed to transfer a significant amount of energy to the electrons through their cyclotron resonance. Thus, here, we consider only the physics of the ion cyclotron resonance as a possible physical mechanism for the dissipation of plasma turbulence.

Evaluating the conditions needed to obtain $\omega/\Omega_i \rightarrow 1$ in terms of the dimensionless parameters of turbulence in the isotropic temperature case, we find

$$\frac{\omega}{\Omega_i} = \bar{\omega} k_{\parallel} d_i = \bar{\omega} \frac{k_{\parallel} \rho_i}{\beta_i^{1/2}}, \tag{5.8}$$

where $\bar{\omega}$ is defined by (5.6). Note that the middle expression indicates that the most natural unit to normalize the length scale parallel to the magnetic field is the ion inertial length $d_i = c/\omega_{pi} = v_A/\Omega_i$, but to maintain consistency with the length normalizations in tables 3 and 4, we substitute $d_i = \rho_i/\beta_i^{1/2}$. Utilizing the general scaling of the parallel wavenumber in terms of the isotropic driving wavenumber

$$k_{\parallel} \rho_i = (k_0 \rho_i)^{(1+\alpha)/(3+\alpha)} (k_{\perp} \rho_i)^{2/(3+\alpha)}, \tag{5.9}$$

to determine the frequency achieved when the cascade reaches $k_{\perp} \rho_i = 1$, we obtain the condition

$$\frac{\omega}{\Omega_i} = \frac{\bar{\omega}}{\beta_i^{1/2}} (k_0 \rho_i)^{(1+\alpha)/(3+\alpha)}. \tag{5.10}$$

This indicates clearly that ion cyclotron damping is more likely to occur for small ion plasma beta $\beta_i \ll 1$ or a smaller turbulent inertial range (meaning a value of $k_0 \rho_i$ that is not too small). Note that, for anisotropic driving with $k_{\parallel 0}/k_{\perp 0} < 1$, such as may occur in the solar corona at low values of β_i , the effective isotropic driving wavenumber $k_0 \rho_i$, given by (3.11), will actually be smaller than the perpendicular driving scale $k_{\perp 0} \rho_i$, leading to yet smaller values of ω/Ω_i . For the GS95 scaling with $\alpha = 0$, we obtain a condition for the onset of ion cyclotron damping of $k_0 \rho_i = \beta_i^{3/2}/\bar{\omega}^3$; for the B06 scaling with $\alpha = 1$, we obtain $k_0 \rho_i = \beta_i/\bar{\omega}^2$. For simplicity, note that at the small-scale end of the inertial range with $k_{\perp} \rho_i \lesssim 1$, the normalized wave frequency $\bar{\omega}$ for Alfvén waves can be approximated in the limit $k_{\parallel} d_i \rightarrow 1$ by the expression (Di Mare & Howes 2024)

$$\bar{\omega} \simeq \frac{1}{\sqrt{1 + (k_{\parallel} d_i)^2}}. \tag{5.11}$$

In summary, ion cyclotron damping is predicted to play a role in the damping of plasma turbulence for conditions with a smaller inertial range and low plasma beta values $\beta_i \ll 1$. The nature of the resulting plasma heating is strictly ion energization $Q_i/Q = 1$ in the perpendicular degrees of freedom¹⁵ $Q_{\perp,i}/Q_i = 1$.

Note that recent theoretical and numerical studies of turbulence with a sufficiently large amount of imbalance $Z_0^+/Z_0^- \gg 1$, such as may be encountered in the inner heliosphere, has uncovered a new phenomenon denoted the helicity barrier, which can lead to the

¹⁵Note, however, that the quasilinear evolution of ions undergoing pitch-angle scattering in the cyclotron wave frame leads to ion motion primarily to higher perpendicular velocity but also to slightly lower parallel velocity, effectively yielding a small amount of parallel cooling (Isenberg 2001; Isenberg *et al.* 2001).

generation of sufficiently high-frequency fluctuations, specifically ion cyclotron waves, that may cause energization of the ions by the cyclotron resonance (Meyrand *et al.* 2021; Squire *et al.* 2022, 2023).

5.6. Stochastic heating

The stochastic heating of ions has long been proposed as a means to energize ions in turbulent plasmas (McChesney *et al.* 1987; Chen *et al.* 2001; Johnson & Cheng 2001; White *et al.* 2002; Voitenko & Goossens 2004; Bourouaine *et al.* 2008), with more recent work providing significant theoretical and numerical evidence for ion stochastic heating as a significant mechanism for turbulent damping in space and astrophysical plasmas (Chandran 2010; Chandran *et al.* 2010, 2011; Bourouaine & Chandran 2013; Chandran *et al.* 2013; Klein & Chandran 2016; Vech, Klein & Kasper 2017; Arzamasskiy *et al.* 2019; Martinović *et al.* 2020; Cerri *et al.* 2021).

Chandran *et al.* (2010) used test particle simulations of randomly phased Alfvén and kinetic Alfvén waves to develop an empirical formula for the rate of ion stochastic heating by turbulent fluctuations with frequencies much lower than the ion cyclotron frequency $\omega/\Omega_i \ll 1$. Following this, Chandran *et al.* (2011) developed a refined implementation to predict the partitioning of turbulent energy among parallel ion heating, perpendicular ion heating, and electron heating (the C11 model in § 4), with a formula for the damping rate by ion stochastic heating given by

$$\gamma_{\text{SH}} = c_1 \left(\frac{\delta v_{\perp}^{(\rho_i)}}{v_{ii}} \right) \Omega_i \exp(-c_2 v_{ii}/\delta v_{\perp}^{(\rho_i)}), \quad (5.12)$$

where $\delta v_{\perp}^{(\rho_i)}$ is the root-mean-square amplitude of the perpendicular velocity fluctuations at the perpendicular scale of the ion Larmor radius, $k_{\perp}\rho_i = 1$. Here, c_1 and c_2 are fitting constants with suggested values $c_1 = 0.18$ and $0.15 \lesssim c_2 \lesssim 0.34$ (Chandran 2010; Chandran *et al.* 2011; Bourouaine & Chandran 2013; Xia *et al.* 2013). The key dimensionless parameter controlling the onset of stochastic heating in this formulation is the ratio of the perpendicular velocity fluctuation to the thermal velocity, $\epsilon \equiv \delta v_{\perp}^{(\rho_i)}/v_{ii}$; these studies found a critical threshold $\epsilon_{\text{crit}} \simeq 0.19$ that determines the minimum fluctuation amplitude required for the onset of stochastic heating (Chandran *et al.* 2010).

Using the relation for Alfvén waves to connect the perpendicular fluid velocity fluctuations to the perpendicular magnetic field fluctuations $\delta v_{\perp}/v_A = \pm \bar{\omega} \delta B_{\perp}/B_0$ (Howes *et al.* 2008a) and the MHD scaling of the turbulent perpendicular magnetic field fluctuation amplitude given by (3.4) with the B06 scaling with $\alpha = 1$, we obtain the expression

$$\frac{\delta v_{\perp}}{v_{ii}} = \bar{\omega} \beta_i^{-1/2} \left(\frac{k_0 \rho_i}{k_{\perp} \rho_i} \right)^{1/4}. \quad (5.13)$$

At $k_{\perp}\rho_i \sim 1$, we obtain the normalized frequency $\bar{\omega} \sim 1$ and find the key relation for the amplitude in terms of our fundamental turbulence parameters

$$\epsilon \equiv \frac{\delta v_{\perp}^{(\rho_i)}}{v_{ii}} = \beta_i^{-1/2} (k_0 \rho_i)^{1/4}. \quad (5.14)$$

To estimate the importance of damping by ion stochastic heating relative to the turbulent cascade rate, we can calculate $\gamma_{\text{SH}}/\omega_{nl} \sim \gamma_{\text{SH}}/\omega$ to obtain the final result

$$\frac{\gamma_{\text{SH}}}{\omega} = c_1 (k_0 \rho_i)^{-1/4} \exp(-c_2 \beta_i^{1/2} (k_0 \rho_i)^{-1/4}), \quad (5.15)$$

where we have used the substitution $\Omega_i/\omega = \beta_i^{1/2}/k_{\parallel}\rho_i$.

In summary, the proposed turbulent damping mechanism of ion stochastic heating depends primarily on the fundamental parameters β_i and $k_0\rho_i$, where lower ion plasma beta and larger isotropic driving wavenumber (which corresponds to a smaller inertial range) both conspire to yield larger turbulent amplitude at the ion Larmor-radius scale $k_{\perp}\rho_i \sim 1$, enhancing stochastic heating of the ions. The exponential effectively provides a threshold turbulent amplitude at the ion scales below which stochastic ion heating is ineffective. Note that the exponential dependence on the constant c_2 makes its accurate determination critical to assess the importance of ion stochastic heating in any particular case; its value is likely to depend on the detailed nature of the turbulent fluctuations at the perpendicular scale of the ion Larmor radius (Chandran *et al.* 2011). This heating mechanism is predicted to lead to strictly ion energization $Q_i/Q = 1$ in the perpendicular degrees of freedom $Q_{\perp,i}/Q_i = 1$.

Note that, because the amplitude of the turbulent fluctuations is typically found to decrease monotonically as the turbulent cascade progresses to smaller scales, it is unlikely that electrons will experience significant stochastic heating, so we do not explore electron stochastic heating here. Further research will be necessary to evaluate thoroughly the potential for electron stochastic heating to damp turbulence at the perpendicular scale of the electron Larmor radius, $k_{\perp}\rho_e \sim 1$. Furthermore, a consideration of the intermittency – which can enhance the amplitude of individual fluctuations – of the turbulent fluctuations at the ion Larmor radius scale suggests that the rate of ion stochastic heating may be dramatically increased in the presence of significant intermittency (Mallet *et al.* 2019).

5.7. Magnetic pumping

Magnetic pumping (Spitzer & Witten 1953; Berger *et al.* 1958; Lichko *et al.* 2017; Lichko & Egedal 2020; Montag & Howes 2022) is a particle energization mechanism in which variations of magnetic field magnitude at low frequency ω lead to an oscillating transfer of energy from parallel to perpendicular degrees of freedom and back, obeying the double-adiabatic (Chew–Goldberger–Low, CGL) equations of state (Chew, Goldberger & Low 1956). In the absence of any collisions, the net change of particle energy over a full oscillation is zero. But, in the presence small but finite collisionality¹⁶, there can be a non-zero transfer of energy from the oscillating electromagnetic fields to the particles over the course of a full oscillation.

As a proposed mechanism for the damping of turbulence, magnetic pumping necessarily requires turbulent fluctuations that involve changes of the magnetic field magnitude from the equilibrium field strength B_0 , or $\delta B \equiv |\mathbf{B}| - B_0 \neq 0$. For Alfvénic turbulence, which is dominantly incompressible¹⁷ in the MHD regime at $k_{\perp}\rho_i \ll 1$, significant fluctuations of the magnetic field magnitude arise only within the KAW regime at $k_{\perp}\rho_i \gtrsim 1$ under conditions of ion plasma beta $\beta_i > 1$. Alternatively, if the turbulence has a significant component of compressible magnetosonic fluctuations with $E_{\text{comp}}/E_{\text{inc}} > 0$, because the turbulent amplitudes typically decrease monotonically with decreasing scale lengths, the largest-amplitude compressible fluctuations occur at the driving scale and may lead to magnetic pumping, directly energizing particles from these large-scale fluctuations.

¹⁶Note that the collisionality can be due to Coulomb collisions or to an effective collisionality due to pitch-angle scattering through collisionless wave–particle interactions with small-scale electromagnetic fluctuations, such as those driven by kinetic temperature anisotropy instabilities (Kunz *et al.* 2018; Arzamasskiy *et al.* 2023).

¹⁷Note, however, that the magnetic field magnitude variations arising from strong turbulent driving at the outer scale with $|\delta B| \sim B_0$ can lead to the ‘interruption’ of linearly polarized Alfvén waves by kinetic temperature anisotropy instabilities at sufficient high $\beta_i \gg 1$ (Squire *et al.* 2016, 2017a, b).

We determine first the parameters controlling magnetic pumping in Alfvénic turbulence, following a similar procedure subsequently to analyse the magnetic pumping arising from compressible turbulence with $E_{\text{comp}}/E_{\text{inc}} > 0$. The foundation of magnetic pumping is the double-adiabatic evolution of the weakly collisional plasma which conserves the particle magnetic moment $\mu_m \equiv mv_{\perp}^2/2B$ and the action integral of the parallel bounce motion $J_{\parallel} \equiv \oint v_{\parallel} dl$ (Lichko *et al.* 2017; Montag 2018). Conservation of these adiabatic invariants requires a scale separation of the perpendicular wavenumber relative to the particle species Larmor radius $k_{\perp}\rho_s \ll 1$ and of the wave parallel phase velocity relative to the particle thermal velocity $\omega/k_{\parallel}v_{ts} \ll 1$.

Kinetic Alfvén waves give rise to non-negligible magnetic field magnitude variations over the perpendicular wavenumber range $1 \lesssim k_{\perp}\rho_i \lesssim (\tau\mu)^{1/2}$ for values of $\beta_i \gtrsim 1$. This range of δB fluctuations is incompatible with the necessary condition $k_{\perp}\rho_i \ll 1$ for the ions, so we expect that magnetic pumping by KAWs cannot energize the ions. For the electrons, on the other hand, the requisite condition $k_{\perp}\rho_e \ll 1$ can be rewritten as $k_{\perp}\rho_i \ll (\tau\mu)^{1/2}$, so we expect that KAWs may be able to damp turbulent fluctuations and energize the electrons under ion plasma beta conditions with $\beta_i \gtrsim 1$. The phase velocity condition for electrons can be expressed as $\bar{\omega} \ll (\beta_i\mu/\tau)^{1/2}$. Under the ion plasma beta condition $\beta_i \gtrsim 1$, the equation for the dimensionless frequency of kinetic Alfvén waves given by (5.7) can be approximated by $\bar{\omega} \simeq k_{\perp}\rho_i/\beta_i^{1/2}$, so this requirement can be converted to a condition on the perpendicular wavenumber given by $k_{\perp}\rho_i \ll \beta_i(\mu/\tau)^{1/2}$, which can certainly be satisfied for the perpendicular wavenumber range of KAWs with significant magnetic field magnitude fluctuations. Therefore, the necessary conditions for the magnetic pumping of electrons to play a role in the dissipation of Alfvénic plasma turbulence with $\beta_i \gtrsim 1$ appear to be satisfied.

Previous studies have shown that the ratio of the damping rate due to magnetic pumping γ_{MP} to the pump wave frequency ω is given by (Lichko *et al.* 2017; Montag & Howes 2022)

$$\frac{\gamma_{\text{MP}}}{\omega} = \frac{\chi_{c,s}}{1 + \chi_{c,s}^2} \left(\frac{\delta B}{B_0} \right)^2, \tag{5.16}$$

where $\chi_{c,s} \equiv 6\nu_s/\omega$ is a dimensionless measure of the collision frequency ν_s for species s and δB is the amplitude of the magnetic field magnitude fluctuations.

To determine the dependence of the magnetic pumping of electrons on the plasma and turbulence parameters in tables 3 and 4, we assume isotropic driving $k_{\parallel 0}/k_{\perp 0} = 1$ for simplicity, write the electron–electron collision frequency as $\nu_e = \nu_{te}/\lambda_{\text{mf},e}$, and use the general parallel wavenumber scaling for arbitrary α given by (3.1) to obtain

$$\chi_{c,e} = \frac{6}{\bar{\omega}(k_{\parallel 0}\lambda_{\text{mf},e})} \left(\frac{\beta_i\mu}{\tau} \right)^{1/2} \left(\frac{k_0\rho_i}{k_{\perp}\rho_i} \right)^{2/(3+\alpha)}. \tag{5.17}$$

For a sufficiently large turbulent inertial range with $k_0\rho_i \ll 1$, KAWs over the perpendicular wavenumber range $1 \lesssim k_{\perp}\rho_i \lesssim (\tau\mu)^{1/2}$ will have relatively small turbulent amplitudes $\delta B_{\perp}/B_0 \ll 1$, so the magnetic field magnitude fluctuations can be expressed to lowest order as variations of the parallel component of the perturbed magnetic field $\delta B \simeq \delta B_{\parallel}$ (Huang *et al.* 2024). The turbulent magnetic field magnitude variations may then be expressed as

$$\frac{\delta B}{B_0} = \left(\frac{\delta B_{\parallel}}{\delta B_{\perp}} \right) \left(\frac{k_0\rho_i}{k_{\perp}\rho_i} \right)^{1/(3+\alpha)}, \tag{5.18}$$

where the ratio $\delta B_{\parallel}/\delta B_{\perp}$ for KAWs over the relevant range from the linear dispersion relation is strictly a function of β_i , or $\delta B_{\parallel}/\delta B_{\perp} = f(\beta_i)$. Therefore, electron magnetic

pumping by Alfvénic turbulent fluctuations at scales $k_{\perp}\rho_i \gtrsim 1$ depends on the parameters β_i , τ , μ , $k_0\rho_i$ and $k_{\parallel 0}\lambda_{\text{mfp},e}$.

Next we consider that case that the turbulence is driven compressibly with $E_{\text{comp}}/E_{\text{inc}} > 0$. In this situation, the magnetic field magnitude fluctuations at the driving scale, which typically have the largest amplitude of $\delta B/B_0$, may contribute to magnetic pumping of both the ions and electrons. In this case of turbulent damping at the driving scale, it is necessary to use the three driving parameters ($k_{\perp 0}\rho_i$, $k_{\parallel 0}/k_{\perp 0}$, χ_0) in table 3, rather than the simplified parameterization through the isotropic driving wavenumber $k_0\rho_i$, to determine the parameter dependence of the turbulent damping via magnetic pumping.

First, the normalized fast and slow magnetosonic wave phase velocities can be expressed by the linear dispersion relation (Klein *et al.* 2012)

$$\tilde{\omega}^4 - \tilde{\omega}^2(1 + \beta) + \beta \cos^2 \Theta = 0, \tag{5.19}$$

which has four solutions given by

$$\tilde{\omega}^2 = \frac{1}{2}[1 + \beta \pm \sqrt{(1 + \beta)^2 - 4\beta \cos^2 \Theta}], \tag{5.20}$$

where the plus (minus) sign corresponds to the two fast (slow) magnetosonic wave modes. Here, we define the normalized wave frequency $\tilde{\omega} \equiv \omega/kv_A$, the total (MHD) plasma beta $\beta = \beta_i(1 + 1/\tau)$, and the wavevector components (k_{\parallel} , k_{\perp}) are alternatively parameterized by (k, Θ) , where $k_{\parallel} = k \cos \Theta$, $k_{\perp} = k \sin \Theta$, $k = (k_{\parallel}^2 + k_{\perp}^2)^{1/2}$ and $\Theta = \tan^{-1}(k_{\perp}/k_{\parallel})$. The dimensionless form of the solutions in (5.20) makes clear that the fast and slow magnetosonic wave phase velocities depend only on two dimensionless parameters, $\tilde{\omega}(\beta, \Theta)$.

We may determine the parameter dependence of the normalized ion collision frequency by using the relation for the ion–ion collision rate in terms of the electron–electron collision rate $\nu_i = \mu^{-1/2}\tau^{-3/2}\nu_e$ and writing the pumping wave frequency at the driving scale as $\omega = \tilde{\omega}_0 k_0 v_A$ to obtain

$$\chi_{c,i} = \frac{6}{\tilde{\omega}_0(k_{\parallel 0}\lambda_{\text{mfp},e})\tau^2}\beta_i^{1/2} \cos \Theta_0. \tag{5.21}$$

Note that the ion collisional mean free path can be expressed in terms of the electron collisional mean free path by the relation $\lambda_{\text{mfp},i} = \lambda_{\text{mfp},e}\tau^2$, so the denominator is actually independent of the ion-to-electron temperature ratio τ , depending rather only on the normalized ion mean free path, $k_{\parallel 0}\lambda_{\text{mfp},i}$.

To evaluate the turbulent magnetic field magnitude variations for ion magnetic pumping by compressible fluctuations at the driving scale, we first note that the phenomenon of dynamic alignment, parameterized by the alignment angle θ_0 , will not play a role: dynamic alignment develops through the nonlinear interactions as the turbulence cascades to smaller scales, but does not come into play at the driving scale, so we set $\theta_0 = 1$, thus reducing the nonlinearity parameter at the driving scale to $\chi_0 = k_{\perp 0}\delta B_{\perp 0}/(k_{\parallel 0}B_0)$. If the magnetic perturbations at the driving scale have $|\delta \mathbf{B}|/B_0 \sim 1$, the linear theory for waves breaks down, and the nonlinearity must be taken into account in the lowest-order description of the wave dynamics; in this case, one may directly take the measured magnetic field magnitude fluctuations $\delta B/B_0$ as the parameter to estimate the damping rate by magnetic pumping in (5.16). However, if the magnetic perturbations at the driving

scale have $\epsilon \equiv |\delta B|/B_0 < 1$, the binomial expansion may be used to obtain the expression

$$\delta B/B_0 \simeq \delta B_{\parallel}/B_0 + (\delta B_{\parallel}/B_0)^2/2 + (\delta B_{\perp}/B_0)^2/2, \quad (5.22)$$

where the first term is of order ϵ and the next two terms are of order ϵ^2 . Thus, to lowest order, we may estimate $\delta B \simeq \delta B_{\parallel}$, where the error in this estimation scales as $\epsilon^2/2$, yielding a fractional error of 25 % for $|\delta B|/B_0 = 1/2$ and of 6 % for $|\delta B|/B_0 = 1/4$.

Using this approximation, we can derive an expression for the normalized fluctuations of the magnetic field magnitude by $\delta B/B_0 \simeq \delta B_{\parallel}/B_0 = (\delta B_{\perp}/B_0)(\delta B_{\parallel}/\delta B_{\perp})$. If we estimate $\delta B_{\parallel}/\delta B_{\perp} \sim (E_{\text{comp}}/E_{\text{inc}})^{1/2}$, we can then obtain the expression for the normalized amplitude of the magnetic field magnitude fluctuations

$$\frac{\delta B}{B_0} = \frac{k_{\parallel 0}}{k_{\perp 0}} \chi_0 \left(\frac{E_{\text{comp}}}{E_{\text{inc}}} \right)^{1/2}. \quad (5.23)$$

Combining the dependencies of $\chi_{c,i}$ in (5.21) and of $\delta B/B_0$ in (5.23), ion magnetic pumping by compressible turbulent fluctuations at the driving scale depends on the parameters β_i , $k_{\parallel 0} \lambda_{\text{mfp},i} = (k_{\parallel 0} \lambda_{\text{mfp},e}) \tau^2$, $k_{\parallel 0}/k_{\perp 0}$, χ_0 and $E_{\text{comp}}/E_{\text{inc}}$.

For magnetic pumping of electrons by compressible turbulent fluctuations at the driving scale, we can follow an analogous procedure to obtain the normalized electron collision frequency

$$\chi_{c,e} = \frac{6}{\tilde{\omega}_0(k_{\parallel 0} \lambda_{\text{mfp},e})} \left(\frac{\beta_i \mu}{\tau} \right)^{1/2} \cos \Theta_0, \quad (5.24)$$

and the same expression in (5.23) for the normalized fluctuations of the magnetic field magnitude by $\delta B/B_0$, which is independent of the species properties. Thus, electron magnetic pumping by compressible turbulent fluctuations at the driving scale depends on the parameters β_i , τ , μ , $k_{\parallel 0} \lambda_{\text{mfp},e}$, $k_{\parallel 0}/k_{\perp 0}$, χ_0 and $E_{\text{comp}}/E_{\text{inc}}$.

In summary, magnetic pumping by Alfvénic turbulent fluctuations can damp turbulence and energize electrons through turbulent fluctuations at perpendicular scales $1 \lesssim k_{\perp} \rho_i \lesssim (\tau \mu)^{1/2}$ for plasma conditions with $\beta_i \gtrsim 1$, but ions are not expected to be energized by Alfvénic fluctuations. The resulting magnetic pumping of electrons by Alfvénic turbulent fluctuations depends on the parameters β_i , τ , μ , $k_0 \rho_i$, and $k_{\parallel 0} \lambda_{\text{mfp},e}$. If the turbulence is driven compressibly with $E_{\text{comp}}/E_{\text{inc}} > 0$, we expect that the turbulent fluctuations at the driving scales, which have the largest amplitude of $\delta B/B_0$, may lead to damping of the turbulence through the magnetic pumping of both the ions and electrons. The resulting magnetic pumping of ions by compressible turbulence at the driving scales depends on the parameters β_i , $k_{\parallel 0} \lambda_{\text{mfp},i} = (k_{\parallel 0} \lambda_{\text{mfp},e}) \tau^2$, $k_{\parallel 0}/k_{\perp 0}$, χ_0 , and $E_{\text{comp}}/E_{\text{inc}}$. Analogously, the magnetic pumping of electrons by compressible turbulence depends on the parameters β_i , τ , μ , $k_{\parallel 0} \lambda_{\text{mfp},e}$, $k_{\parallel 0}/k_{\perp 0}$, χ_0 , and $E_{\text{comp}}/E_{\text{inc}}$. These parameter dependencies for magnetic pumping of ions and electrons are summarized in table 5. Note that magnetic pumping energizes particles in energy over all pitch angles (Montag & Howes 2022), so that both the parallel and perpendicular degrees of freedom gain energy, yielding for either ion or electron species $Q_{\perp,s}/Q_{\parallel,s} \sim 1$.

5.8. Kinetic viscous heating

As discussed above for the case of magnetic pumping, low-frequency turbulent fluctuations that generate variations in the magnetic field magnitude will lead to a double-adiabatic (CGL) (Chew *et al.* 1956) evolution of weakly collisional plasmas that preserves to lowest order the particle magnetic moment μ_m and the action integral of the

parallel bounce motion J_{\parallel} (Lichko *et al.* 2017; Montag 2018; Arzamasskiy *et al.* 2023). This dynamics leads to the development of anisotropies in the velocity distribution of the plasma particles, yielding temperature and pressure anisotropies with $p_{\parallel} \neq p_{\perp}$. These deviations from local thermodynamic equilibrium can trigger rapidly growing kinetic instabilities that can disrupt the linear wave dynamics (Squire *et al.* 2016, 2017a, b) and mediate the non-local transfer of turbulent energy directly from the large driving scales to kinetic length scales (Kunz *et al.* 2018; Arzamasskiy *et al.* 2023), as illustrated by the red arrow in figure 1(b). The effect of these kinetic instabilities on the turbulent dynamics has recently been modelled as an effective ‘viscosity’ (Arzamasskiy *et al.* 2023).

Here we use the term ‘kinetic viscous heating’ to describe the transfer of energy by this effective viscosity mediated by temperature anisotropy instabilities (Arzamasskiy *et al.* 2023) to avoid confusion with the usual viscous heating arising from microscopic Coulomb collisions. We note that, although this effect can be grossly modelled as an effective viscosity that leads to diffusion of the bulk fluid velocity field, its properties are entirely distinct from the standard viscosity in fluid dynamics mediated by microscopic collisions between neutral particles (Chapman & Cowling 1970) or by microscopic Coulomb collisions between charged particles in a plasma under strongly collisional conditions (Spitzer 1962; Grad 1963; Braginskii 1965). Standard viscosity is a linear mechanism that may be modelled mathematically by a Laplacian differential operator in the fluid momentum equation, and thus its effect increases monotonically with k^2 in Fourier space; this kinetic viscosity is a nonlinear mechanism operating only under weakly collisional conditions that strongly depends on the value of the ion plasma beta β_i , and its effect diminishes at higher wavenumber k with the monotonically decreasing amplitudes of the turbulent fluctuations. Determining how this kinetic viscosity may tap some fraction of the energy from the turbulent fluctuations at the large, driving scales and non-locally transfer that energy directly to fluctuations at the small, ion kinetic length scales remains an open line of investigation.

To properly describe the kinetic physics of turbulence in temperature anisotropic plasmas, it is necessary to employ the full set of plasma and turbulence parameters in table 3. The relevant kinetic instabilities driven by anisotropies in the ion velocity distribution are the four ion temperature anisotropy instabilities: (i) the parallel (or whistler) firehose instability (Kennel 1966; Gary *et al.* 1976) and (ii) the Alfvén (or oblique) firehose instability (Hellinger & Matsumoto 2000), which are both relevant to plasmas with an ion temperature anisotropy sufficiently less than unity $A_i = T_{\perp,i}/T_{\parallel,i} < 1$ and with a parallel ion plasma beta $\beta_{\parallel,i} > 1$; and (iii) the mirror instability (Vedenov & Sagdeev 1958; Tajiri 1967; Southwood & Kivelson 1993) and (iv) the ion cyclotron instability (Gary *et al.* 1976), which are both relevant to plasmas with an ion temperature anisotropy sufficiently greater than unity $A_i = T_{\perp,i}/T_{\parallel,i} > 1$ for any value of the parallel ion plasma beta $\beta_{\parallel,i}$. When the plasma exceeds a threshold value of the ion temperature anisotropy (Boris & Manheimer 1977; Matteini *et al.* 2006; Hellinger & Trávníček 2008; Klein & Howes 2015), these instabilities can tap the free energy associated with the anisotropic ion temperature, driving electromagnetic fluctuations and ultimately reducing the temperature anisotropy, thereby moving the plasma back toward a state of marginal stability.

Hellinger *et al.* (2006) has compiled values for the marginal stability boundaries for these four ion temperature anisotropy instabilities over the $(\beta_{\parallel,i}, T_{\perp,i}/T_{\parallel,i})$ plane. Using a linear Vlasov-Maxwell dispersion relation solver with bi-Maxwellian equilibrium ion velocity distributions in a fully ionized, hydrogenic (proton and electron) plasma, the marginal stability boundary is determined by calculating the complex eigenfrequency $\omega(\mathbf{k})$ for a fixed $\beta_{\parallel,i}$ over all possible wavevectors \mathbf{k} . The ion temperature anisotropy

Instability	a	b	β_0
Ion Cyclotron	0.43	0.42	-0.0004
Parallel Firehose	-0.47	0.53	0.59
Alfvén Firehose	-1.4	1.0	-0.11
Mirror	0.77	0.76	-0.016

TABLE 6. Instability threshold parameters for a maximum growth rate $|\gamma|/\Omega_i = 10^{-3}$ from Hellinger *et al.* (2006).

$T_{\perp,i}/T_{\parallel,i}$ is then varied until the most unstable wavevector has a growth rate of $|\gamma|/\Omega_i = 10^{-3}$, thus establishing the instability criterion. For the four ion temperature anisotropy instabilities, the corresponding instability criteria on the $(\beta_{\parallel,i}, T_{\perp,i}/T_{\parallel,i})$ plane are generally well fit by an expression of the form

$$\frac{T_{\perp,i}}{T_{\parallel,i}} = 1 + \frac{a}{(\beta_{\parallel,i} - \beta_0)^b}, \quad (5.25)$$

where a , b , and β_0 are unique values for each of the four instabilities, computed by Hellinger *et al.* (2006) and found here in table 6. These instability thresholds are plotted in figure 8, and observational studies of measured intervals in the solar wind generally show that the measurements are more or less constrained by these threshold limits on the $(\beta_{\parallel,i}, T_{\perp,i}/T_{\parallel,i})$ plane (Hellinger *et al.* 2006; Bale *et al.* 2009; Maruca, Kasper & Bale 2011).

Recent theoretical and numerical studies have highlighted the fact that, at sufficiently high parallel ion plasma beta $\beta_{\parallel,i} \gg 1$, the marginal stability boundary for these kinetic ion temperature anisotropy instabilities asymptotes towards isotropy, as shown in figure 8, so the double-adiabatic evolution of turbulent fluctuations can easily exceed these boundaries and trigger these rapidly growing instabilities. Large-scale Alfvén waves in the MHD limit at $k_{\perp}\rho_i \ll 1$ yield only perpendicular magnetic field perturbations $\delta B_{\perp} \neq 0$ with $\delta B_{\parallel} = 0$, so the variation in the magnetic field magnitude δB is negligible in the limit of small-amplitude waves $\delta B_{\perp}/B_0 \ll 1$. However, at sufficiently large amplitudes $\delta B_{\perp}/B_0 \rightarrow 1$, these fluctuations can lead to significant variation in the magnetic field magnitude, as made clear by (5.22). Thus, at sufficiently high values of parallel ion plasma beta $\beta_{\parallel,i} \gg 1$, the physics of linearly polarized¹⁸ Alfvén waves can be ‘interrupted’ by these kinetic ion temperature anisotropy instabilities (Squire *et al.* 2016, 2017a, b).

Further examination of the effect of kinetic instabilities on the turbulent cascade under conditions of high parallel ion plasma beta, $\beta_{\parallel,i} \gg 1$, has found that these instabilities can non-locally transfer energy directly to kinetic length scales (Arzamasskiy *et al.* 2023), as illustrated by the red arrow in figure 1(b). This new channel of energy transfer can compete with the traditional local transfer of energy to smaller scales of the turbulent cascade that is mediated by nonlinear interactions, as illustrated by the black arrows in figure 1(a). The effect of these kinetic instabilities on the large-scale turbulent dynamics has been quantified as an effective viscosity by Arzamasskiy *et al.* (2023). Here, we denote this kinetic-instability-mediated viscosity as the kinetic viscosity¹⁹ to distinguish it from the

¹⁸Note that circularly polarized Alfvénic fluctuations, which have no magnetic field magnitude variation, do not suffer this kinetic-instability-driven interruption (Squire *et al.* 2016).

¹⁹This kinetic viscosity terminology for kinetic-instability-mediated viscosity should not be confused with the kinematic viscosity defined in hydrodynamic fluids.

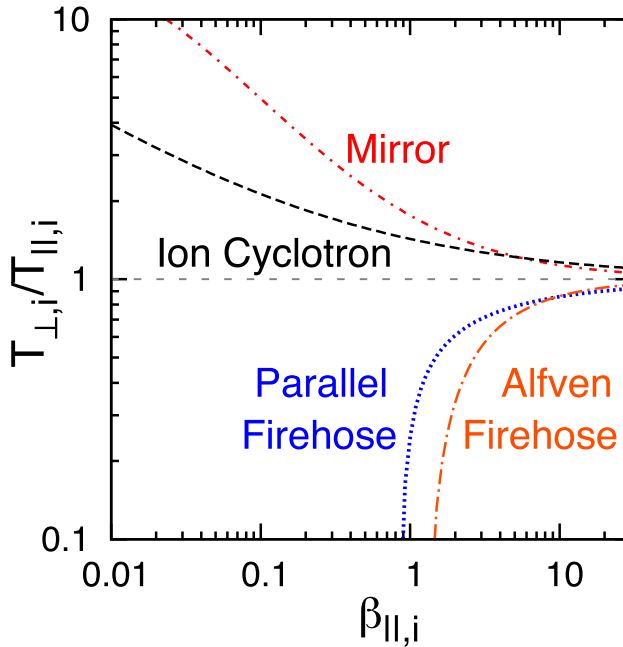


FIGURE 8. Marginal linear stability thresholds for the four ion temperature anisotropy instabilities using (5.25) and the parameters in table 6.

usual definition of viscosity that arises through Coulomb collisions among the charged plasma particles.

These ion kinetic instabilities act to limit the ion pressure anisotropy in the plasma to values corresponding to marginal stability, given by $\Delta p_i/p_i \lesssim 1/\beta_{\parallel,i}$, where $\Delta p_i \equiv p_{\perp,i} - p_{\parallel,i}$ and $p_i \equiv (2p_{\perp,i} + p_{\parallel,i})/3$ (Kunz, Schekochihin & Stone 2014; Melville, Schekochihin & Kunz 2016; Arzamasskiy *et al.* 2023). Using this marginal stability scaling with $\beta_{\parallel,i}$, one can estimate an effective collision frequency (Arzamasskiy *et al.* 2023)

$$\nu_{\text{eff}} \sim \beta_{\parallel,i} \omega (\delta B_{\perp}/B_0)^2, \tag{5.26}$$

where ω is the linear wave frequency at the scale where the dynamics generates the largest pressure anisotropy, thus leading to the maximum instability growth rate. Since the turbulent fluctuation amplitudes generally decrease monotonically with scale, the kinetic temperature anisotropy instabilities will be driven most strongly by turbulent fluctuations at the driving scale. As with the case for magnetic pumping by compressible fluctuations that is dominated by the driving-scale dynamics, here, we must use the three driving parameters ($k_{\perp,0}\rho_i, k_{\parallel,0}/k_{\perp,0}, \chi_0$) in table 3, rather than $k_0\rho_i$, to estimate the turbulent damping rate by the kinetic viscosity.

Using the effective collision frequency ν_{eff} above as an estimate of the damping rate by this kinetic viscous heating γ_{VH} , we can calculate the ratio of the damping rate arising from kinetic viscous heating to the wave frequency at the driving scale, obtaining

$$\frac{\gamma_{\text{VH}}}{\omega} \sim \beta_{\parallel,i} \left(\chi_0 \frac{k_{\parallel,0}}{k_{\perp,0}} \right)^2, \tag{5.27}$$

where the definition of the nonlinearity parameter $\chi_0 = (k_{\perp 0}/k_{\parallel 0})(\delta B_{\perp 0}/B_0)\theta_0$ with $\theta_0 = 1$ at the driving scale is used to replace the amplitude of the driving-scale turbulent fluctuations $\delta B_{\perp 0}/B_0$.

In summary, the kinetic viscous heating due to ion temperature anisotropy instabilities arising from the non-thermal velocity distributions driven by the large-scale turbulent motions occurs in weakly collisional turbulent plasmas with parallel ion plasma beta $\beta_{\parallel, i} \gg 1$. The kinetic viscous damping rate depends on the parallel ion plasma beta $\beta_{\parallel, i}$, the nonlinearity parameter χ_0 , and the anisotropy of the turbulent driving $k_{\perp 0}/k_{\parallel 0}$. It is important to keep in mind that the scaling used to derive the form of the effective collision frequency ν_{eff} depends on the scaling of the marginal stability boundaries that are generally calculated in quiescent plasmas in the absence of turbulence. The scaling of the marginal stability boundaries – such as those quantified by (5.25) and the coefficients in table 6 – may differ in the presence of strong plasma turbulence, although evidence from spacecraft observations (Hellinger *et al.* 2006; Bale *et al.* 2009; Maruca *et al.* 2011) and from hybrid kinetic ion and fluid electron simulations of temperature anisotropic plasma turbulence (Kunz *et al.* 2014; Bott *et al.* 2021; Arzamasskiy *et al.* 2023) appear to suggest that any modifications of these boundaries due to the presence of turbulence are relatively small.

5.9. Collisionless magnetic reconnection

Numerical simulations of plasma turbulence demonstrate the ubiquitous development of current sheets at small scales (Matthaeus & Montgomery 1980; Meneguzzi *et al.* 1981; Biskamp & Welter 1989; Spangler 1998, 1999; Biskamp & Müller 2000; Maron & Goldreich 2001; Merrifield *et al.* 2005; Greco *et al.* 2008), and it has been found that the dissipation of the turbulence is largely concentrated in the vicinity of these current sheets (Uritsky *et al.* 2010; Wan *et al.* 2012; Karimabadi *et al.* 2013; TenBarge & Howes 2013; Wu *et al.* 2013; Zhdankin *et al.* 2013), giving rise to the proposal that magnetic reconnection may play a role in the damping of plasma turbulence. Motivated by these findings, statistical analyses of observations of turbulence in the solar wind have sought evidence for such spatially localized heating (Borovsky & Denton 2011; Osman *et al.* 2011, 2012a, b; Perri *et al.* 2012; Wang *et al.* 2013; Wu *et al.* 2013; Osman *et al.* 2014b). Yet the physical mechanisms that lead to the development of these current sheets in plasma turbulence is yet to be fully understood.

Under the B06 theory for the scaling of MHD turbulence, the phenomenon of dynamic alignment (Boldyrev 2006) is predicted to lead to the development of current sheets with a width $w \sim 1/k_i$ to thickness $a \sim 1/k_{\perp}$ ratio in the plane perpendicular to the magnetic field given by $w/a = k_{\perp}/k_i = [(k_{\perp}\rho_i)/(k_0\rho_i)]^{1/4}$, according to the scaling in (3.2) for $\alpha = 1$. The geometry of the current sheets expected to develop in plasma turbulence is illustrated in figure 9, where for sufficiently small perpendicular scales relative to the driving scale, $k_{\perp}\rho_i \gg k_0\rho_i$, the current sheets have a parallel extent along the mean magnetic field \mathbf{B}_0 , given by $l \sim 1/k_{\parallel}$, and a scale separation of thickness to width to length obeying $a \ll w \ll l$; the corresponding three components of the wavevector have the complementary scaling $k_{\parallel} \ll k_i \ll k_{\perp}$. In figure 9, the wavelength of a mode that is unstable to the collisionless tearing instability is illustrated by $\lambda \sim 1/k$ (red). Note that the minimum value of this tearing unstable wavenumber k is equal to the intermediate wavenumber k_i corresponding to the width of the current sheet, $w \sim 1/k_i$. The maximum value of k assumed in calculations of the linear collisionless tearing instability (Loureiro & Boldyrev 2017a; Mallet *et al.* 2017b) must be much smaller than the perpendicular wavenumber k_{\perp} characterizing the current sheet thickness ($a \sim 1/k_{\perp}$), thereby yielding

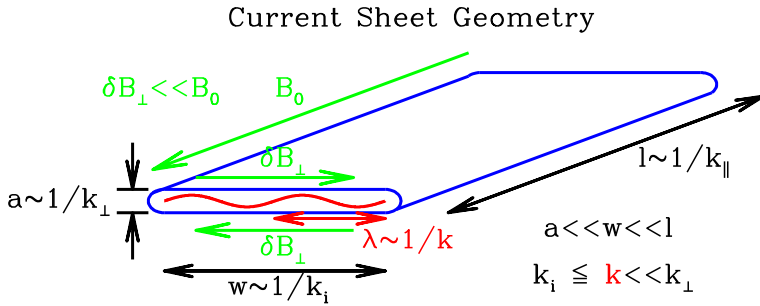


FIGURE 9. Diagram of the current sheet geometry generated self-consistently in plasma turbulence in the MHD regime at $k_{\perp}\rho_i \lesssim 1$, with the scalings of $(k_{\perp}, k_i, k_{\parallel})$ given by the B06 scaling. The current sheet has thickness $a \sim 1/k_{\perp}$ and width $w \sim 1/k_i$ in the perpendicular plane and length $l \sim 1/k_{\parallel}$ along the equilibrium magnetic field B_0 . The wavelength of the mode unstable to the collisionless tearing instability is given by $\lambda \sim 1/k$ (red), and must fall within the bounds determined by the current sheet scaling, yielding an ordering $k_i \lesssim k \ll k_{\perp}$.

$k/k_{\perp} = ka \ll 1$. Thus, the range of the unstable wavenumbers k is given by

$$k_i\rho_i = (k_0\rho_i)^{1/4}(k_{\perp}\rho_i)^{3/4} \lesssim k\rho_i \ll k_{\perp}\rho_i \lesssim 1, \quad (5.28)$$

where the final constraint $k_{\perp}\rho_i \lesssim 1$ is needed for the tearing instability to arise for a current sheet thickness within the MHD regime, otherwise different scalings for electron-only reconnection (Phan *et al.* 2018) in the regime $k_{\perp}\rho_i \gtrsim 1$ would need to be incorporated.

Note that, in turbulence obeying the B06 scaling, the self-consistent generation of current sheets arises only at sufficiently small perpendicular scales relative to the driving scale, $k_{\perp}\rho_i \gg k_0\rho_i$. Therefore, the ratio of the perpendicular magnetic field perturbation to the mean magnetic field will be small, $\delta B_{\perp}/B_0 = (k_0\rho_i/k_{\perp}\rho_i)^{1/4} \ll 1$, so the reconnection that arises in plasma turbulence necessarily falls in the limit of strong-guide-field magnetic reconnection, as illustrated in figure 9 (green). An implication of this fact is that, if numerical simulations are employed to assess the importance of magnetic reconnection in turbulence, it is critical that those simulations be modelled in three spatial dimensions. Previous studies of two-dimensional vs. three-dimensional plasma turbulence have shown that three-dimensional simulations exhibit a significantly faster turbulent cascade rate (Li *et al.* 2016), so enabling full three-dimensional evolution is likely to be essential to determine the competition between the turbulent cascade and magnetic reconnection.

The tearing instability growth rate typically increases with an increasing perpendicular aspect ratio w/a ratio of the current sheets. If this ratio reaches a sufficiently large value, it was recently recognized that the growth rate of the tearing instability could exceed the turbulent cascade rate at that scale, $\gamma/\omega_{nl} \gtrsim 1$, triggering a reconnection flow that would disrupt the turbulent dynamics, deviating from the scaling relations summarized in § 3. Such changes in the scaling of the turbulent fluctuations may potentially lead to differences in which physical mechanisms dominate the damping of the turbulent cascade at small scales (Boldyrev & Loureiro 2017; Loureiro & Boldyrev 2017a, b; Mallet *et al.* 2017a, b; Walker *et al.* 2018).

It is worth noting here that an alternative explanation for the development of current sheets in plasma turbulence due to the nonlinear interactions between counterpropagating Alfvén waves – a phenomenon often denoted Alfvén wave collisions (Howes & Nielson 2013) – was proposed by Howes (2016), but no scaling for the resulting aspect ratio of the current sheets was provided. If the scaling of this alternative mechanism differs from that

of the B06 theory, than the scaling predictions for the onset of reconnection would also change.

Here, we adopt the B06 scaling for the development of current sheets, with the goal to determine the dependence of magnetic reconnection as a turbulent damping mechanism on the fundamental plasma and turbulence parameters for the isotropic temperature case in table 4. This calculation follows previous investigations that assess the conditions under which collisionless magnetic reconnection may disrupt the turbulent cascade and thereby impact how the turbulent energy is channelled into particle energy (Loureiro & Boldyrev 2017a; Mallet *et al.* 2017b).

The growth rate of the collisionless tearing instability, which is the instability that initiates the process of magnetic reconnection under the weakly collisional conditions typical of space and astrophysical plasmas, has been derived in the limit of very low electron plasma beta $\beta_e \sim \mu^{-1}$ (Zocco & Schekochihin 2011), where we convert $\beta_e = \beta_i/\tau$. The physics of the collisionless tearing instability depends on three length scales: (i) the thickness of the current sheet $a \sim 1/k_{\perp}$, assumed here to occur on MHD scales with $k_{\perp}\rho_i \ll 1$; (ii) the ion sound Larmor radius $\rho_s \equiv \rho_i/(2\tau)^{1/2}$ where two fluid effects begin to lead to differences between the ion and electron dynamics; and (iii) the inner boundary layer scale δ_{in} where the magnetic flux can be unfrozen from the electron fluid flow. We will restrict our analysis to $\beta_e \gg \mu^{-1}$, such that the flux unfreezing arises from electron inertia (Zocco & Schekochihin 2011; Loureiro & Boldyrev 2017a; Mallet *et al.* 2017b), occurring approximately at the electron inertial length scale $d_e \equiv c/\omega_{pe} = \rho_i/(\beta_i\mu)^{1/2}$. These scales are ordered by $\delta_{in} \sim d_e \ll \rho_s \ll a$. Together, these restrictions limit us to moderately small plasma beta

$$\mu^{-1} \ll \beta_i/\tau \ll 1. \tag{5.29}$$

The tearing instability depends on the tearing mode instability parameter Δ' , determined by the outer-region solution (at MHD scales $k_{\perp}\rho_i \ll 1$) (Zocco & Schekochihin 2011). This parameter can be expressed over two limiting regimes in a dimensionless form (Loureiro & Boldyrev 2017a) as

$$\Delta' a = (ka)^{-n} \quad \text{for } 1 < n \leq 2, \tag{5.30}$$

where k is the unstable wavenumber along the width of the current layer governing the reconnection flow, as illustrated in figure 9 by the red sinusoidal curve. Here $n = 1$ corresponds to a Harris current sheet (a hyperbolic tangent profile of the reconnecting magnetic field across the current sheet thickness, Harris 1962), while $n = 2$ corresponds to a sinusoidal variation of the reconnection magnetic field (Loureiro & Boldyrev 2017a), which may be the more likely case for the onset of reconnection at current sheets that self-consistently arise in a turbulent plasma. The tearing instability growth rates are solved in two limits of Δ' (Zocco & Schekochihin 2011; Loureiro & Boldyrev 2017a; Mallet *et al.* 2017b): (i) $\Delta'\delta_{in} \ll 1$

$$\gamma \sim kv_{A\perp} \frac{d_e \rho_s \Delta'}{a} \quad \text{with } \delta_{in} \sim d_e \rho_s^{1/2} \Delta'^{1/2}, \tag{5.31}$$

and (ii) $\Delta'\delta_{in} \gtrsim 1$

$$\gamma \sim kv_{A\perp} \frac{d_e^{1/3} \rho_s^{2/3}}{a} \quad \text{with } \delta_{in} \sim d_e^{2/3} \rho_s^{1/3}, \tag{5.32}$$

where $v_{A\perp} \equiv \delta B_{\perp}/(4\pi n_i m_i)^{1/2}$ is the Alfvén speed based on the magnitude of only the reconnecting component of the magnetic field δB_{\perp} . Since the growth rates above are calculated in the limit $k_{\perp}\rho_i \ll 1$, we will focus our assessment on whether magnetic reconnection will disrupt the turbulent cascade at MHD scales $k_{\perp}\rho_i \lesssim 1$, which is the same approach as taken in previous studies (Loureiro & Boldyrev 2017a; Mallet *et al.* 2017b).

Using (5.30) and either (5.31) or (5.32) for δ_{in} , the normalized tearing mode instability parameter $\Delta'\delta_{in}$ can be expressed in terms of the dimensionless quantities in table 4 by

$$\Delta'\delta_{in} = \frac{k_{\perp}\rho_i}{(2\tau\beta_i^2\mu^2)^{1/6}} \left(\frac{k_{\perp}\rho_i}{k\rho_i}\right)^n. \tag{5.33}$$

This equation shows that $\Delta'\delta_{in}$ increases as the perpendicular wavenumber $k_{\perp}\rho_i$ increases, corresponding to a thinner current sheet, or as the unstable wavenumber $k\rho_i$ decreases, requiring to a wider current sheet. Since the width $w \sim 1/k_i$ of the current sheets in B06 scaling theory governed by (3.2) bounds the unstable wavenumber k from below by the intermediate wavenumber, $k > k_i$, the maximum value of instability parameter $\Delta'\delta_{in}$ increases with the perpendicular aspect ratio of the current sheets $w/a = k_{\perp}/k_i \gg 1$. Note also that $\Delta'\delta_{in} \propto \beta_i^{-1/3}$, so that lower values of ion plasma beta also lead to a larger instability parameter.

Note that the value of the unstable wavenumber $k\rho_i$ at the transition between the limiting regimes of the tearing mode instability parameter, where $\Delta'\delta_{in} = 1$, is given by

$$k\rho_i = k_t\rho_i \equiv \frac{(k_{\perp}\rho_i)^{(n+1)/n}}{(2\tau\beta_i^2\mu^2)^{1/6n}}, \tag{5.34}$$

which provides a bound on the value of $k\rho_i$ for the validity of the tearing growth rate formulas in (5.31) and (5.32).

To assess whether the collisionless tearing instability grows fast enough to enable the onset of magnetic reconnection to disrupt the turbulent cascade, we will assess $\gamma_{RXN}/\omega_{nl} \sim \gamma_{RXN}/\omega$, assuming critical balance of linear and nonlinear time scales $\omega_{nl} \sim \omega$ (Goldreich & Sridhar 1995; Mallet *et al.* 2015). Taking the linear wave frequency for MHD Alfvén waves $\omega = k_{\parallel}v_A = (k_{\parallel}\rho_i)^{1/2}(k_{\perp}\rho_i)^{1/2}v_A/\rho_i$ using (3.1) with $\alpha = 1$ for the B06 scaling of k_{\parallel} , and substituting $v_{A\perp} = v_A(\delta B_{\perp}/B_0) = v_A[(k_0\rho_i)/(k_{\perp}\rho_i)]^{1/4}$ using (3.4), we find that the growth rate in the $\Delta'\delta_{in} \ll 1$ limit, which corresponds to the large unstable wavenumber k limit by inspection of (5.33), can be expressed as

$$\frac{\gamma_{RXN}}{\omega} \sim \frac{(k_{\perp}\rho_i)^{(5+4n)/4}}{(k\rho_i)^{n-1}(k_0\rho_i)^{1/4}(2\tau\beta_i\mu)^{1/2}}, \tag{5.35}$$

where this expression is formally valid in the MHD limit with $k_{\perp}\rho_i \ll 1$. Combining the limitations on the possible unstable wavenumber from (5.28) and the requirement $\Delta'\delta_{in} \lesssim 1$ using (5.34), the formula in (5.35) is valid over the range of normalized unstable wavenumbers

$$\max \left[(k_0\rho_i)^{1/4}(k_{\perp}\rho_i)^{3/4}, \frac{(k_{\perp}\rho_i)^{(n+1)/n}}{(2\tau\beta_i^2\mu^2)^{1/6n}} \right] \lesssim k\rho_i \ll k_{\perp}\rho_i \lesssim 1. \tag{5.36}$$

Note that this valid unstable wavenumber range can be used to show that no range with $\Delta'\delta_{in} \lesssim 1$ exists if $\beta_i \lesssim (2\tau\mu^2)^{-1/2}$. For typical values of $\tau \sim 1$, however, the very low

values of β_i required to violate this condition would already have violated the assumed moderate beta limit given by (5.29), so this limitation is of no practical concern.

The tearing growth rate in (5.35) demonstrates that, in the large k limit, the normalized growth rate is independent of k with $\gamma_{\text{RXN}}/\omega \propto k^0$ for Harris-type current sheets with $n = 1$, and is inversely proportional to k with $\gamma_{\text{RXN}}/\omega \propto k^{-1}$ for the $n = 2$ case of sinusoidal variations of the perpendicular magnetic field component that may be expected to occur in plasma turbulence.

The maximum growth rate $\gamma_{\text{RXN}}/\omega$ from (5.35) increases with $k_{\perp}\rho_i$, but also requires the limit $k_{\perp}\rho_i \ll 1$ for the validity of this linear tearing growth-rate calculation. Therefore, to estimate quantitatively the maximum normalized tearing growth rate, we take $k_{\perp}\rho_i \rightarrow \mathcal{F}$, where $\mathcal{F} \ll 1$ is the maximum value of the normalized perpendicular wavenumber for which (5.35) remains valid; numerical simulations of collisionless magnetic reconnection will be invaluable to provide estimates of the maximum value of \mathcal{F} . The maximum growth rate $\gamma_{\text{RXN}}/\omega$ also occurs for the minimum unstable wavenumber $k\rho_i$ allowed by the range in (5.36). Thus, taking these two limits and requiring a collisionless tearing instability growth rate sufficient to disrupt the turbulent cascade, $\gamma_{\text{RXN}}/\omega \gtrsim 1$, yields the constraint

$$k_0\rho_i \lesssim \frac{\mathcal{F}^{(4+5n)/n}}{(2\tau)^{(4n+2)/3n}(\beta_i\mu)^{(2n+4)/3n}}, \quad (5.37)$$

if the minimum $k\rho_i$ is constrained by the condition $\Delta'\delta_{in} \lesssim 1$. Alternatively, if the minimum $k\rho_i$ is constrained by the width of the current sheet given by (5.28), then the condition $\gamma_{\text{RXN}}/\omega \gtrsim 1$ yields the constraint

$$k_0\rho_i \lesssim \frac{\mathcal{F}^{(5+4n)/n}}{(2\tau\beta_i\mu)^{2/n}}. \quad (5.38)$$

The normalized growth rates in the $\Delta'\delta_{in} \lesssim 1$ limit vs. normalized unstable wavenumber $k\rho_i$ are illustrated in figure 10(a) for $n = 1$ (thin blue) and $n = 2$ (thick blue) for turbulent parameters $\beta_i = 0.01$, $\tau = 1$, $\mu = 1836$ and $k_0\rho_i = 10^{-4}$ and for three values of the maximum of $k_{\perp}\rho_i$ given by $\mathcal{F} = 1.0$ (solid), 0.3 (dashed) and 0.1 (dotted). The corresponding values of $\Delta'\delta_{in}$ vs. $k\rho_i$ are presented in figure 10(b) for each of the n and $k_{\perp}\rho_i$ cases. For the turbulence parameters specified in this example, we find $\gamma_{\text{RXN}}/\omega \gtrsim 1$ only for the $\mathcal{F} = k_{\perp}\rho_i = 1.0$ case over the unstable wavenumber range $0.3 \lesssim k\rho_i \lesssim 1$ for the $n = 1$ case (thin solid blue) and over $0.6 \lesssim k\rho_i \lesssim 1$ for the $n = 2$ case (thick solid blue).

Next, we assess the initiation of collisionless tearing in the $\Delta'\delta_{in} \gtrsim 1$ limit with the growth rate given by (5.32). Using similar substitutions for ω and $v_{A\perp}$ (as detailed above for the $\Delta'\delta_{in} \ll 1$ limit), we find that the growth rate in the $\Delta'\delta_{in} \gtrsim 1$ limit, which is the small unstable wavenumber k limit as shown by (5.33), can be expressed as

$$\frac{\gamma_{\text{RXN}}}{\omega} \sim \frac{(k\rho_i)(k_{\perp}\rho_i)^{1/4}}{(k_0\rho_i)^{1/4}(4\tau^2\beta_i\mu)^{1/6}}, \quad (5.39)$$

where this expression is formally valid in the MHD limit with $k_{\perp}\rho_i \ll 1$. Combining the limitations on the possible unstable wavenumber from (5.28) and the requirement $\Delta'\delta_{in} \gtrsim 1$ using (5.34), the formula in (5.39) is valid over the range of normalized unstable

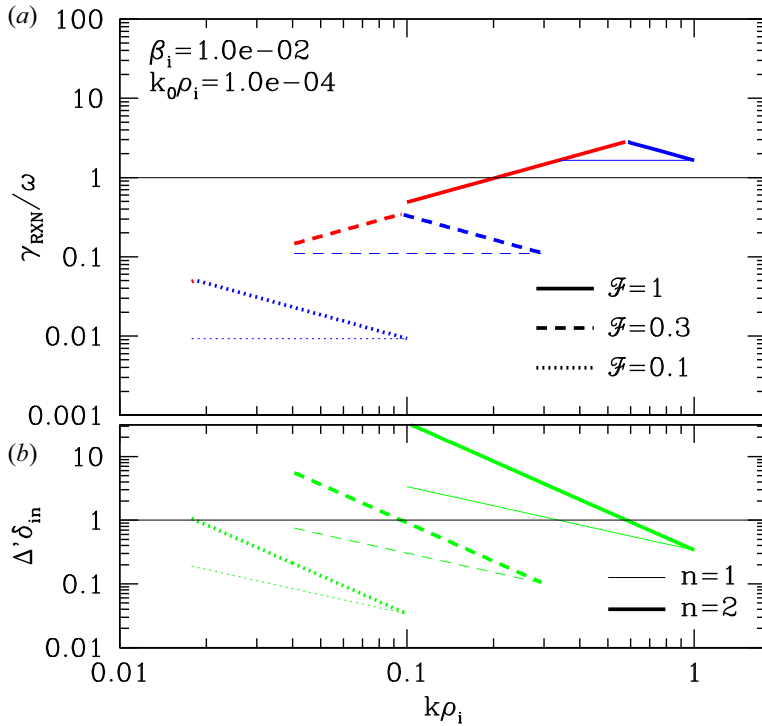


FIGURE 10. (a) Scaling the normalized collisionless tearing instability growth rate γ_{RXN}/ω for a turbulent plasma with $\beta_i = 0.01$, $\tau = 1$, $\mu = 1836$ and $k_0\rho_i = 10^{-4}$ as a function of the normalized unstable wavenumber $k\rho_i$. Colours indicate the solutions in the low k limit (corresponding to $\Delta'\delta_{in} \gtrsim 1$) (red) and in the high k limit (corresponding to $\Delta'\delta_{in} \ll 1$) (blue). Line thickness indicates the either a sinusoidal current profile with $n = 2$ (thick) or a Harris-like hyperbolic tangent current profile with $n = 1$ (thin). Line styles indicate different values of maximum perpendicular wavenumber $\mathcal{F} = 1.0$ (solid), 0.3 (dashed) and 0.1 (dotted). (b) The corresponding normalized tearing mode instability parameter $\Delta'\delta_{in}$ vs. $k\rho_i$ for each case.

wavenumbers

$$(k_0\rho_i)^{1/4}(k_{\perp}\rho_i)^{3/4} \lesssim k\rho_i \ll \max \left[k_{\perp}\rho_i, \frac{(k_{\perp}\rho_i)^{(n+1)/n}}{(2\tau\beta_i^2\mu^2)^{1/6n}} \right] \lesssim 1. \tag{5.40}$$

This valid unstable wavenumber range can be used to show that no range with $\Delta'\delta_{in} \gtrsim 1$ exists if

$$k_{\perp}\rho_i \lesssim (k_0\rho_i)^{n/(n+4)}(2\tau\beta_i^2\mu^2)^{2/3(n+4)}. \tag{5.41}$$

This finding is consistent with the fact that the value of $\Delta'\delta_{in}$ decreases with decreasing $k_{\perp}\rho_i$ in (5.33), so by decreasing $k_{\perp}\rho_i$ enough, one will always reach a point where there is no range of $k\rho_i$ with $\Delta'\delta_{in} \gtrsim 1$.

The tearing growth rate in (5.39) shows that, in the small k limit, the normalized growth rate increases linearly with the unstable wavenumber k and increases weakly with the perpendicular wavenumber $k_{\perp}\rho_i$, independent of whether the turbulently generated current sheets are Harris-like or sinusoidal (thus, independent of n).

Once again the maximum growth rate γ_{RXN}/ω from (5.39) increases with $k_{\perp}\rho_i$ (although weakly with the $1/4$ power), so once again we take the limit $k_{\perp}\rho_i \rightarrow \mathcal{F}$, where $\mathcal{F} \ll 1$

is the maximum value of the normalized perpendicular wavenumber for which (5.39) remains valid. The maximum growth rate will also occur for the maximum unstable wavenumber $k\rho_i$ given by (5.40). Thus, taking these two limits and requiring a collisionless tearing instability growth rate sufficient to disrupt the turbulent cascade, $\gamma_{\text{RXN}}/\omega \gtrsim 1$, yields the constraint

$$k_0\rho_i \lesssim \frac{\mathcal{F}^{(4+5n)/n}}{(2\tau)^{(4n+2)/3n}(\beta_i\mu)^{(2n+4)/3n}}, \quad (5.42)$$

if the maximum $k\rho_i$ is constrained by the condition $\Delta'\delta_{in} \gtrsim 1$. Note that this condition is the same as (5.37), as it must be since this maximum growth rate occurs at $\Delta'\delta_{in} = 1$, where the growth rates for the $\Delta'\delta_{in} \lesssim 1$ and $\Delta'\delta_{in} \gtrsim 1$ limits cross. Alternatively, if the maximum $k\rho_i$ is constrained by the maximum $k_{\perp}\rho_i \rightarrow \mathcal{F}$, then the condition $\gamma_{\text{RXN}}/\omega \gtrsim 1$ yields the constraint

$$k_0\rho_i \lesssim \frac{\mathcal{F}^{(5+4n)/n}}{(4\tau^2\beta_i\mu)^{2/3}}. \quad (5.43)$$

The normalized growth rates in the $\Delta'\delta_{in} \gtrsim 1$ limit vs. normalized unstable wavenumber $k\rho_i$ are illustrated in figure 10(a) (thick red) for turbulent parameters $\beta_i = 0.01$, $\tau = 1$, $\mu = 1836$ and $k_0\rho_i = 10^{-4}$ and for three values of the maximum of $k_{\perp}\rho_i$ given by $\mathcal{F} = 1.0$ (solid), 0.3 (dashed) and 0.1 (dotted). The corresponding values of $\Delta'\delta_{in}$ vs. $k\rho_i$ are presented in figure 10(b) for each of the n and $k_{\perp}\rho_i$ cases. For the turbulence parameters specified in this example, we find $\gamma_{\text{RXN}}/\omega \gtrsim 1$ only for the $k_{\perp}\rho_i = 1.0$ case over the unstable wavenumber range $0.2 \lesssim k\rho_i \lesssim 0.3$ for the $n = 1$ case (thick solid red) and over $0.2 \lesssim k\rho_i \lesssim 0.6$ for the $n = 2$ case (thick solid red).

It is necessary to highlight here a few important caveats in using the linear collisionless tearing mode growth rates and MHD turbulence scaling theory to predict when magnetic reconnection may disrupt the dynamics of the turbulent cascade. First, the linear tearing mode growth rates used here are rigorously derived in asymptotic limits, but we employ these same rates up to the extreme boundary of those limits. For example, the linear growth rates formally require $k_{\perp}\rho_i \ll 1$, but we take $k_{\perp}\rho_i \rightarrow 1$ to estimate the maximum growth rate; also, the $\Delta'\delta_{in} \ll 1$ limit is used to estimate the tearing mode growth rates as $\Delta'\delta_{in} \rightarrow 1$. Such rates derived in asymptotic limits, however, may not remain quantitatively accurate as we extend beyond their formal regime of validity. We adopt the viewpoint that the growth rates calculated in these limits are at least reasonable lowest-order estimates of the rates even beyond their formally limited range. Furthermore, the growth rates for the collisionless tearing mode are determined under smooth conditions, whereas to determine whether reconnection arises in the current sheets that naturally arise in plasma turbulence, one needs to determine the collisionless tearing growth rates in the presence of turbulence; once again, the estimated tearing mode growth rates used here are taken simply as the lowest-order estimation. Computing the tearing mode growth rates in a turbulent plasma and determining the competition of the tearing mode with the nonlinear cascade of energy due to turbulence are both necessary for more accurate calculations, which likely will require detailed kinetic numerical simulations. Finally, alternative proposed mechanisms for the development of current sheets in plasma turbulence – such as the nonlinear interaction of counterpropagating Alfvén wave collisions (Howes 2016), as opposed to dynamic alignment (Boldyrev 2006) – may yield a different scaling for the width and thickness of current sheets; the resulting predictions for the onset of magnetic reconnection in a turbulent plasma would thereby also likely change.

In summary, we have followed previous investigations (Loureiro & Boldyrev 2017a; Mallet *et al.* 2017b) to estimate how the collisionless tearing mode may arise in the

current sheets that develop self-consistently in plasma turbulence, potentially disrupting the nonlinear cascade of turbulent energy to small scales. We restrict ourselves to the moderately low electron plasma beta limit $\mu^{-1} \ll \beta_e \ll 1$, which can be expressed in terms of the plasma and turbulence parameters in table 4 as the limit $1 \ll \beta_i \mu / \tau \ll \mu$. In this limit, magnetic flux conservation is broken due to electron inertia at electron inertial length scales d_e (Zocco & Schekochihin 2011; Loureiro & Boldyrev 2017a; Mallet *et al.* 2017b). We consider only the case when collisionless magnetic reconnection arises in current sheets with thicknesses $a \sim 1/k_{\perp}$ in the MHD regime $k_{\perp} \rho_i \lesssim 1$. We find that the growth rate of reconnection relative to the turbulent fluctuation frequencies $\gamma_{\text{RXN}}/\omega$ is a function of the isotropic driving wavenumber $k_0 \rho_i$, ion plasma beta β_i , and ion-to-electron temperature ratio τ , as well as the ion-to-electron mass ratio μ .

In general, the normalized collisionless tearing instability growth rates $\gamma_{\text{RXN}}/\omega$ – given by (5.35) in the $\Delta' \delta_{in} \ll 1$ limit and by (5.39) in the $\Delta' \delta_{in} \gtrsim 1$ limit – increase as both $k_0 \rho_i$ and β_i decrease. For specified values of the plasma parameters β_i and τ , we obtain different conditions on how small $k_0 \rho_i$ must be for reconnection to arise, given by (5.37) and (5.38) in the $\Delta' \delta_{in} \ll 1$ limit and by (5.42) and (5.43) in the $\Delta' \delta_{in} \gtrsim 1$ limit. These scalings mean that reconnection is more likely to arise in turbulence with a very large driving scale relative to the ion Larmor-radius scale – meaning a smaller value of $k_0 \rho_i \ll 1$ – and for low ion plasma beta conditions $\beta_i \ll 1$.

It is worthwhile emphasizing that these estimates on the importance of magnetic reconnection in plasma turbulence are calculated only for current sheets with a thickness $a \sim 1/k_{\perp}$ in the MHD regime $k_{\perp} \rho_i \ll 1$ so that the MHD scaling predictions in § 3 apply. It is also possible that electron-only magnetic reconnection (Phan *et al.* 2018) could occur within the range of scales in the kinetic dissipation range $k_{\perp} \rho_i \gtrsim 1$, but to estimate whether this will occur would require the use of modified turbulence scalings appropriate for the dissipation range (Howes *et al.* 2008a, 2011a).

Finally, how the incorporation of magnetic reconnection into the turbulent cascade impacts the damping of the turbulence and the resulting energization of the plasma remains an open question. Collisionless magnetic reconnection effectively converts magnetic energy into other forms, specifically the kinetic energy of the bulk plasma outflows and possibly internal energy in the particle velocity distribution functions (Drake *et al.* 2005; Egedal *et al.* 2008; Drake & Swisdak 2012; Egedal, Daughton & Le 2012; Loureiro, Schekochihin & Zocco 2013; Janssen *et al.* 2018; Muñoz & Büchner 2018; Pucci *et al.* 2018; Dahlin 2020; McCubbin, Howes & TenBarge 2022). But such conversion between magnetic energy and the bulk kinetic energy of turbulent plasma motions already occurs ubiquitously in plasma turbulence: the linear terms in the equations of evolution for the turbulent plasma mediate the ongoing oscillation of energy from magnetic energy to the kinetic energy of the turbulent bulk plasma motions and back (Howes 2015a). For example, the physics of undamped Alfvén waves involve the transformation of the bulk kinetic energy of the perpendicular wave motions to magnetic energy as the frozen-in magnetic field is stretched; magnetic tension serves as the restoring force for the wave, decelerating the perpendicular wave motions and ultimately re-accelerating them back towards the state where the magnetic field is not bent, thereby converting magnetic energy back to kinetic energy. Thus, collisionless magnetic reconnection does not necessarily lead directly to damping of the turbulent motions (unless a significant fraction of the released magnetic energy is converted into internal energy of the particle velocity distributions), but rather is simply a channel, in addition to magnetic tension, for converting magnetic to kinetic energy. The triggering of magnetic reconnection, however, will impact the scaling of the characteristic three-dimensional wavevector of the turbulent motions that result from the reconnection flow (Boldyrev & Loureiro 2017; Loureiro & Boldyrev

2017a, b; Mallet *et al.* 2017a, b; Walker *et al.* 2018), and these different scalings may channel energy through different kinetic physical mechanisms that ultimately transfer turbulent energy to internal particle energy. Furthermore, the onset of reconnection in the turbulent cascade will alter the spectral index of the turbulent energy spectrum as a function of wavenumber, and will also reduce intermittency since the largest-amplitude current sheets will preferentially succumb to the tearing instability. Thus, the partitioning of turbulent energy between ions and electrons, Q_i/Q_e , and between degrees of freedom for both species, $Q_{\perp,i}/Q_{\parallel,i}$ and $Q_{\perp,e}/Q_{\parallel,e}$, remains to be ascertained in situations where collisionless magnetic reconnection is triggered in plasma turbulence.

6. Phase diagrams for plasmas turbulence

The scalings of the different proposed kinetic dissipation mechanisms listed in § 5.1 enable us to map the importance of the different mechanisms for the damping of turbulence as a function of the fundamental plasma parameters by creating phase diagrams for plasma turbulence, analogous to a similar effort to create a phase diagram for magnetic reconnection (Ji & Daughton 2011). Here, we present two such phase diagrams based on the plasma and turbulence parameters estimated for different space and astrophysical plasmas.

6.1. Collisionality of the dissipation range of plasma turbulence

We first create a phase diagram indicating that, for many plasmas of interest, even if the turbulence is driven at fluid scales with $k_{\parallel,0}\lambda_{\text{mfp},e} \ll 1$, the end of the inertial range generally occurs at scales that are weakly collisional. Therefore, the kinetic damping mechanisms analysed here are responsible for removing energy from the turbulent cascade, rather than viscosity and resistivity, which are based on microscopic Coulomb collisions between particles in the limit of strong collisionality (Braginskii 1965; Chapman & Cowling 1970). Since the mean free path must be compared with the parallel length scales of the turbulent fluctuations characterized by k_{\parallel} , we must first determine the parallel length scales associated with the small-scale end of the inertial range at the transition to the dissipation range, corresponding to a perpendicular scale $k_{\perp}\rho_i \sim 1$. Specifying the GS95 scaling with $\alpha = 0$ for this example, the parallel wavenumber at the transition to the dissipation range $k_{\parallel T}$, determined by (3.1), is given by $k_{\parallel T}\rho_i = (k_0\rho_i)^{1/3}(k_{\perp}\rho_i)^{2/3} = (k_0\rho_i)^{1/3}$, here taking $k_{\perp}\rho_i \sim 1$ as the end of the inertial range. For simplicity, we assume here that the turbulence is driven strongly and isotropically with $\chi_0 = 1$ and $k_{\parallel 0}/k_{\perp 0} = 1$. Normalizing this parallel scale in terms of the electron collisional mean free path $\lambda_{\text{mfp},e}$, we obtain $k_{\parallel T}\lambda_{\text{mfp},e} = (k_0\rho_i)^{1/3}(\lambda_{\text{mfp},e}/\rho_i)$.

The range of plasma and turbulence parameters for a number of plasma systems of interest are denoted by the coloured boxes in figure 11. Plotted on the horizontal axis of figure 11 is the range of parallel scales bounding the turbulent inertial range normalized to the electron collisional mean free path $\lambda_{\text{mfp},e}$: (i) the normalized parallel driving scale $k_{\parallel 0}\lambda_{\text{mfp},e}$ of the turbulence is represented by the left end of each box; (ii) the turbulent energy cascades to smaller scales to the right within each box (wavy red arrow below plot); and (iii) the parallel scale corresponding to the small-scale end of the inertial range at $k_{\parallel T}\lambda_{\text{mfp},e}$ is represented by the right end of each box. The vertical extent of the coloured boxes indicates the range of ion plasma beta β_i for each of the chosen systems. The fluid regime (yellow region) indicates conditions under which the dynamics of the turbulent fluctuations occurs on parallel scales that are strongly collisional with $k_{\parallel 0}\lambda_{\text{mfp},e} \ll 1$; the kinetic regime (light blue region) indicates conditions under which the dynamics of the turbulent fluctuations occurs on parallel scales that are weakly collisional with $k_{\parallel 0}\lambda_{\text{mfp},e} \gg 1$.

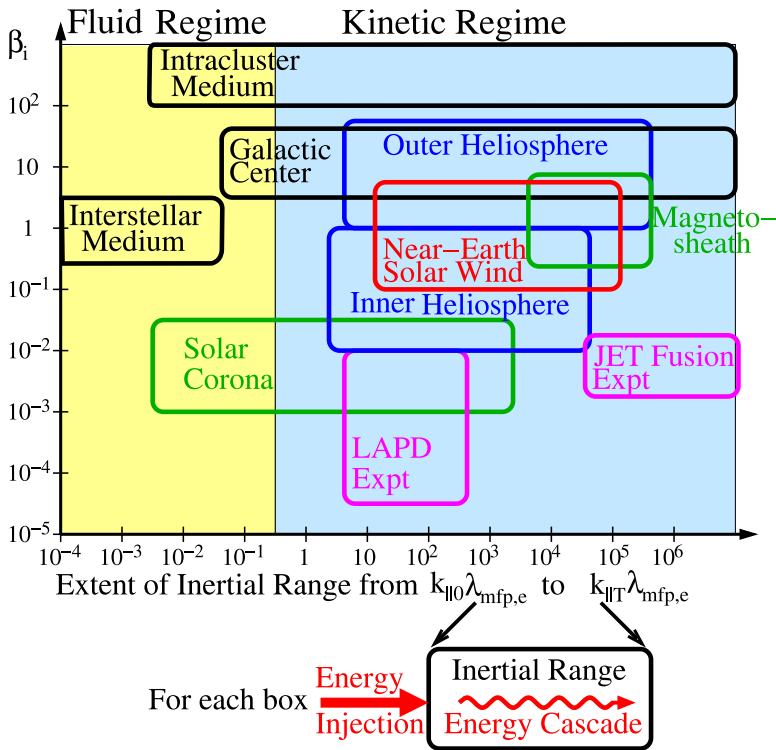


FIGURE 11. Phase diagram of the extent of the turbulent inertial range from driving scales at $k_{\parallel 0} \lambda_{mfpe}$ to the transition to the dissipation range at $k_{\parallel T} \lambda_{mfpe}$ vs. the ion plasma beta β_i . The plot indicates that, at the small-scale end of the inertial range where damping mechanisms can remove energy from the turbulence, for many plasma systems of interest the governing dynamics is weakly collisional with $k_{\parallel T} \lambda_{mfpe} \gg 1$, so kinetic plasma theory is necessary to capture the physics of turbulent dissipation.

In figure 11 are shown these parameter ranges for a variety of plasma systems: the near Earth solar wind (red); the Earth’s magnetosheath and the solar corona (green); the inner heliosphere at heliocentric radii $R \ll 1$ AU and the outer heliosphere at $R \gg 1$ AU (blue); the warm ionized interstellar medium, the Galactic centre and the intracluster medium (black); and terrestrial laboratory experiments including the Large Plasma Device (LAPD) at UCLA (Gekelman *et al.* 1991, 2016) and the Joint European Torus (JET) Fusion experiment (JET Team 1992). The main message of figure 11 is that, for most turbulent plasma systems of interest, the parallel length scales associated with the end of the inertial range correspond to weakly collisional plasma conditions with $k_{\parallel T} \lambda_{mfpe} \gg 1$. Therefore, to explore the physical damping mechanisms responsible for removing energy from the turbulent fluctuations and consequently energizing the plasma particles, plasma kinetic theory is essential.

6.2. Turbulent damping mechanisms on the $(\beta_i, k_0 \rho_i)$ plane

A single phase diagram that demonstrates the power of using the dimensionless plasma and turbulence parameters for the isotropic temperature case presented in table 4 is a plot of the predicted regions on the $(\beta_i, k_0 \rho_i)$ plane where different kinetic mechanisms are expected to play a role in the damping of weakly collisional plasma turbulence, presented

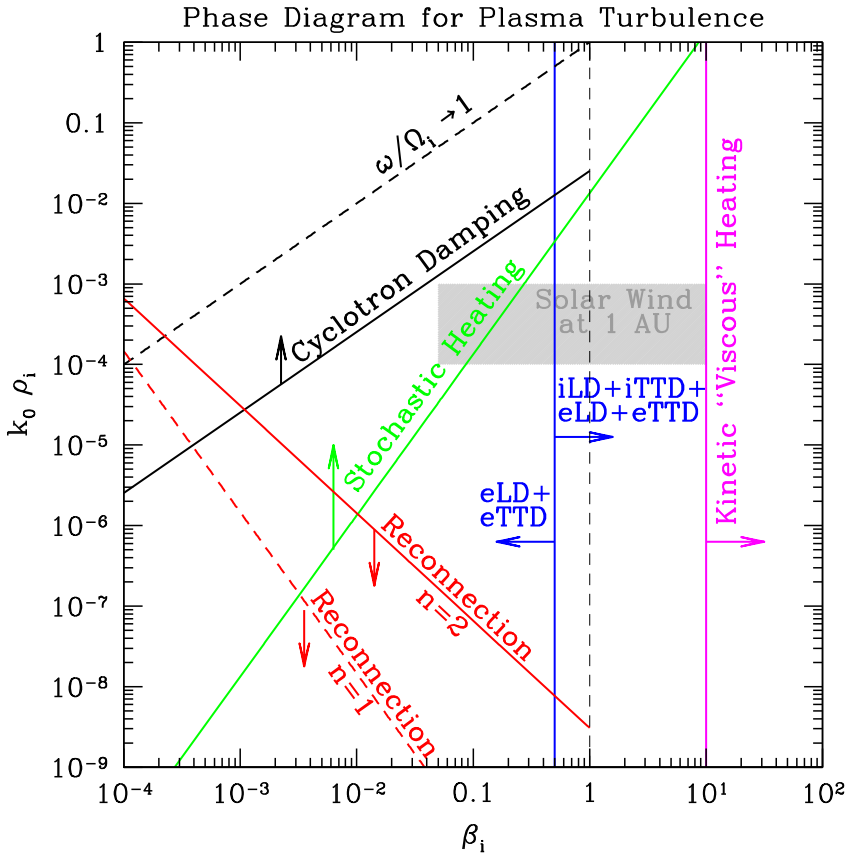


FIGURE 12. Phase diagram for the kinetic damping mechanisms of weakly collisional plasma turbulence as a function of isotropic driving wavenumber $k_0 \rho_i$ and ion plasma beta β_i , showing regions of this parameter space where different mechanisms are likely to contribute to the heating of the plasma species: iLD and iTTD (blue); eLD and eTTD (blue); ion cyclotron damping (iCD) (black); ion stochastic heating (iSH) (green); ion kinetic viscous heating (iVH) (magenta); and collisionless magnetic reconnection (RXN) (red) for intermittent current sheets ($n = 1$, red dashed) and sinusoidal current sheets ($n = 2$, red solid). The extent of the turbulent near-Earth solar wind on the $(\beta_i, k_0 \rho_i)$ plane is indicated (grey shading).

here in figure 12. This phase diagram of the turbulent damping mechanisms is the key result of this study.

For this phase diagram, we specify the ion-to-electron temperature ratio $\tau = 1$ and the ion-to-electron mass ratio $\mu = 1836$. For the isotropic temperature case, the species temperature anisotropies are $A_i = A_e = 1$, and we take the turbulence to be driven strongly ($\chi_0 = 1$) and isotropically ($k_{\parallel 0}/k_{\perp 0} = 1$) so that the turbulent driving can be characterized by the isotropic driving wavenumber $k_0 \rho_i$. Furthermore, we assume the turbulence driving to be balanced ($Z_0^+/Z_0^- = 1$) and incompressible ($E_{\text{comp}}/E_{\text{inc}} = 0$). In addition, the turbulence is assumed to be weakly collisional with $k_{\parallel 0} \lambda_{\text{mfp},e} \ll 1$, eliminating magnetic pumping as a potential turbulent damping mechanism. Finally, we specifically choose to use the B06 scaling for MHD turbulence with $\alpha = 1$ to assess the contributions of the different proposed damping mechanisms.

We use the dependencies discussed in § 5 of the proposed turbulent damping mechanisms on the dimensionless parameters in table 4 to assess the regions of the two-dimensional $(\beta_i, k_0\rho_i)$ parameter space over which each mechanism is expected to contribute.

For the Landau-resonant ($n = 0$) collisionless damping mechanisms – Landau damping (LD) and transit-time damping (TTD) – the primary parameter dependencies summarized in § 5.4 are β_i for iLD and iTTD and (β_i, τ, μ) for eLD and eTTD. Since the sum of LD and TTD for each species always leads to damping in the case of isotropic equilibrium temperatures, but separately the net energy transfer by either mechanism to that species over a full wave period can be positive or negative – as discussed in § 5.4 and illustrated in figure 7 – we do not separate the contributions of LD and TTD for a single species. Furthermore, since any turbulent cascade energy not deposited onto the ions by iLD and iTTD at the ion scales $k_\perp\rho_i \sim 1$ will cascade to $k_\perp\rho_i \gg 1$ and ultimately be transferred to the electrons, the partitioning of energy between ions and electrons by these Landau-resonant mechanisms is simply a function of β_i . Solutions of the linear Vlasov–Maxwell dispersion relation for the normalized ion damping rate by iLD and iTTD, $(\gamma_{iLD} + \gamma_{iTDD})/\omega$ indicate that ion damping is non-negligible for $\beta_i \gtrsim 0.5$, so iLD and iTTD will contribute in this region (blue line with right arrow), independent of the driving scale $k_0\rho_i$. For $\beta_i \lesssim 0.5$, eLD and eTTD will dominate the Landau-resonant damping (blue line with left arrow), but eLD and eTTD will still contribute to terminate the remaining turbulent cascade energy not removed by ions at $\beta_i \gtrsim 0.5$ (blue right arrow).

As discussed in § 5.5, ion cyclotron damping (iCD) will contribute to the damping of turbulence if the turbulent frequencies approach the ion cyclotron frequency $\omega/\Omega_i \rightarrow 1$, with the scaling of this ratio given by (5.10). We can solve this equation for $k_0\rho_i$ in terms of β_i with $\alpha = 1$ for the B06 scaling, yielding

$$k_0\rho_i = \left(\frac{\omega}{\Omega_i} \frac{1}{\bar{\omega}} \right)^2 \beta_i. \tag{6.1}$$

Taking the factor $(\omega/\Omega_i)/\bar{\omega} = 1$ gives an estimate for when $\omega/\Omega_i = 1$ (black dotted line), but iCD often becomes significant at lower values of the frequency, $\omega/\Omega_i \lesssim 1$. Thus, we estimate the onset of iCD by taking $(\omega/\Omega_i)/\bar{\omega} = 1/2\pi$ (black solid line and upward arrow).

The impact of ion stochastic heating (iSH) on turbulent fluctuations for the B06 scaling is given by (5.15) in § 5.6. The exponential dependence in this equation for γ_{SH}/ω yields a strong inhibition of iSH unless $c_2\beta_i^{1/2}(k_0\rho_i)^{-1/4} \lesssim 1$. Thus, we obtain a condition for $k_0\rho_i$ in terms of β_i for the onset of iSH, given by

$$k_0\rho_i \gtrsim c_2^4\beta_i^2. \tag{6.2}$$

Note that the dependence of this condition on c_2^4 means that an accurate determination of this constant is critical to assess the role of iSH on the damping of plasma turbulence. Taking the value of $c_2 = 0.34$ from Chandran *et al.* (2010), we plot (6.2) for the onset of ion stochastic heating (green line and upward arrow) on figure 12.

Kinetic viscous heating of ions mediated by temperature anisotropy instabilities²⁰ at high values of ion plasma beta $\beta_i \gg 1$ depends on the β_i and the amplitude of the turbulent fluctuations at the driving scale, as shown by (5.27) in § 5.8. Because this mechanism only contributes when β_i is sufficiently high that the temperature anisotropy can exceed

²⁰Recall that this mechanism is not the standard viscous heating mediated by microscopic Coulomb collisions between charged plasma particles, as emphasized in § 5.8.

the threshold values for the proton temperature anisotropy instabilities given by [table 6](#) and shown in [figure 8](#), we take the threshold for this kinetic damping mechanism to be dependent only on the value of the ion plasma beta, with an estimated onset at $\beta_i \gtrsim 10$ (magenta line and right arrow).

Finally, if the isotropic driving wavenumber $k_0\rho_i \ll 1$ and the ion plasma beta $\beta_i \ll 1$ of the turbulence are sufficiently low, current sheets with a large width-to-thickness ratio in the plane perpendicular to the equilibrium magnetic field can be unstable to a rapid collisionless tearing instability in the large-guide-field limit, as detailed in § 5.9. If growth rate of the tearing instability is faster than the rate of the nonlinear cascade of energy to small scales in the turbulence $\gamma_{\text{RXN}}/\omega_{nl} \gtrsim 1$, collisionless magnetic reconnection can disrupt the turbulent cascade. The condition that the normalized collisionless tearing instability growth rate satisfies $\gamma_{\text{RXN}}/\omega \gtrsim 1$ (for the unstable wavenumber with the maximum growth rate) is given by either (5.37) or (5.42) (both expressions yield the same maximum value at the transitional value of $\Delta'\delta_{in} = 1$). In these expressions, $n = 1$ corresponds to a Harris-like current sheet with a hyperbolic tangent profile, and $n = 2$ corresponds to a sinusoidal variation of the reconnecting magnetic field. The determination of the tearing growth rate demands $k_{\perp}\rho_i \ll 1$ for the validity of this linear tearing growth-rate calculation, so we take $k_{\perp}\rho_i \rightarrow \mathcal{F}$, where $\mathcal{F} \ll 1$ is the maximum value of the normalized perpendicular wavenumber for which the growth-rate derivations remain valid. Here, we specify a value $\mathcal{F} = 0.3$ for our estimation of the onset of collisionless magnetic reconnection, plotting the threshold boundaries for reconnection of intermittent current sheets ($n = 1$) (dashed red line and downward arrow) and for reconnection of sinusoidal current sheets ($n = 2$) (solid red line and downward arrow). Note that the dependence of $k_0\rho_i$ on \mathcal{F} in both (5.37) and (5.42) is very strong, scaling as \mathcal{F}^9 for $n = 1$ and as \mathcal{F}^7 for $n = 2$, so the determination of the maximal value of $k_{\perp}\rho_i \equiv \mathcal{F}$ for the tearing instability growth has a strong influence on whether reconnection will arise. Also, as discussed in the last paragraph of § 5.9, the onset of collisionless magnetic reconnection may not directly lead to damping of the turbulent fluctuations, but rather is expected to change the nature of turbulent fluctuations, such as the wavevector anisotropy, the scaling of the energy spectrum and the degree of intermittency. Thus, below the red lines in [figure 12](#), the onset of reconnection may not directly damp turbulent fluctuations but instead may alter the scalings of the other turbulent damping mechanisms.

The phase diagram for the turbulent damping mechanisms on the $(\beta_i, k_0\rho_i)$ plane in [figure 12](#) can be used in the following manner to predict which damping mechanisms will contribute to the dissipation of turbulence in a specific space or astrophysical plasma system. In the near-Earth solar wind, the observed ion plasma beta values span the range $0.05 \lesssim \beta_i \lesssim 10$ (Wilson *et al.* 2018), taking a 5% and 95% limit on the distribution of β_i values. Furthermore, the isotropic driving wavenumber in the near-Earth solar wind spans the typical values $10^{-4} \lesssim k_0\rho_i \lesssim 10^{-3}$ (Tu & Marsch 1990, 1995; Matthaeus *et al.* 2005; Howes *et al.* 2008a; Kiyani *et al.* 2015). This range of parameters for the solar wind at 1 AU is plotted as the grey shaded region on [figure 12](#). Reading the phase diagram, the prediction for the damping mechanisms in the near-Earth solar wind is that Landau-resonant damping for ions (iLD and iTTD) and electrons (eLD and eTTD) will contribute to the damping over the full range of solar wind turbulence parameters. At lower values of $\beta_i \lesssim 0.3$ and higher values of $k_0\rho_i$, stochastic heating is predicted to play a role. Indeed, in the Earth's magnetosheath (which has a similar footprint on the $(\beta_i, k_0\rho_i)$ plane as the near-Earth solar wind), there is direct evidence from Magnetospheric MultiScale spacecraft observations of eLD playing a significant role in the damping of the turbulent fluctuations (Chen *et al.* 2019; Afshari *et al.* 2021). In addition, for the solar wind in the inner heliosphere, where the values of β_i tend to be lower than in the near-Earth

solar wind, analysis of observations from the Ulysses spacecraft (Bourouaine & Chandran 2013), the Helios spacecraft (Martinović, Klein & Bourouaine 2019) and the Parker Solar Probe spacecraft (Martinović *et al.* 2020) find evidence for iSH in the turbulent plasma. Thus, phase diagrams like figure 12 can play a valuable role in predicting the mechanisms that will contribute to the damping of weakly collisional plasma turbulence in space and astrophysical plasmas.

7. Conclusions

Turbulence is a ubiquitous phenomenon that arises in space and astrophysical plasmas and mediates the transfer of the energy of large-scale plasma flows and electromagnetic fields to sufficiently small scales that dissipation mechanisms can convert that energy into the microscopic energy of the plasma particles. A grand challenge problem in heliophysics and astrophysics is to predict the heating or acceleration of the different plasma species by the turbulence in terms of the dimensionless parameters that characterize the plasma and the nature of the turbulence. In particular, a long-term goal is to develop predictive models of the turbulent plasma heating that determine the partitioning of energy between the ion and electron species, Q_i/Q_e , and between the perpendicular and parallel degrees of freedom for each species, $Q_{\perp,i}/Q_{\parallel,i}$ and $Q_{\perp,e}/Q_{\parallel,e}$. An essential step in the development of such predictive turbulent heating models is to identify the microphysical kinetic processes that govern the transfer of the turbulent energy to the particles as a function of the dimensionless parameters, information that can be summarized in a phase diagram for the dissipation of plasma turbulence, as shown in figure 12.

The first step in this long term effort is to specify a set of the key dimensionless parameters upon which the turbulent energy cascade and its dissipation depend. In this paper, we propose a specific set of ten dimensionless parameters that characterize the state of the plasma and the nature of the turbulence

$$(\beta_{\parallel,i}, \tau_{\parallel}, A_i, A_e, k_{\parallel 0} \lambda_{\text{mfp},e}; k_{\perp 0} \rho_i, k_{\parallel 0}/k_{\perp 0}, \chi_0, Z_0^+/Z_0^-, E_{\text{comp}}/E_{\text{inc}}), \quad (7.1)$$

summarized in table 3. Although this set of ten parameters is sufficient to characterize a wide variety of turbulent space and astrophysical plasmas, the development of completely general turbulent heating models on a ten-dimensional parameter space is unlikely to be successful. Fortunately, we can capture many of the dominant dependencies of the turbulence and its damping mechanisms by adopting of reduced set of parameters in the limits that (i) the equilibrium velocity distribution for each species is an isotropic Maxwellian and (ii) the turbulence is driven at sufficiently large scale or sufficiently strongly that the turbulent fluctuations at the small-scale end of the inertial range $k_{\perp} \rho_i \sim 1$ satisfy a state of strong turbulence, with a nonlinearity parameter at those small scales of $\chi \sim 1$. With these idealizations we arrive at the isotropic temperature case, where just three dimensionless parameters remain

$$(\beta_i, \tau; k_0 \rho_i), \quad (7.2)$$

summarized in table 4.

A number of kinetic mechanisms have been proposed to govern the damping of weakly collisional plasma turbulence, as enumerated in § 5.1. The critical advance presented in this paper is to express the dependence of each of these mechanisms on the same set of fundamental plasma and turbulence parameters. The result of this analysis of the dependencies for each of the turbulent damping mechanisms is summarized in table 5.

Finally, the scalings of each of the turbulent damping mechanisms with the isotropic driving wavenumber $k_0\rho_i$ and the ion plasma beta β_i can be synthesized to generate the first phase diagram for turbulent damping mechanisms as a function of $(\beta_i, k_0\rho_i)$, presented in [figure 12](#). For a chosen space or astrophysical plasma system, such as the near-Earth solar wind, the range of dimensionless plasma and turbulence parameters can be plotted on the phase diagram, as illustrated by the grey shaded region in the figure. One may then read off which mechanisms are predicted to contribute to the damping of the turbulence in that system. Kinetic numerical simulations and spacecraft observations of weakly collisional turbulence in space or astrophysical plasmas can be used to update and refine this phase diagram, or to extend its applicability as additional dimensionless parameters are varied, such as the ion-to-electron temperature ratio $\tau = T_i/T_e$. It is worthwhile emphasizing that, if kinetic simulations are used to identify the turbulent damping mechanisms and to quantify the associated energy density transfer rates with each plasma species, it is essential that those simulations be performed in the full three spatial dimensions. Utilizing reduced dimensionality for such simulations may unphysically restrict the available channels of energy transfer from the turbulent fluctuations to the particles, potentially changing which physical turbulent damping mechanisms are dominant and thereby artificially altering the resulting partitioning of energy among particle species and degrees of freedom.

Ultimately, the goal is to produce more accurate and complete predictive turbulent heating models than those reviewed in §4, facilitating improved global modelling of important turbulent space and astrophysical plasmas, such as the mesoscale and macroscale energy transport through the heliosphere or the interpretation of Event Horizon Telescope observations of accretion disks around supermassive black holes.

Acknowledgements

More than fifteen years of turbulent modelling efforts are synthesized here, having benefited from interactions over many years with S. Cowley, B. Dorland, E. Quataert, A. Schekochihin, G. Hammett, T. Tatsuno, R. Numata, B. Chandran, S. Bale, K. Nielson, J. TenBarge, J. Drake, F. Skiff, C. Kletzing, S. Vincena, T. Carter, C. Salem, K. Klein, C. Chen, J. Schroeder, D. Told, F. Jenko, F. Sahaoui, T.C. Li, S. Ruhunusiri, J. Halekas, S. Bourouaine, J. Verniero, M. Kunz, A. McCubbin, F. Valentini, R. Wicks, D. Verscharen, L. Woodham, S. Conley, A. Afshari, P. Montag, D. McGinnis, C. Brown, R. Huang and A. Felix. I also thank H. Karimabadi for first suggesting the idea of creating a phase diagram for plasma turbulence.

Editor Nuno Loureiro thanks the referees for their advice in evaluating this article.

Funding

This work in this long-term project was supported by the National Science Foundation (grant numbers PHY-10033446, CAREER AGS-1054061, AGS-1842561); the Department of Energy (grant number DE-SC0014599); and NASA (grant numbers NNX10AC91G, 80NSSC18K0643, 80NSSC18K1217, 80NSSC18K1371).

Declaration of interests

The author reports no conflict of interest.

REFERENCES

- ABRAHAM-SHRAUNER, B. & FELDMAN, W.C. 1977 Electromagnetic ion-cyclotron wave growth rates and their variation with velocity distribution function shape. *J. Plasma Phys.* **17**, 123–131.
- ADHIKARI, L., ZANK, G.P., ZHAO, L.L., KASPER, J.C., KORRECK, K.E., STEVENS, M., CASE, A.W., WHITTLESEY, P., LARSON, D., LIVI, R., *et al.* 2020 Turbulence transport modeling and first orbit parker solar probe (PSP) observations. *Astrophys. J. Suppl.* **246** (2), 38.
- AFSHARI, A.S., HOWES, G.G., KLETZING, C.A., HARTLEY, D.P. & BOARDSEN, S.A. 2021 The importance of electron landau damping for the dissipation of turbulent energy in terrestrial magnetosheath plasma. *J. Geophys. Res.* **126** (12), e29578.
- AFSHARI, A.S., HOWES, G.G., SHUSTER, J.R., KLEIN, K.G., MCGINNIS, D., MARTINOVIC, M.M., BOARDSEN, S.A., BROWN, C.R., HUANG, R., *et al.* 2024 Direct observation of ion cyclotron damping of turbulence in Earth's magnetosheath plasma. *Nature Comm.*
- ALEXANDROVA, O., CARBONE, V., VELTRI, P. & SORRISO-VALVO, L. 2008 Small-scale energy cascade of the solar wind turbulence. *Astrophys. J.* **674**, 1153–1157.
- ALEXANDROVA, O., SAUR, J., LACOMBE, C., MANGENEY, A., MITCHELL, J., SCHWARTZ, S.J. & ROBERT, P. 2009 Universality of solar-wind turbulent spectrum from MHD to electron scales. *Phys. Rev. Lett.* **103** (16), 165003.
- AMBROSIANO, J., MATTHAEUS, W.H., GOLDSTEIN, M.L. & PLANTE, D. 1988 Test particle acceleration in turbulent reconnecting magnetic fields. *J. Geophys. Res.* **93**, 14383–14400.
- ANTONSEN, T.M., JR. & LANE, B. 1980 Kinetic equations for low frequency instabilities in inhomogeneous plasmas. *Phys. Fluids* **23**, 1205–1214.
- ARMSTRONG, T.P., PAONESSA, M.T., BELL, E.V., & KRIMIGIS II, S.M. 1983 Voyager observations of saturnian ion and electron phase space densities. *J. Geophys. Res.* **88** (A11), 8893–8904.
- ARZAMASSKIY, L., KUNZ, M.W., CHAND RAN, B.D.G. & QUATAERT, E. 2019 Hybrid-kinetic simulations of ion heating in Alfvénic turbulence. *Astrophys. J.* **879** (1), 53.
- ARZAMASSKIY, L., KUNZ, M.W., SQUIRE, J., QUATAERT, E. & SCHEKOCIHIN, A.A. 2023 Kinetic turbulence in collisionless high- β plasmas. *Phys. Rev. X* **13** (2), 021014.
- BALBUS, S.A. & HAWLEY, J.F. 1991 A powerful local shear instability in weakly magnetized disks. I. Linear analysis. *Astrophys. J.* **376**, 214–222.
- BALBUS, S.A. & HAWLEY, J.F. 1998 Instability, turbulence, and enhanced transport in accretion disks. *Rev. Mod. Phys.* **70**, 1–53.
- BALE, S.D., KASPER, J.C., HOWES, G.G., QUATAERT, E., SALEM, C. & SUNDKVIST, D. 2009 Magnetic fluctuation power near proton temperature anisotropy instability thresholds in the solar wind. *Phys. Rev. Lett.* **103**, 211101.
- BARBHUIYA, M.H. & CASSAK, P. A. 2022 Pressure-strain interaction. III. Particle-in-cell simulations of magnetic reconnection. *Phys. Plasmas* **29** (12), 122308.
- BARENBLATT, G.I. 1996 *Scaling, Self-Similarity, and Intermediate Asymptotics*. Cambridge University Press.
- BARNES, A. 1966 Collisionless damping of hydromagnetic waves. *Phys. Fluids* **9**, 1483–1495.
- BELCHER, J.W. & DAVIS, L. 1971 Large-amplitude Alfvén waves in the interplanetary medium, 2. *J. Geophys. Res.* **76**, 3534–3563.
- BERGER, J.M., NEWCOMB, W.A., DAWSON, J.M., FRIEMAN, E.A., KULSRUD, R.M. & LENARD, A. 1958 Heating of a confined plasma by oscillating electromagnetic fields. *Phys. Fluids* **1** (4), 301–307.
- BISKAMP, D. & MÜLLER, W.-C. 2000 Scaling properties of three-dimensional isotropic magnetohydrodynamic turbulence. *Phys. Plasmas* **7**, 4889–4900.
- BISKAMP, D. & WELTER, H. 1989 Dynamics of decaying two-dimensional magnetohydrodynamic turbulence. *Phys. Fluids B* **1**, 1964–1979.
- BISKAMP, D., SCHWARZ, E., ZEILER, A., CELANI, A. & DRAKE, J.F. 1999 Electron magnetohydrodynamic turbulence. *Phys. Plasmas* **6**, 751–758.
- BOLDYREV, S. 2006 Spectrum of magnetohydrodynamic turbulence. *Phys. Rev. Lett.* **96** (11), 115002.
- BOLDYREV, S. & LOUREIRO, N.F. 2017 Magnetohydrodynamic turbulence mediated by reconnection. *Astrophys. J.* **844**, 125.

- BOLDYREV, S., MASON, J. & CATTANEO, F. 2009 Dynamic alignment and exact scaling laws in magnetohydrodynamic turbulence. *Astrophys. J. Lett.* **699**, L39–L42.
- BOLDYREV, S. & PEREZ, J.C. 2009 Spectrum of weak magnetohydrodynamic turbulence. *Phys. Rev. Lett.* **103** (22), 225001.
- BORIS, J.P. & MANHEIMER, W. 1977 Marginal stability analysis: a simpler approach to anomalous transport in plasmas. *Tech. Rep.*
- BOROVSKY, J.E. 2008 Flux tube texture of the solar wind: strands of the magnetic carpet at 1 AU? *J. Geophys. Res.* **113**, A08110.
- BOROVSKY, J.E. & DENTON, M.H. 2011 No evidence for heating of the solar wind at strong current sheets. *Astrophys. J. Lett.* **739**, L61.
- BOTT, A.F.A., ARZAMASSKIY, L., KUNZ, M.W., QUATAERT, E. & SQUIRE, J. 2021 Adaptive critical balance and firehose instability in an expanding, turbulent, collisionless plasma. *Astrophys. J. Lett.* **922** (2), L35.
- BOUROUAINE, S. & CHANDRAN, B.D.G. 2013 Observational test of stochastic heating in low- β fast-solar-wind streams. *Astrophys. J.* **774**, 96.
- BOUROUAINE, S., MARSCH, E. & VOCKS, C. 2008 On the efficiency of nonresonant ion heating by coronal Alfvén waves. *Astrophys. J. Lett.* **684**, L119–L122.
- BRAGINSKII, S.I. 1965 Transport processes in a plasma. *Rev. Plasma Phys.* **1**, 205.
- BRIZARD, A. 1992 Nonlinear gyrofluid description of turbulent magnetized plasmas. *Phys. Fluids B* **4**, 1213–1228.
- BRIZARD, A.J. & HAHM, T.S. 2007 Foundations of nonlinear gyrokinetic theory. *Rev. Mod. Phys.* **79**, 421–468.
- BROWN, C.R., JUNO, J., HOWES, G.G., HAGGERTY, C.C. & CONSTANTINOU, S. 2023 Isolation and phase-space energization analysis of the instabilities in collisionless shocks. *J. Plasma Phys.* **89** (3), 905890308.
- BRUNO, R. & CARBONE, V. 2013 The solar wind as a turbulence laboratory. *Liv. Rev. Solar Phys.* **10**, 2.
- BUCKINGHAM, E. 1914 On physically similar systems; illustrations of the use of dimensional equations. *Phys. Rev.* **4**, 345–376.
- CASSAK, P.A. & BARBHUIYA, M.H. 2022 Pressure-strain interaction. I. On compression, deformation, and implications for Pi-D. *Phys. Plasmas* **29** (12), 122306.
- CASSAK, P.A., BARBHUIYA, M.H., LIANG, H. & ARGALL, M.R. 2023 Quantifying energy conversion in higher-order phase space density moments in plasmas. *Phys. Rev. Lett.* **130** (8), 085201.
- CASSAK, P.A., BARBHUIYA, M.H. & WELDON, H.A. 2022 Pressure-strain interaction. II. Decomposition in magnetic field-aligned coordinates. *Phys. Plasmas* **29** (12), 122307.
- CATTO, P.J. 1978 Linearized gyro-kinetics. *Plasma Phys.* **20**, 719–722.
- CATTO, P.J., TANG, W.M. & BALDWIN, D.E. 1981 Generalized gyrokinetics. *Plasma Phys.* **23**, 639–650.
- CERRI, S.S., ARZAMASSKIY, L. & KUNZ, M.W. 2021 On stochastic heating and its phase-space signatures in low-beta kinetic turbulence. *Astrophys. J.* **916** (2), 120.
- CHAEL, A., NARAYAN, R. & JOHNSON, M.D. 2019 Two-temperature, magnetically arrested disc simulations of the jet from the supermassive black hole in M87. *Mon. Not. R. Astron. Soc.* **486** (2), 2873–2895.
- CHANDRAN, B.D.G. 2010 Alfvén-wave turbulence and perpendicular ion temperatures in coronal holes. *Astrophys. J.* **720**, 548–554.
- CHANDRAN, B.D.G., DENNIS, T.J., QUATAERT, E. & BALE, S.D. 2011 Incorporating kinetic physics into a two-fluid solar-wind model with temperature anisotropy and low-frequency Alfvén-wave turbulence. *Astrophys. J.* **743**, 197.
- CHANDRAN, B.D.G., LI, B., ROGERS, B.N., QUATAERT, E. & GERMASCHEWSKI, K. 2010 Perpendicular ion heating by low-frequency Alfvén-wave turbulence in the solar wind. *Astrophys. J.* **720**, 503–515.
- CHANDRAN, B.D.G. & PEREZ, J.C. 2019 Reflection-driven magnetohydrodynamic turbulence in the solar atmosphere and solar wind. *J. Plasma Phys.* **85** (4), 905850409.
- CHANDRAN, B.D.G., VERSCHAREN, D., QUATAERT, E., KASPER, J.C., ISENBERG, P.A. & BOUROUAINE, S. 2013 Stochastic heating, differential flow, and the alpha-to-proton temperature ratio in the solar wind. *Astrophys. J.* **776** (1), 45.

- CHAPMAN, S. & COWLING, T.G. 1970 *The Mathematical Theory of Non-uniform Gases. An Account of the Kinetic Theory of Viscosity, Thermal Conduction and Diffusion in Gases*. Cambridge University Press.
- CHEN, C.H.K., HORBURY, T.S., SCHEKOCHIHIN, A.A., WICKS, R.T., ALEXANDROVA, O. & MITCHELL, J. 2010 Anisotropy of solar wind turbulence between ion and electron scales. *Phys. Rev. Lett.* **104** (25), 255002.
- CHEN, C.H.K., HOWES, G.G., BONNELL, J.W., MOZER, F.S., KLEIN, K.G. & BALE, S.D. 2013 Kinetic scale density fluctuations in the solar wind. In *American Institute of Physics Conference Series* (ed. G.P. Zank, J. Borovsky, R. Bruno, J. Cirtain, S. Cranmer, H. Elliott, J. Giacalone, W. Gonzalez, G. Li, E. Marsch, E. Moebius, N. Pogorelov, J. Spann & O. Verkhoglyadova), *American Institute of Physics Conference Series*, vol. 1539, pp. 143–146.
- CHEN, C.H.K., KLEIN, K.G. & HOWES, G.G. 2019 Evidence for electron Landau damping in space plasma turbulence. *Nat. Commun.* **10** (1), 740.
- CHEN, C.H.K., MALLET, A., SCHEKOCHIHIN, A.A., HORBURY, T.S., WICKS, R.T. & BALE, S.D. 2012 Three-dimensional structure of solar wind turbulence. *Astrophys. J.* **758**, 120.
- CHEN, C.H.K., MALLET, A., YOUSEF, T.A., SCHEKOCHIHIN, A.A. & HORBURY, T.S. 2011 Anisotropy of Alfvénic turbulence in the solar wind and numerical simulations. *Mon. Not. R. Astron. Soc.* **415**, 3219–3226.
- CHEN, L., LIN, Z. & WHITE, R. 2001 On resonant heating below the cyclotron frequency. *Phys. Plasmas* **8**, 4713–4716.
- CHEW, G.L., GOLDBERGER, M.L. & LOW, F.E. 1956 The Boltzmann equation and the one-fluid hydromagnetic equations in the absence of particle collisions. *Proc. R. Soc. Lond. A* **236**, 112–118.
- CHO, J. & LAZARIAN, A. 2003 Compressible magnetohydrodynamic turbulence: mode coupling, scaling relations, anisotropy, viscosity-damped regime and astrophysical implications. *Mon. Not. R. Astron. Soc.* **345**, 325–339.
- CHO, J. & LAZARIAN, A. 2004 The anisotropy of electron magnetohydrodynamic turbulence. *Astrophys. J. Lett.* **615**, L41–L44.
- CHO, J., LAZARIAN, A. & VISHNIAC, E.T. 2002 Simulations of magnetohydrodynamic turbulence in a strongly magnetized medium. *Astrophys. J.* **564**, 291–301.
- CHO, J. & VISHNIAC, E.T. 2000 The anisotropy of magnetohydrodynamic Alfvénic turbulence. *Astrophys. J.* **539**, 273–282.
- COBURN, J.T., FORMAN, M.A., SMITH, C.W., VASQUEZ, B.J. & STAWARZ, J.E. 2015 Third-moment descriptions of the interplanetary turbulent cascade, intermittency and back transfer. *Phil. Trans. R. Soc. A* **373** (2041), 20140150–20140150.
- COBURN, J.T., SMITH, C.W., VASQUEZ, B.J., FORMAN, M.A. & STAWARZ, J.E. 2014 Variable cascade dynamics and intermittency in the solar wind at 1 AU. *Astrophys. J.* **786** (1), 52.
- COLEMAN, P.J., JR. 1968 Turbulence, viscosity, and dissipation in the solar-wind plasma. *Astrophys. J.* **153**, 371–388.
- CONLEY, S.A., HOWES, G.G. & MCCUBBIN, A.J. 2023 Characterizing the velocity-space signature of electron Landau damping. *J. Plasma Phys.* **89** (5), 905890514.
- DAHLIN, J.T. 2020 Prospectus on electron acceleration via magnetic reconnection. *Phys. Plasmas* **27** (10).
- DALENA, S., RAPPAZZO, A.F., DMITRUK, P., GRECO, A. & MATTHAEUS, W.H. 2014 Test-particle acceleration in a hierarchical three-dimensional turbulence model. *Astrophys. J.* **783**, 143.
- DENSKAT, K.U., BEINROTH, H.J. & NEUBAUER, F.M. 1983 Interplanetary magnetic field power spectra with frequencies from 2.4×10 to the -5 th Hz to 470 Hz from HELIOS-observations during solar minimum conditions. *J. Geophys.* **54**, 60–67.
- DI MARE, F. & HOWES, G.G. 2024 New regime of Alfvén wave turbulence in auroral ionosphere. *Phys. Rev. Lett.* (in press).
- DMITRUK, P., MATTHAEUS, W.H. & SEENU, N. 2004 Test particle energization by current sheets and nonuniform fields in magnetohydrodynamic turbulence. *Astrophys. J.* **617**, 667–679.
- DOBROWOLNY, M., MANGENEY, A. & VELTRI, P. 1980 Fully developed anisotropic hydromagnetic turbulence in interplanetary space. *Phys. Rev. Lett.* **45**, 144–147.
- DORLAND, W. & HAMMETT, G.W. 1993 Gyrofluid turbulence models with kinetic effects. *Phys. Fluids B* **5**, 812–835.

- DRAKE, D.J., SCHROEDER, J.W.R., HOWES, G.G., KLETZING, C.A., SKIFF, F., CARTER, T.A. & AUERBACH, D.W. 2013 Alfvén wave collisions, the fundamental building block of plasma turbulence. IV. Laboratory experiment. *Phys. Plasmas* **20** (7), 072901.
- DRAKE, J.F., SHAY, M.A., THONGTHAI, W. & SWISDAK, M. 2005 Production of energetic electrons during magnetic reconnection. *Phys. Rev. Lett.* **94** (9), s 095001.
- DRAKE, J.F. & SWISDAK, M. 2012 Ion heating and acceleration during magnetic reconnection relevant to the corona. *Space Sci. Rev.* **172**, 227–240.
- DUBIN, D.H.E., KROMMES, J.A., OBERMAN, C. & LEE, W.W. 1983 Nonlinear gyrokinetic equations. *Phys. Fluids* **26**, 3524–3535.
- EGEDAL, J., DAUGHTON, W. & LE, A. 2012 Large-scale electron acceleration by parallel electric fields during magnetic reconnection. *Nat. Phys.* **8**, 321–324.
- EGEDAL, J., FOX, W., KATZ, N., PORKOLAB, M., ØIEROSET, M., LIN, R.P., DAUGHTON, W. & DRAKE, J.F. 2008 Evidence and theory for trapped electrons in guide field magnetotail reconnection. *J. Geophys. Res.* **113**, 12207.
- ELSASSER, W.M. 1950 The hydromagnetic equations. *Phys. Rev.* **79**, 183.
- EVENT HORIZON TELESCOPE COLLABORATION, AKIYAMA, K., ALBERDI, A., ALEF, W., Algaba, J.C., Anantua, R., Asada, K., Azulay, R., Bach, U., Baczkó, A.-K., *et al.* 2022 First sagittarius A* event horizon telescope results. V. Testing astrophysical models of the galactic center black hole. *Astrophys. J. Lett.* **930** (2), L16.
- EVENT HORIZON TELESCOPE COLLABORATION, AKIYAMA, K., ALBERDI, A., ALEF, W., Asada, K., Azulay, R., Baczkó, A.-K., Ball, D., Baloković, M., Barrett, J., *et al.* 2019 First M87 event horizon telescope results. V. Physical origin of the asymmetric ring. *Astrophys. J. Lett.* **875** (1), L5.
- FOX, N.J., VELLI, M.C., BALE, S.D., DECKER, R., DRIESMAN, A., HOWARD, R.A., KASPER, J.C., KINNISON, J., KUSTERER, M., LARIO, D., *et al.* 2016 The solar probe plus mission: humanity's first visit to our star. *Space Sci. Rev.* **204**, 7–48.
- FRIEMAN, E.A. & CHEN, L. 1982 Nonlinear gyrokinetic equations for low-frequency electromagnetic waves in general plasma equilibria. *Phys. Fluids* **25**, 502–508.
- FURTH, H.P., KILLEEN, J. & ROSENBLUTH, M.N. 1963 Finite-resistivity instabilities of a sheet pinch. *Phys. Fluids* **6** (4), 459–484.
- GALTIER, S., NAZARENKO, S.V., NEWELL, A.C. & POUQUET, A. 2000 A weak turbulence theory for incompressible magnetohydrodynamics. *J. Plasma Phys.* **63**, 447–488.
- GARY, S.P. 1999 Collisionless dissipation wavenumber: linear theory. *J. Geophys. Res.* **104**, 6759–6762.
- GARY, S.P., MONTGOMERY, M.D., FELDMAN, W.C. & FORSLUND, D.W. 1976 Proton temperature anisotropy instabilities in the solar wind. *J. Geophys. Res.* **81**, 1241–1246.
- GEKELMAN, W., PFISTER, H., LUCKY, Z., BAMBER, J., LENEMAN, D. & MAGGS, J. 1991 Design, construction, and properties of the large plasma research device - The LAPD at UCLA. *Rev. Sci. Instrum.* **62**, 2875–2883.
- GEKELMAN, W., PRIBYL, P., LUCKY, Z., DRANDELL, M., LENEMAN, D., MAGGS, J., VINCENA, S., VAN COMPENOLLE, B., TRIPATHI, S.K.P., MORALES, G., *et al.* 2016 The upgraded large plasma device, a machine for studying frontier basic plasma physics. *Rev. Sci. Instrum.* **87** (2), 025105.
- GLATZMAIER, G.A. 1984 Numerical simulations of stellar convective dynamos. I. The model and method. *J. Comput. Phys.* **55**, 461–484.
- GLATZMAIER, G.A. 1985 Numerical simulations of stellar convective dynamos. II - Field propagation in the convection zone. *Astrophys. J.* **291**, 300–307.
- GOLDREICH, P. & SRIDHAR, S. 1995 Toward a theory of interstellar turbulence. II. Strong Alfvénic turbulence. *Astrophys. J.* **438**, 763–775.
- GOLDSTEIN, M.L., ROBERTS, D.A. & FITCH, C.A. 1994 Properties of the fluctuating magnetic helicity in the inertial and dissipation ranges of solar wind turbulence. *J. Geophys. Res.* **99**, 11519–11538.
- GORMAN, W. & KLEIN, K.G. 2024 Mind the gap: non-local cascades and preferential heating in high- β Alfvénic turbulence. *Mon. Not. R. Astron. Soc.* **531** (1), L1–L7.
- GOSLING, J.T., ASBRIDGE, J.R., BAME, S.J., FELDMAN, W.C., ZWICKL, R.D., PASCHMANN, G., SCKOPKE, N. & HYND, R.J. 1981 Interplanetary ions during an energetic storm particle event:

- the distribution function from solar wind thermal energies to 1.6 MeV. *J. Geophys. Res.* **86** (A2), 547–554.
- GRAD, H. 1963 Asymptotic theory of the Boltzmann equation. *Phys. Fluids* **6**, 147–181.
- GRECO, A., CHUYCHAI, P., MATTHAEUS, W.H., SERVIDIO, S. & DMITRUK, P. 2008 Intermittent MHD structures and classical discontinuities. *Geophys. Res. Lett.* **35**, 19111.
- GROŠELJ, D., CHEN, C.H.K., MALLETT, A., SAMTANEY, R., SCHNEIDER, K. & JENKO, F. 2019 Kinetic turbulence in astrophysical plasmas: waves and/or structures? *Phys. Rev. X* **9** (3), 031037.
- GRUZINOV, A.V. 1998 Radiative efficiency of collisionless accretion. *Astrophys. J.* **501**, 787.
- GURNETT, D.A. & BHATTACHARJEE, A. 2017 *Introduction to Plasma Physics: With Space, Laboratory and Astrophysical Applications*, 2nd ed. Cambridge University Press.
- HAHM, T.S., LEE, W.W. & BRIZARD, A. 1988 Nonlinear gyrokinetic theory for finite-beta plasmas. *Phys. Fluids* **31**, 1940–1948.
- HAMMETT, G.W., DORLAND, W. & PERKINS, F.W. 1992 Fluid models of phase mixing, Landau damping, and nonlinear gyrokinetic dynamics. *Phys. Fluids B* **4**, 2052–2061.
- HARRIS, E.G. 1962 On a plasma sheath separating regions of oppositely directed magnetic field. *Il Nuovo Cimento* **23** (1), 115–121.
- HAWLEY, J.F. & BALBUS, S.A. 1991 A powerful local shear instability in weakly magnetized disks. II. Nonlinear evolution. *Astrophys. J.* **376**, 223.
- HELLINGER, P. & MATSUMOTO, H. 2000 New kinetic instability: oblique Alfvén fire hose. *J. Geophys. Res.* **105**, 10519–10526.
- HELLINGER, P., TRÁVNÍČEK, P., KASPER, J.C. & LAZARUS, A.J. 2006 Solar wind proton temperature anisotropy: linear theory and WIND/SWE observations. *Geophys. Res. Lett.* **33**, 9101.
- HELLINGER, P. & TRÁVNÍČEK, P.M. 2008 Oblique proton fire hose instability in the expanding solar wind: hybrid simulations. *J. Geophys. Res.* **113**, 10109.
- HNAT, B., CHAPMAN, S.C. & ROWLANDS, G. 2003 Intermittency, scaling, and the Fokker-Planck approach to fluctuations of the solar wind bulk plasma parameters as seen by the WIND spacecraft. *Phys. Rev. E* **67** (5), 056404.
- HOLLWEG, J.V. & ISENBERG, P.A. 2002 Generation of the fast solar wind: a review with emphasis on the resonant cyclotron interaction. *J. Geophys. Res.* **107**, 1147.
- VAN DER HOLST, B., SOKOLOV, I.V., MENG, X., JIN, M., MANCHESTER IV, W.B., TÓTH, G. & GOMBOSI, T.I. 2014 Alfvén wave solar model (AWSOM): coronal heating. *Astrophys. J.* **782**, 81.
- HORVATH, S.A., HOWES, G.G. & MCCUBBIN, A.J. 2020 Electron Landau damping of kinetic Alfvén waves in simulated magnetosheath turbulence. *Phys. Plasmas* **27** (10), 102901.
- HOWES, G.G. 2008 Inertial range turbulence in kinetic plasmas. *Phys. Plasmas* **15** (5), 055904.
- HOWES, G.G. 2010 A prescription for the turbulent heating of astrophysical plasmas. *Mon. Not. R. Astron. Soc.* **409**, L104–L108.
- HOWES, G.G. 2015a A dynamical model of plasma turbulence in the solar wind. *Phil. Trans. R. Soc. Lond. A* **373** (2041), 20140145.
- HOWES, G.G. 2015b The inherently three-dimensional nature of magnetized plasma turbulence. *J. Plasma Phys.* **81**, 3203.
- HOWES, G.G. 2016 The dynamical generation of current sheets in astrophysical plasma turbulence. *Astrophys. J. Lett.* **82**, L28.
- HOWES, G.G. 2017 A prospectus on kinetic heliophysics. *Phys. Plasmas* **24** (5), 055907.
- HOWES, G.G., BALE, S.D., KLEIN, K.G., CHEN, C.H.K., SALEM, C.S. & TENBARGE, J.M. 2012a The slow-mode nature of compressible wave power in solar wind turbulence. *Astrophys. J. Lett.* **753**, L19.
- HOWES, G.G., COWLEY, S.C., DORLAND, W., HAMMETT, G.W., QUATAERT, E. & SCHEKOCHIHIN, A.A. 2006 Astrophysical gyrokinetics: basic equations and linear theory. *Astrophys. J.* **651**, 590–614.
- HOWES, G.G., COWLEY, S.C., DORLAND, W., HAMMETT, G.W., QUATAERT, E. & SCHEKOCHIHIN, A.A. 2008a A model of turbulence in magnetized plasmas: implications for the dissipation range in the solar wind. *J. Geophys. Res.* **113** (A12), A05103.

- HOWES, G.G., DORLAND, W., COWLEY, S.C., HAMMETT, G.W., QUATAERT, E., SCHEKOCIHIN, A.A. & TATSUNO, T. 2008*b* Kinetic simulations of magnetized turbulence in astrophysical plasmas. *Phys. Rev. Lett.* **100** (6), 065004.
- HOWES, G.G., DRAKE, D.J., NIELSON, K.D., CARTER, T.A., KLETZING, C.A. & SKIFF, F. 2012*b* Toward astrophysical turbulence in the laboratory. *Phys. Rev. Lett.* **109** (25), 255001.
- HOWES, G.G., HUANG, R. & FELIX, A.A. 2024 The physics of the magnetic mirror force and transit-time damping: asymptotic solution. *J. Plasma Phys.* (in preparation).
- HOWES, G.G., KLEIN, K.G. & LI, T.C. 2017 Diagnosing collisionless energy transfer using field-particle correlations: Vlasov-Poisson plasmas. *J. Plasma Phys.* **83** (1), 705830102.
- HOWES, G.G., KLEIN, K.G. & TENBARGE, J.M. 2014 Validity of the Taylor hypothesis for linear kinetic waves in the weakly collisional solar wind. *Astrophys. J.* **789**, 106.
- HOWES, G.G., MCCUBBIN, A.J. & KLEIN, K.G. 2018 Spatially localized particle energization by Landau damping in current sheets produced by strong Alfvén wave collisions. *J. Plasma Phys.* **84** (1), 905840105.
- HOWES, G.G. & NIELSON, K.D. 2013 Alfvén wave collisions, the fundamental building block of plasma turbulence. I. Asymptotic solution. *Phys. Plasmas* **20** (7), 072302.
- HOWES, G.G., NIELSON, K.D., DRAKE, D.J., SCHROEDER, J.W.R., SKIFF, F., KLETZING, C.A. & CARTER, T.A. 2013 Alfvén wave collisions, the fundamental building block of plasma turbulence. III. Theory for experimental design. *Phys. Plasmas* **20** (7), 072304.
- HOWES, G.G., TENBARGE, J.M. & DORLAND, W. 2011*a* A weakened cascade model for turbulence in astrophysical plasmas. *Phys. Plasmas* **18**, 102305.
- HOWES, G.G., TENBARGE, J.M., DORLAND, W., QUATAERT, E., SCHEKOCIHIN, A.A., NUMATA, R. & TATSUNO, T. 2011*b* Gyrokinetic simulations of solar wind turbulence from ion to electron scales. *Phys. Rev. Lett.* **107**, 035004.
- HUANG, R., HOWES, G.G. & MCCUBBIN, A.J. 2024 The velocity-space signature of transit-time damping. *J. Plasma Phys.* **90** (4), 535900401.
- HUNANA, P., LAVEDER, D., PASSOT, T., SULEM, P.L. & BORGOGNO, D. 2011 Reduction of compressibility and parallel transfer by Landau damping in turbulent magnetized plasmas. *Astrophys. J.* **743**, 128.
- ISENBERG, P.A. 2001 The kinetic shell model of coronal heating and acceleration by ion cyclotron waves. 2. Inward and outward propagating waves. *J. Geophys. Res.* **106** (A12), 29249–29260.
- ISENBERG, P.A. & HOLLWEG, J.V. 1983 On the preferential acceleration and heating of solar wind heavy ions. *J. Geophys. Res.* **88**, 3923–3935.
- ISENBERG, P.A., LEE, M.A. & HOLLWEG, J.V. 2001 The kinetic shell model of coronal heating and acceleration by ion cyclotron waves. 1. Outward propagating waves. *J. Geophys. Res.* **106**, 5649–5660.
- ISENBERG, P.A. & VASQUEZ, B.J. 2019 Perpendicular ion heating by cyclotron resonant dissipation of turbulently generated kinetic Alfvén waves in the solar wind. *Astrophys. J.* **887** (1), 63.
- JET TEAM 1992 Fusion energy production from a deuterium-tritium plasma in the JET tokamak. *Nuclear Fusion* **32** (2), 187–203.
- JIANSEN, H., XINGYU, Z., YAJIE, C., CHADI, S., MICHAEL, S., HUI, L., WENZHI, R., LEI, Z. & CHUANYI, T. 2018 Plasma heating and Alfvénic turbulence enhancement during two steps of energy conversion in magnetic reconnection exhaust region of solar wind. *Astrophys. J.* **856** (2), 148.
- JI, H. & DAUGHTON, W. 2011 Phase diagram for magnetic reconnection in heliophysical, astrophysical, and laboratory plasmas. *Phys. Plasmas* **18** (11), 111207–111207.
- JOHNSON, J.R. & CHENG, C.Z. 2001 Stochastic ion heating at the magnetopause due to kinetic Alfvén waves. *Geophys. Res. Lett.* **28**, 4421–4424.
- KARIMABADI, H., ROYTERSHTEYN, V., WAN, M., MATTHAEUS, W.H., DAUGHTON, W., WU, P., SHAY, M., LORING, B., BOROVSKY, J., LEONARDIS, E., *et al.* 2013 Coherent structures, intermittent turbulence, and dissipation in high-temperature plasmas. *Phys. Plasmas* **20** (1), 012303.
- KASPER, J.C., LAZARUS, A.J. & GARY, S.P. 2002 Wind/SWE observations of firehose constraint on solar wind proton temperature anisotropy. *Geophys. Res. Lett.* **29**, 20–1.
- KAWAMORI, E. 2013 Experimental verification of entropy cascade in two-dimensional electrostatic turbulence in magnetized plasma. *Phys. Rev. Lett.* **110** (9), 095001.

- KAWAZURA, Y. 2022 CALLIOPE: pseudospectral shearing magnetohydrodynamics code with a pencil decomposition. *Astrophys. J.* **928** (2), 113.
- KAWAZURA, Y. & BARNES, M. 2018 A hybrid gyrokinetic ion and isothermal electron fluid code for astrophysical plasma. *J. Comput. Phys.* **360**, 57–73.
- KAWAZURA, Y., BARNES, M. & SCHEKOCHIHIN, A.A. 2019 Thermal disequilibrium of ions and electrons by collisionless plasma turbulence. *Proc. Natl Acad. Sci. USA* **116**, 771–776.
- KAWAZURA, Y., SCHEKOCHIHIN, A.A., BARNES, M., DORLAND, W. & BALBUS, S.A. 2022 Energy partition between Alfvénic and compressive fluctuations in magnetorotational turbulence with near-azimuthal mean magnetic field. *J. Plasma Phys.* **88** (3), 905880311.
- KAWAZURA, Y., SCHEKOCHIHIN, A.A., BARNES, M., TENBARGE, J.M., TONG, Y., KLEIN, K.G. & DORLAND, W. 2020 Ion versus electron heating in compressively driven astrophysical gyrokinetic turbulence. *Phys. Rev. X* **10** (4), 041050.
- KENNEL, C. 1966 Low-frequency whistler mode. *Phys. Fluids* **9**, 2190–2202.
- KIYANI, K.H., CHAPMAN, S.C., KHOTYAINTEV, Y.V., DUNLOP, M.W. & SAHRAOUI, F. 2009 Global scale-invariant dissipation in collisionless plasma turbulence. *Phys. Rev. Lett.* **103**, 075006.
- KIYANI, K.H., OSMAN, K.T. & CHAPMAN, S.C. 2015 Introduction: dissipation and heating in solar wind turbulence: from the macro to the micro and back again. *Phil. Trans. R. Soc. Lond. A* **373**, 40155.
- KLEIN, K.G. & CHANDRAN, B.D.G. 2016 Evolution of the proton velocity distribution due to stochastic heating in the near-sun solar wind. *Astrophys. J.* **820**, 47.
- KLEIN, K.G. & HOWES, G.G. 2015 Predicted impacts of proton temperature anisotropy on solar wind turbulence. *Phys. Plasmas* **22** (3), 032903.
- KLEIN, K.G. & HOWES, G.G. 2016 Measuring collisionless damping in heliospheric plasmas using field-particle correlations. *Astrophys. J. Lett.* **826**, L30.
- KLEIN, K.G., HOWES, G.G. & TENBARGE, J.M. 2017 Diagnosing collisionless energy transfer using field-particle correlations: gyrokinetic turbulence. *J. Plasma Phys.* **83** (4), 535830401.
- KLEIN, K.G., HOWES, G.G., TENBARGE, J.M., BALE, S.D., CHEN, C.H.K. & SALEM, C.S. 2012 Using synthetic spacecraft data to interpret compressible fluctuations in solar wind turbulence. *Astrophys. J.* **755**, 159.
- KLEIN, K.G., HOWES, G.G., TENBARGE, J.M. & VALENTINI, F. 2020 Diagnosing collisionless energy transfer using field-particle correlations: Alfvén-ion cyclotron turbulence. *J. Plasma Phys.* **86** (4), 905860402.
- KOLMOGOROV, A.N. 1941 The local structure of turbulence in incompressible viscous fluid for very large Reynolds numbers. *Dokl. Akad. Nauk SSSR* **30**, 9.
- KRAICHNAN, R.H. 1965 Inertial range spectrum of hydromagnetic turbulence. *Phys. Fluids* **8**, 1385–1387.
- KRALL, N.A. & TRIVELPIECE, A.W. 1973 *Principles of Plasma Physics*, International Student Edition - International Series in Pure and Applied Physics. McGraw-Hill Kogakusha.
- KRISHAN, V. & MAHAJAN, S.M. 2004 Magnetic fluctuations and Hall magnetohydrodynamic turbulence in the solar wind. *J. Geophys. Res.* **109** (A18), A11105.
- KULSRUD, R.M. 1983 MHD description of plasma. In *Handbook of Plasma Physics: Basic Plasma Physics I* (ed. A.A. Galeev & R.N. Sudan), vol. 1, chap. 1.4, pp. 115–145. North Holland.
- KUNZ, M.W., ABEL, I.G., KLEIN, K.G. & SCHEKOCHIHIN, A.A. 2018 Astrophysical gyrokinetics: turbulence in pressure-anisotropic plasmas at ion scales and beyond. *J. Plasma Phys.* **84** (2), 715840201.
- KUNZ, M.W., SCHEKOCHIHIN, A.A. & STONE, J.M. 2014 Firehose and mirror instabilities in a collisionless shearing plasma. *Phys. Rev. Lett.* **112** (20), 205003.
- LANDAU, L.D. 1946 On the vibrations of the electronic plasma. *J. Phys.* **10**, 25.
- LEAMON, R.J., MATTHAEUS, W.H., SMITH, C.W. & WONG, H.K. 1998a Contribution of cyclotron-resonant damping to kinetic dissipation of interplanetary turbulence. *Astrophys. J.* **507**, L181–L184.
- LEAMON, R.J., MATTHAEUS, W.H., SMITH, C.W., ZANK, G.P., MULLAN, D.J. & OUGHTON, S. 2000 MHD-driven kinetic dissipation in the solar wind and corona. *Astrophys. J.* **537**, 1054–1062.
- LEAMON, R.J., SMITH, C.W., NESS, N.F., MATTHAEUS, W.H. & WONG, H.K. 1998b Observational constraints on the dynamics of the interplanetary magnetic field dissipation range. *J. Geophys. Res.* **103**, 4775–4787.

- LEAMON, R.J., SMITH, C.W., NESS, N.F. & WONG, H.K. 1999 Dissipation range dynamics: kinetic Alfvén waves and the importance of β_e . *J. Geophys. Res.* **104**, 22331–22344.
- LICHKO, E. & EGEDAL, J. 2020 Magnetic pumping model for energizing superthermal particles applied to observations of the Earth's bow shock. *Nat. Commun.* **11**, 2942.
- LICHKO, E., EGEDAL, J., DAUGHTON, W. & KASPER, J. 2017 Magnetic pumping as a source of particle heating and power-law distributions in the solar wind. *Astrophys. J. Lett.* **850**, L28.
- LIONELLO, R., LINKER, J.A. & MIKIĆ, Z. 2009 Multispectral emission of the sun during the first whole sun month: magnetohydrodynamic simulations. *Astrophys. J.* **690** (1), 902–912.
- LI, T.C., HOWES, G.G., KLEIN, K.G. & TENBARGE, J.M. 2016 Energy dissipation and Landau damping in two- and three-dimensional plasma turbulence. *Astrophys. J. Lett.* **832**, L24.
- LITHWICK, Y. & GOLDBREICH, P. 2001 Compressible magnetohydrodynamic turbulence in interstellar plasmas. *Astrophys. J.* **562** (1), 279–296.
- LIVADIOTIS, G., DESAI, M.I. & WILSON III, L.B. 2018 Generation of kappa distributions in solar wind at 1 Au. *Astrophys. J. Lett.* **853** (2), 142.
- LIVADIOTIS, G. & MCCOMAS, D.J. 2013 Understanding kappa distributions: a toolbox for space science and astrophysics. *Space Sci. Rev.* **175** (1–4), 183–214.
- LOUREIRO, N.F. & BOLDYREV, S. 2017a Collisionless reconnection in magnetohydrodynamic and kinetic turbulence. *Astrophys. J.* **850**, 182.
- LOUREIRO, N.F. & BOLDYREV, S. 2017b Role of magnetic reconnection in magnetohydrodynamic turbulence. *Phys. Rev. Lett.* **118** (24), 245101.
- LOUREIRO, N.F., SCHEKOCHIHIN, A.A. & ZOCCO, A. 2013 Fast collisionless reconnection and electron heating in strongly magnetized plasmas. *Phys. Rev. Lett.* **111** (2), 025002.
- LUI, A.T.Y. & KRIMIGIS, S.M. 1981 Earthward transport of energetic protons in the Earth's plasma sheet. *Geophys. Res. Lett.* **8** (5), 527–530.
- MALLET, A., KLEIN, K.G., CHANDRAN, B.D.G., GROŠELJ, D., HOPPOCK, I.W., BOWEN, T.A., SALEM, C.S. & BALE, S.D. 2019 Interplay between intermittency and dissipation in collisionless plasma turbulence. *J. Plasma Phys.* **85** (3), 175850302.
- MALLET, A., SCHEKOCHIHIN, A.A. & CHANDRAN, B.D.G. 2015 Refined critical balance in strong Alfvénic turbulence. *Mon. Not. R. Astron. Soc.* **449**, L77–L81.
- MALLET, A., SCHEKOCHIHIN, A.A. & CHANDRAN, B.D.G. 2017a Disruption of Alfvénic turbulence by magnetic reconnection in a collisionless plasma. *J. Plasma Phys.* **83** (6), 905830609.
- MALLET, A., SCHEKOCHIHIN, A.A. & CHANDRAN, B.D.G. 2017b Disruption of sheet-like structures in Alfvénic turbulence by magnetic reconnection. *Mon. Not. R. Astron. Soc.* **468** (4), 4862–4871.
- MARKOVSKII, S.A. & VASQUEZ, B.J. 2011 A short-timescale channel of dissipation of the strong solar wind turbulence. *Astrophys. J.* **739**, 22.
- MARON, J. & GOLDBREICH, P. 2001 Simulations of incompressible magnetohydrodynamic turbulence. *Astrophys. J.* **554**, 1175–1196.
- MARSCH, E. & TU, C.Y. 1990 On the radial evolution of MHD turbulence in the inner heliosphere. *J. Geophys. Res.* **95** (A6), 8211–8229.
- MARTINOVIĆ, M.M., KLEIN, K.G. & BOUROUAINE, S. 2019 Radial evolution of stochastic heating in low- β solar wind. *Astrophys. J.* **879** (1), 43.
- MARTINOVIĆ, M.M., KLEIN, K.G., KASPER, J.C., CASE, A.W., KORRECK, K.E., LARSON, D., Livi, R., Stevens, M., Whittlesey, P., Chandran, B.D.G., *et al.* 2020 The enhancement of proton stochastic heating in the near-sun solar wind. *Astrophys. J. Suppl.* **246** (2), 30.
- MARUCA, B.A., KASPER, J.C. & BALE, S.D. 2011 What are the relative roles of heating and cooling in generating solar wind temperature anisotropies? *Phys. Rev. Lett.* **107** (20), 201101.
- MASON, J., CATTANEO, F. & BOLDYREV, S. 2006 Dynamic alignment in driven magnetohydrodynamic turbulence. *Phys. Rev. Lett.* **97** (25), 255002.
- MATTEINI, L., LANDI, S., HELLINGER, P. & VELLI, M. 2006 Parallel proton fire hose instability in the expanding solar wind: hybrid simulations. *J. Geophys. Res.* **111** (A10), 10101.
- MATTHAEUS, W.H., DASSO, S., WEYGAND, J.M., MILANO, L.J., SMITH, C.W. & KIVELSON, M.G. 2005 Spatial correlation of solar-wind turbulence from two-point measurements. *Phys. Rev. Lett.* **95** (23), 231101.

- MATTHAEUS, W.H., GOLDSTEIN, M.L. & SMITH, C. 1982 Evaluation of magnetic helicity in homogeneous turbulence. *Phys. Rev. Lett.* **48** (18), 1256–1259.
- MATTHAEUS, W.H. & MONTGOMERY, D. 1980 Selective decay hypothesis at high mechanical and magnetic Reynolds numbers. *Ann. N. Y. Acad. Sci.* **357**, 203–222.
- MATTHAEUS, W.H., OUGHTON, S., OSMAN, K.T., SERVIDIO, S., WAN, M., GARY, S.P., SHAY, M.A., VALENTINI, F., ROYTERSHTEYN, V., KARIMABADI, H., *et al.* 2014 Nonlinear and linear timescales near kinetic scales in solar wind turbulence. *Astrophys. J.* **790** (2), 155.
- MATTHAEUS, W.H. & VELLI, M. 2011 Who needs turbulence? A review of turbulence effects in the heliosphere and on the fundamental process of reconnection. *Space Sci. Rev.* **160**, 145–168.
- MCCHESENEY, J.M., STERN, R.A. & BELLAN, P.M. 1987 Observation of fast stochastic ion heating by drift waves. *Phys. Rev. Lett.* **59** (13), 1436–1439.
- MCCUBBIN, A.J., HOWES, G.G. & TENBARGE, J.M. 2022 Characterizing velocity-space signatures of electron energization in large-guide-field collisionless magnetic reconnection. *Phys. Plasmas* **29** (5), 052105.
- MELVILLE, S., SCHEKOCHIHIN, A.A. & KUNZ, M.W. 2016 Pressure-anisotropy-driven microturbulence and magnetic-field evolution in shearing, collisionless plasma. *Mon. Not. R. Astron. Soc.* **459**, 2701–2720.
- MENEGUZZI, M., FRISCH, U. & POUQUET, A. 1981 Helical and nonhelical turbulent dynamos. *Phys. Rev. Lett.* **47**, 1060–1064.
- MERRIFIELD, J.A., MÜLLER, W. -C., CHAPMAN, S.C. & DENDY, R.O. 2005 The scaling properties of dissipation in incompressible isotropic three-dimensional magnetohydrodynamic turbulence. *Phys. Plasmas* **12** (2), 022301.
- MEYRAND, R., KANEKAR, A., DORLAND, W. & SCHEKOCHIHIN, A.A. 2019 Fluidization of collisionless plasma turbulence. *Proc. Natl Acad. Sci. USA* **116**, 1185–1194.
- MEYRAND, R., SQUIRE, J., SCHEKOCHIHIN, A.A. & DORLAND, W. 2021 On the violation of the zeroth law of turbulence in space plasmas. *J. Plasma Phys.* **87** (3), 535870301.
- MIKIĆ, Z., LINKER, J.A., SCHNACK, D.D., LIONELLO, R. & TARDITI, A. 1999 Magnetohydrodynamic modeling of the global solar corona. *Phys. Plasmas* **6** (5), 2217–2224.
- MONTAG, P. & HOWES, G.G. 2022 A field-particle correlation analysis of magnetic pumping. *Phys. Plasmas* **29** (3), 032901.
- MONTAG, P.K. 2018 Modeling the formation of current sheets in symmetric and asymmetric reconnection. PhD thesis, Massachusetts Institute of Technology.
- MUÑOZ, P.A. & BÜCHNER, J. 2018 Two-stage electron acceleration by 3D collisionless guide-field magnetic reconnection. *Astrophys. J.* **864** (1), 92.
- NARITA, Y., GLASSMEIER, K.-H., SAHRAOUI, F. & GOLDSTEIN, M.L. 2010 Wave-vector dependence of magnetic-turbulence spectra in the solar wind. *Phys. Rev. Lett.* **104** (17), 171101.
- NATIONAL RESEARCH COUNCIL 2013 *Solar and Space Physics: A Science for a Technological Society*. The National Academies Press, Committee on a Decadal Strategy for Solar and Space Physics (Heliophysics); Space Studies Board; Aeronautics and Space Engineering Board; Division of Earth and Physical Sciences; National Research Council.
- NAVARRO, A.B., TEACA, B., TOLD, D., GROSELI, D., CRANDALL, P. & JENKO, F. 2016 Structure of plasma heating in gyrokinetic Alfvénic turbulence. *Phys. Rev. Lett.* **117** (24), 245101.
- NG, C.S. & BHATTACHARJEE, A. 1996 Interaction of shear-Alfvén wave packets: implication for weak magnetohydrodynamic turbulence in astrophysical plasmas. *Astrophys. J.* **465**, 845.
- NIELSON, K.D., HOWES, G.G. & DORLAND, W. 2013 Alfvén wave collisions, the fundamental building block of plasma turbulence. II. Numerical solution. *Phys. Plasmas* **20** (7), 072303.
- OPHER, M., LOEB, A., DRAKE, J. & TOTH, G. 2020 A small and round heliosphere suggested by magnetohydrodynamic modelling of pick-up ions. *Nat. Astron.* **4**, 675–683.
- OSMAN, K.T., KIYANI, K.H., CHAPMAN, S.C. & HNAT, B. 2014a Anisotropic intermittency of magnetohydrodynamic turbulence. *Astrophys. J. Lett.* **783**, L27.
- OSMAN, K.T., MATTHAEUS, W.H., GOSLING, J.T., GRECO, A., SERVIDIO, S., HNAT, B., CHAPMAN, S.C. & PHAN, T.D. 2014b Magnetic reconnection and intermittent turbulence in the solar wind. *Phys. Rev. Lett.* **112** (21), 215002.

- OSMAN, K.T., MATTHAEUS, W.H., GRECO, A. & SERVIDIO, S. 2011 Evidence for inhomogeneous heating in the solar wind. *Astrophys. J. Lett.* **727**, L11.
- OSMAN, K.T., MATTHAEUS, W.H., HNAT, B. & CHAPMAN, S.C. 2012a Kinetic signatures and intermittent turbulence in the solar wind plasma. *Phys. Rev. Lett.* **108** (26), 261103.
- OSMAN, K.T., MATTHAEUS, W.H., WAN, M. & RAPPAZZO, A.F. 2012b Intermittency and local heating in the solar wind. *Phys. Rev. Lett.* **108** (26), 261102.
- OSSENDRIJVER, M. 2003 The solar dynamo. *Astron. Astrophys. Rev.* **11** (4), 287–367.
- PAO, Y.-H. 1965 Structure of turbulent velocity and scalar fields at large wavenumbers. *Phys. Fluids* **8** (6), 1063–1075.
- PARKER, E.N. 1955 Hydromagnetic dynamo models. *Astrophys. J.* **122**, 293–314.
- PARKER, E.N. 1993 A solar dynamo surface wave at the interface between convection and nonuniform rotation. *Astrophys. J.* **408**, 707.
- PARKER, J.T., HIGHCOCK, E.G., SCHEKOCHIHIN, A.A. & DELLAR, P.J. 2016 Suppression of phase mixing in drift-kinetic plasma turbulence. *Phys. Plasmas* **23** (7), 070703.
- PEREZ, J.C. & BOLDYREV, S. 2009 Role of cross-helicity in magnetohydrodynamic turbulence. *Phys. Rev. Lett.* **102** (2), 025003.
- PEREZ, J.C. & BOLDYREV, S. 2010 Strong magnetohydrodynamic turbulence with cross helicity. *Phys. Plasmas* **17** (5), 055903.
- PEREZ, J.C. & CHANDRAN, B.D.G. 2013 Direct numerical simulations of reflection-driven, reduced magnetohydrodynamic turbulence from the sun to the Alfvén critical point. *Astrophys. J.* **776**, 124.
- PEREZ, J.C., MASON, J., BOLDYREV, S. & CATTANEO, F. 2012 On the energy spectrum of strong magnetohydrodynamic turbulence. *Phys. Rev. X* **2** (4), 041005.
- PERRI, S., GOLDSTEIN, M.L., DORELLI, J.C. & SAHRAOUI, F. 2012 Detection of small-scale structures in the dissipation regime of solar-wind turbulence. *Phys. Rev. Lett.* **109** (19), 191101.
- PHAN, T.D., EASTWOOD, J.P., SHAY, M.A., DRAKE, J.F., SONNERUP, B.U.Ö., FUJIMOTO, M., CASSAK, P.A., ØIEROSET, M., BURCH, J.L., TORBERT, R.B., *et al.* 2018 Electron magnetic reconnection without ion coupling in earth’s turbulent magnetosheath. *Nature* **557** (7704), 202–206.
- PLUNK, G.G. 2013 Landau damping in a turbulent setting. *Phys. Plasmas* **20** (3), 032304.
- PLUNK, G.G., COWLEY, S.C., SCHEKOCHIHIN, A.A. & TATSUNO, T. 2010 Two-dimensional gyrokinetic turbulence. *J. Fluid Mech.* **664**, 407–435.
- PLUNK, G.G. & TATSUNO, T. 2011 Energy transfer and dual cascade in kinetic magnetized plasma turbulence. *Phys. Rev. Lett.* **106** (16), 165003.
- PODESTA, J.J., BOROVSKY, J.E. & GARY, S.P. 2010 A kinetic Alfvén wave cascade subject to collisionless damping cannot reach electron scales in the solar wind at 1 AU. *Astrophys. J.* **712**, 685–691.
- PUCCI, F., USAMI, S., JI, H., GUO, X., HORIUCHI, R., OKAMURA, S., FOX, W., JARA-ALMONTE, J., YAMADA, M. & YOO, J. 2018 Energy transfer and electron energization in collisionless magnetic reconnection for different guide-field intensities. *Phys. Plasmas* **25** (12).
- QUATAERT, E. 1998 Particle heating by Alfvénic turbulence in hot accretion flows. *Astrophys. J.* **500**, 978–991.
- QUATAERT, E. & GRUZINOV, A. 1999 Turbulence and particle heating in advection-dominated accretion flows. *Astrophys. J.* **520**, 248–255.
- RIPPERDA, B., MAHLMANN, J.F., CHERNOGLAZOV, A., TENBARGE, J.M., MOST, E.R., JUNO, J., YUAN, Y., PHILIPPOV, A.A. & BHATTACHARJEE, A. 2021 Weak Alfvénic turbulence in relativistic plasmas. Part 2. Current sheets and dissipation. *J. Plasma Phys.* **87** (5), 905870512.
- ROBERTS, O.W., LI, X. & JESKA, L. 2015 A statistical study of the solar wind turbulence at ion kinetic scales using the k-filtering technique and cluster data. *Astrophys. J.* **802**, 2.
- ROWAN, M.E., SIRONI, L. & NARAYAN, R. 2017 Electron and proton heating in transrelativistic magnetic reconnection. *Astrophys. J.* **850** (1), 29.
- RUTHERFORD, P.H. & FRIEMAN, E.A. 1968 Drift instabilities in general magnetic field configurations. *Phys. Fluids* **11**, 569–585.
- SAHRAOUI, F., GOLDSTEIN, M.L., BELMONT, G., CANU, P. & REZEAU, L. 2010 Three dimensional anisotropic k spectra of turbulence at subproton scales in the solar wind. *Phys. Rev. Lett.* **105** (13), 131101.

- SAHRAOUI, F., GOLDSTEIN, M.L., ROBERT, P. & KHOTYAINTEV, Y.V. 2009 Evidence of a cascade and dissipation of solar-wind turbulence at the electron gyroscale. *Phys. Rev. Lett.* **102** (23), 231102.
- SAHRAOUI, F., HUANG, S.Y., BELMONT, G., GOLDSTEIN, M.L., RÉTINO, A., ROBERT, P. & De Patoul, J. 2013 Scaling of the electron dissipation range of solar wind turbulence. *Astrophys. J.* **777**, 15.
- SCHEKOCHIHIN, A.A., COWLEY, S.C., DORLAND, W., HAMMETT, G.W., HOWES, G.G., QUATAERT, E. & TATSUNO, T. 2009 Astrophysical gyrokinetics: kinetic and fluid turbulent cascades in magnetized weakly collisional plasmas. *Astrophys. J. Suppl.* **182**, 310–377.
- SCHEKOCHIHIN, A.A., KAWAZURA, Y. & BARNES, M.A. 2019 Constraints on ion versus electron heating by plasma turbulence at low beta. *J. Plasma Phys.* **85** (3), 905850303.
- SCHEKOCHIHIN, A.A., PARKER, J.T., HIGHCOCK, E.G., DELLAR, P.J., DORLAND, W. & HAMMETT, G.W. 2016 Phase mixing versus nonlinear advection in drift-kinetic plasma turbulence. *J. Plasma Phys.* **82** (2), 905820212.
- SCHREINER, A. & SAUR, J. 2017 A model for dissipation of solar wind magnetic turbulence by kinetic Alfvén waves at electron scales: comparison with observations. *Astrophys. J.* **835** (2), 133.
- SERVIDIO, S., GRECO, A., MATTHAEUS, W.H., OSMAN, K.T. & DMITRUK, P. 2011 Statistical association of discontinuities and reconnection in magnetohydrodynamic turbulence. *J. Geophys. Res.* **116**, 9102.
- SHAIKH, D. & ZANK, G.P. 2005 Driven dissipative whistler wave turbulence. *Phys. Plasmas* **12** (12), 122310.
- SHANKARAPPA, N., KLEIN, K.G. & MARTINOVIĆ, M.M. 2023 Estimation of turbulent proton and electron heating rates via Landau damping constrained by Parker solar probe observations. *Astrophys. J.* **946** (2), 85.
- SNYDER, P.B., HAMMETT, G.W. & DORLAND, W. 1997 Landau fluid models of collisionless magnetohydrodynamics. *Phys. Plasmas* **4**, 3974–3985.
- SOUTHWOOD, D.J. & KIVELSON, M.G. 1993 Mirror instability. I - Physical mechanism of linear instability. *J. Geophys. Res.* **98**, 9181–9187.
- SPANGLER, S.R. 1998 Magnetohydrodynamic turbulence and enhanced atomic processes in astrophysical plasmas. *Phys. Plasmas* **5**, 3006–3020.
- SPANGLER, S.R. 1999 Two-dimensional magnetohydrodynamics and interstellar plasma turbulence. *Astrophys. J.* **522**, 879–896.
- SPITZER, L. 1962 *Physics of Fully Ionized Gases*, 2nd edn. Interscience.
- SPITZER, L., JR. & WITTEN, L. 1953 On the ionization and heating of plasma. *Tech. Rep.* NYO-999 (PM-S-6). US Atomic Energy Commission.
- SQUIRE, J., KUNZ, M.W., QUATAERT, E. & SCHEKOCHIHIN, A.A. 2017a Kinetic simulations of the interruption of large-amplitude shear-Alfvén waves in a high- β plasma. *Phys. Rev. Lett.* **119** (15), 155101.
- SQUIRE, J., MEYRAND, R. & KUNZ, M.W. 2023 Electron-ion heating partition in imbalanced solar-wind turbulence. *Astrophys. J. Lett.* **957** (2), L30.
- SQUIRE, J., MEYRAND, R., KUNZ, M.W., ARZAMASSKIY, L., SCHEKOCHIHIN, A.A. & QUATAERT, E. 2022 High-frequency heating of the solar wind triggered by low-frequency turbulence. *Nat. Astron.* **6**, 715–723.
- SQUIRE, J., QUATAERT, E. & SCHEKOCHIHIN, A.A. 2016 A stringent limit on the amplitude of Alfvénic perturbations in high-beta low-collisionality plasmas. *Astrophys. J. Lett.* **830**, L25.
- SQUIRE, J., SCHEKOCHIHIN, A.A. & QUATAERT, E. 2017b Amplitude limits and nonlinear damping of shear-Alfvén waves in high-beta low-collisionality plasmas. *New J. Phys.* **19** (5), 055005.
- SRIDHAR, S. & GOLDREICH, P. 1994 Toward a theory of interstellar turbulence. 1. Weak Alfvénic turbulence. *Astrophys. J.* **432**, 612–621.
- STIX, T.H. 1992 *Waves in Plasmas*. American Institute of Physics.
- ŠTVERÁK, Š., MAKSIMOVIC, M., TRÁVNÍČEK, P.M., MARSCH, E., FAZAKERLEY, A.N. & SCIME, E.E. 2009 Radial evolution of nonthermal electron populations in the low-latitude solar wind: helios, cluster, and ulysses observations. *J. Geophys. Res.* **114** (A5), A05104.

- ŠTVERÁK, Š., TRÁVNÍČEK, P., MAKSIMOVIC, M., MARSCH, E., FAZAKERLEY, A.N. & SCIME, E.E. 2008 Electron temperature anisotropy constraints in the solar wind. *J. Geophys. Res.* **113** (A3), A03103.
- SUMMERS, D. & THORNE, R.M. 1991 The modified plasma dispersion function. *Phys. Fluids B* **3**, 1835–1847.
- SUMMERS, D., XUE, S. & THORNE, R.M. 1994 Calculation of the dielectric tensor for a generalized Lorentzian (κ) distribution function. *Phys. Plasmas* **1**, 2012–2025.
- SVIDZINSKI, V.A., LI, H., ROSE, H.A., ALBRIGHT, B.J. & BOWERS, K.J. 2009 Particle in cell simulations of fast magnetosonic wave turbulence in the ion cyclotron frequency range. *Phys. Plasmas* **16** (12), 122310.
- SWANSON, D.G. 2003 *Plasma Waves*, 2nd ed. Institute of Physics Publishing.
- TAJIRI, M. 1967 Propagation of hydromagnetic waves in collisionless plasma. II. Kinetic approach. *J. Phys. Soc. Japan* **22**, 1482.
- TATSUNO, T., SCHEKOCIHIN, A.A., DORLAND, W., PLUNK, G., BARNES, M.A., COWLEY, S.C. & HOWES, G.G. 2009 Nonlinear phase mixing and phase-space cascade of entropy in gyrokinetic plasma turbulence. *Phys. Rev. Lett.* **103** (1), 015003.
- TAYLOR, J.B. & HASTIE, R.J. 1968 Stability of general plasma equilibria. I. Formal theory. *Plasma Phys.* **10**, 479–494.
- TENBARGE, J.M. & HOWES, G.G. 2012 Evidence of critical balance in kinetic Alfvén wave turbulence simulations. *Phys. Plasmas* **19** (5), 055901.
- TENBARGE, J.M. & HOWES, G.G. 2013 Current sheets and collisionless damping in kinetic plasma turbulence. *Astrophys. J. Lett.* **771**, L27.
- TENBARGE, J.M., HOWES, G.G. & DORLAND, W. 2013 Collisionless damping at electron scales in solar wind turbulence. *Astrophys. J.* **774**, 139.
- TENBARGE, J.M., HOWES, G.G., DORLAND, W. & HAMMETT, G.W. 2014 An oscillating Langevin antenna for driving plasma turbulence simulations. *Comput. Phys. Commun.* **185**, 578–589.
- TENBARGE, J.M., PODESTA, J.J., KLEIN, K.G. & HOWES, G.G. 2012 Interpreting magnetic variance anisotropy measurements in the solar wind. *Astrophys. J.* **753**, 107.
- TENBARGE, J.M., RIPPERDA, B., CHERNOGLAZOV, A., BHATTACHARJEE, A., MAHLMANN, J.F., MOST, E.R., JUNO, J., YUAN, Y. & PHILIPPOV, A.A. 2021 Weak Alfvénic turbulence in relativistic plasmas. Part I. Dynamical equations and basic dynamics of interacting resonant triads. *J. Plasma Phys.* **87** (6), 905870614.
- THORNE, R.M. & SUMMERS, D. 1991 Landau damping in space plasmas. *Phys. Fluids B* **3** (8), 2117–2123.
- TOLD, D., JENKO, F., TENBARGE, J.M., HOWES, G.G. & HAMMETT, G.W. 2015 Multiscale nature of the dissipation range in gyrokinetic simulations of Alfvénic turbulence. *Phys. Rev. Lett.* **115** (2), 025003.
- TU, C.-Y. & MARSCH, E. 1990 Evidence for a ‘background’ spectrum of solar wind turbulence in the inner heliosphere. *J. Geophys. Res.* **95**, 4337–4341.
- TU, C.-Y. & MARSCH, E. 1995 MHD structures, waves and turbulence in the solar wind: observations and theories. *Space Sci. Rev.* **73**, 1–2.
- URITSKY, V.M., POUQUET, A., ROSENBERG, D., MININNI, P.D. & DONOVAN, E.F. 2010 Structures in magnetohydrodynamic turbulence: detection and scaling. *Phys. Rev. E* **82** (5), 056326.
- VASYLIUNAS, V.M. 1968 A survey of low-energy electrons in the evening sector of the magnetosphere with OGO 1 and OGO 3. *J. Geophys. Res.* **73** (9), 2839–2884.
- VECH, D., KLEIN, K.G. & KASPER, J.C. 2017 Nature of stochastic ion heating in the solar wind: testing the dependence on plasma beta and turbulence amplitude. *Astrophys. J. Lett.* **850** (1), L11.
- VEDENOV, A.A. & SAGDEEV, R.Z. 1958 Some properties of a plasma with an anisotropic ion velocity distribution in a magnetic field. In *Plasma Physics and the Problem of Controlled Thermonuclear Reactions* (ed. M.A. Leontovich), vol. 3, p. 332. Pergamon.
- VERNIERO, J.L. & HOWES, G.G. 2018 The Alfvénic nature of energy transfer mediation in localized, strongly nonlinear Alfvén wavepacket collisions. *J. Plasma Phys.* **84** (1), 905840109.
- VERNIERO, J.L., HOWES, G.G. & KLEIN, K.G. 2018 Nonlinear energy transfer and current sheet development in localized Alfvén wavepacket collisions in the strong turbulence limit. *J. Plasma Phys.* **84** (1), 905840103.

- VERSCHAREN, D., CHANDRAN, B.D.G., KLEIN, K.G. & QUATAERT, E. 2016 Collisionless isotropization of the solar-wind protons by compressive fluctuations and plasma instabilities. *Astrophys. J.* **831** (2), 128.
- VOITENKO, Y. & GOOSSENS, M. 2004 Cross-field heating of coronal ions by low-frequency kinetic Alfvén waves. *Astrophys. J. Lett.* **605** (2), L149–L152.
- WALKER, J., BOLDYREV, S. & LOUREIRO, N.F. 2018 Influence of tearing instability on magnetohydrodynamic turbulence. *Phys. Rev. E* **98** (3), 033209.
- WANG, X., TU, C., HE, J., MARSCH, E. & WANG, L. 2013 On intermittent turbulence heating of the solar wind: differences between tangential and rotational discontinuities. *Astrophys. J. Lett.* **772**, L14.
- WAN, M., MATTHAEUS, W.H., KARIMABADI, H., ROYTERSHEYN, V., SHAY, M., WU, P., DAUGHTON, W., LORING, B. & CHAPMAN, S.C. 2012 Intermittent dissipation at kinetic scales in collisionless plasma turbulence. *Phys. Rev. Lett.* **109** (19), 195001.
- WHITE, R., CHEN, L. & LIN, Z. 2002 Resonant plasma heating below the cyclotron frequency. *Phys. Plasmas* **9**, 1890–1897.
- WILSON III, L.B., STEVENS, M.L., KASPER, J.C., KLEIN, K.G., MARUCA, B.A., BALE, S.D., BOWEN, T.A., PULUPA, M.P. & SALEM, C.S. 2018 The statistical properties of solar wind temperature parameters near 1 Au. *Astrophys. J. Suppl.* **236** (2), 41.
- WU, P., PERRI, S., OSMAN, K., WAN, M., MATTHAEUS, W.H., SHAY, M.A., GOLDSTEIN, M.L., KARIMABADI, H. & CHAPMAN, S. 2013 Intermittent heating in solar wind and kinetic simulations. *Astrophys. J. Lett.* **763**, L30.
- XIA, Q., PEREZ, J.C., CHANDRAN, B.D.G. & QUATAERT, E. 2013 Perpendicular ion heating by reduced magnetohydrodynamic turbulence. *Astrophys. J.* **776** (2), 90.
- YANG, Y., MATTHAEUS, W.H., PARASHAR, T.N., HAGGERTY, C.C., ROYTERSHEYN, V., DAUGHTON, W., WAN, M., SHI, Y. & CHEN, S. 2017a Energy transfer, pressure tensor, and heating of kinetic plasma. *Phys. Plasmas* **24** (7), 072306.
- YANG, Y., MATTHAEUS, W.H., PARASHAR, T.N., WU, P., WAN, M., SHI, Y., CHEN, S., ROYTERSHEYN, V. & DAUGHTON, W. 2017b Energy transfer channels and turbulence cascade in Vlasov-Maxwell turbulence. *Phys. Rev. E* **95** (6), 061201.
- YANG, Y., SHI, Y., WAN, M., MATTHAEUS, W.H. & CHEN, S. 2016 Energy cascade and its locality in compressible magnetohydrodynamic turbulence. *Phys. Rev. E* **93** (6), 061102.
- ZHAO, J.S., WU, D.J. & LU, J.Y. 2013 Kinetic Alfvén turbulence and parallel electric fields in flare loops. *Astrophys. J.* **767** (2), 109.
- ZHDANKIN, V., BOLDYREV, S., MASON, J. & PEREZ, J.C. 2012 Magnetic discontinuities in magnetohydrodynamic turbulence and in the solar wind. *Phys. Rev. Lett.* **108** (17), 175004.
- ZHDANKIN, V., UZDENSKY, D.A. & BOLDYREV, S. 2015a Temporal analysis of dissipative structures in magnetohydrodynamic turbulence. *Astrophys. J.* **811**, 6.
- ZHDANKIN, V., UZDENSKY, D.A. & BOLDYREV, S. 2015b Temporal intermittency of energy dissipation in magnetohydrodynamic turbulence. *Phys. Rev. Lett.* **114** (6), 065002.
- ZHDANKIN, V., UZDENSKY, D.A., PEREZ, J.C. & BOLDYREV, S. 2013 Statistical analysis of current sheets in three-dimensional magnetohydrodynamic turbulence. *Astrophys. J.* **771**, 124.
- ZHOU, M., LIU, Z. & LOUREIRO, N.F. 2023 Electron heating in kinetic-Alfvén-wave turbulence. *Proc. Natl Acad. Sci. USA* **120** (23), e2220927120.
- ZOCCO, A. & SCHEKOCIHIN, A.A. 2011 Reduced fluid-kinetic equations for low-frequency dynamics, magnetic reconnection, and electron heating in low-beta plasmas. *Phys. Plasmas* **18** (10), 102309.